RECEIVED
MAR 17 1998
OSTI

BNL-64772
Informal Report
CONF-9705259--Vugraphs

Proceedings of the Workshop on:

X-ray Computed Microtomography

May 19-21, 1997

Brookhaven National Laboratory
National Synchrotron Light Source

DISTRIBUTION OF THIS DOCUMENT IS UNLIMITED

Prepared for the U.S. Department of Energy under Contract No. DE-AC02-76CH00016

MASTER

DISCLAIMER

This report was prepared as an account of work sponsored by an agency of the United States Government. Neither the United States Government nor any agency thereof, nor any of their employees, make any warranty, express or implied, or assumes any legal liability or responsibility for the accuracy, completeness, or usefulness of any information, apparatus, product, or process disclosed, or represents that its use would not infringe privately owned rights. Reference herein to any specific commercial product, process, or service by trade name, trademark, manufacturer, or otherwise does not necessarily constitute or imply its endorsement, recommendation, or favoring by the United States Government or any agency thereof. The views and opinions of authors expressed herein do not necessarily state or reflect those of the United States Government or any agency thereof.

DISCLAIMER

Portions of this document may be illegible in electronic image products. Images are produced from the best available original document.

BNL-64772
Informal Report

Proceedings of the Workshop on:

X-ray Computed Microtomography

May 19-21, 1997

Presenters:

John Dunsmuir, Exxon
Per Spanne, ESRF
Chris Jacobsen, SUNY Stony Brook
Avraham Dilmanian, BNL
Zhong Zhong, BNL
Betsy Dowd, BNL
Barbara Illman, USDA/FS Forest Products Laboratory, University of Wisconsin
Brent Lindquist, SUNY Stony Brook
Sheng-Rong Song, Dept of Geology, National Taiwan University
Ballard Andrews, BNL

Published: February 1998

Brookhaven National Laboratory
P.O. Box 5000
Upton, New York 11973-5000

Prepared for the U.S. Department of Energy under Contract No. DE-AC02-76CH00016

Order of Presentations:

Part I	John Dunsmuir (Exxon) "CMT: Applications and Techniques"
Part II	Per Spanne (ESRF) - "Computer Microtomography Using X-rays from Third Generation Synchrotron X-ray"
Part III	Chris Jacobsen (SUNY, Stony Brook) - "Approaches to Soft X-ray Nanotomography"
Part IV	Avraham Dilmanian and Zhong Zhong (BNL) - "Diffraction Enhanced Tomography"
Part V	Betsy Dowd (BNL) - "X-ray Computed Microtomography Applications at the NSLS"
Part VI	Barbara Illman (USDA/FS Forest Products Laboratory, University of Wisconsin) - "XCMT Applications in Forestry and Forest Products"
Part VII	Brent Lindquist (SUNY, Stony Brook) - "3DMA: Investigating Three Dimensional Pore Geometry from High Resolution Images"
Part VIII	Sheng-Rong Song (Dept of Geology, National Taiwan University) - "X-ray Computed Microtomography Studies on Volcanic Rock"
Part IX	Ballard Andrews (NSLS, BNL) - "3-D Visualization of Tomographic Volumes"

Part I

John Dunsmuir
Exxon

"CMT: Applications and Techniques"

Microtomography at X2-B

Techniques and Applications

J.H. Dunsmuir

Exxon Research & Engineering

NSLS workshop May 19, 1997

Experimental
K.L. D'Amico
H.W. Deckman
J.H. Dunsmuir
P. Eisenberger

Computing
B. Bannett
S. Ferguson
J. Hardenbergh
M. Wangert

Theory
B.P. Flannery
W. Roberge

Users
T. Halsey
M. Zhou
P. Sheng

Imaging X-ray DetectorAccuracy and Resolution

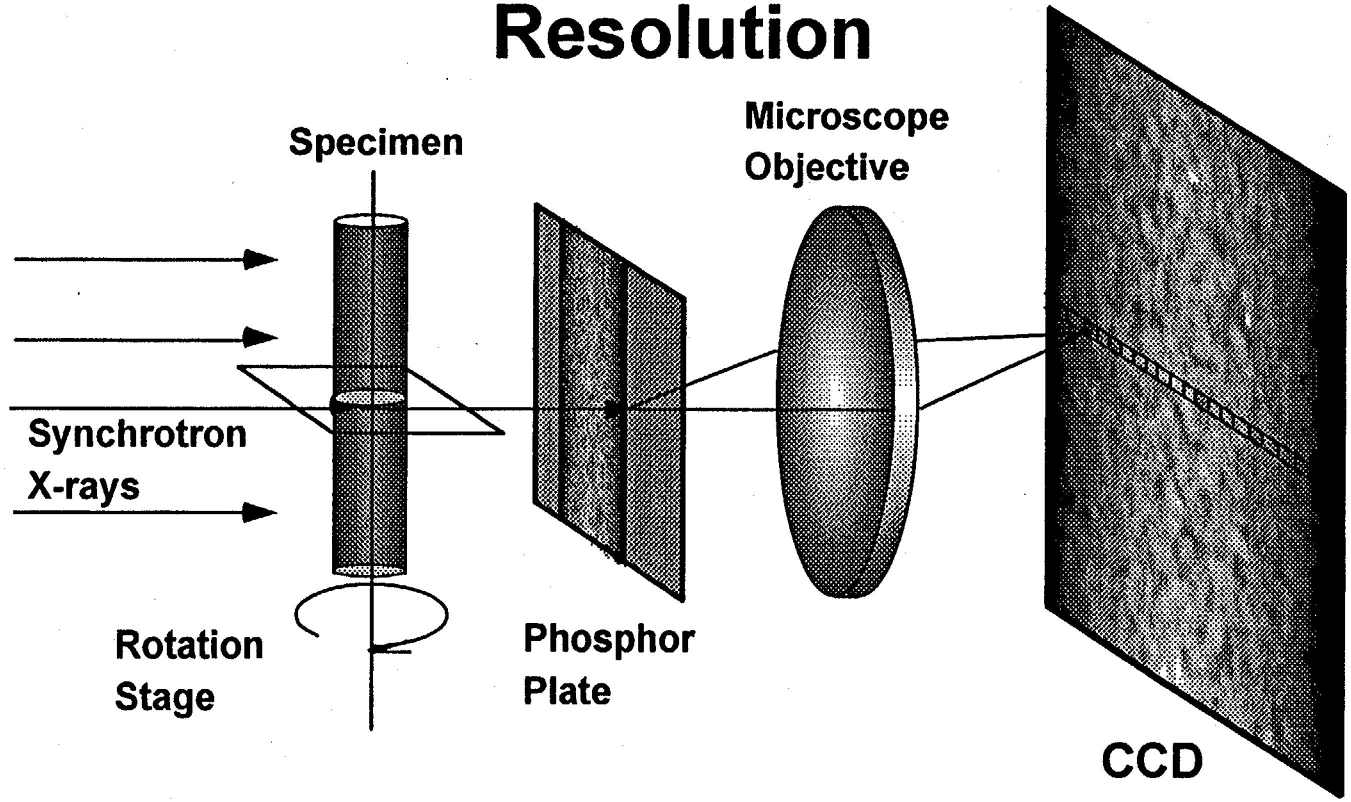

$$N_0 \longrightarrow \frac{N_1 Opt}{X\text{-}ray} \longrightarrow \frac{N_2 Col}{Gen} \longrightarrow \frac{N_3 e^-}{Opt}$$

- $S_d = N_0 \times N_1 \times N_2 \times N_3$
- $\mu_d = \mu_0 + \mu_1/N_0 + \mu_2/N_0N_1 + \mu_3/N_0N_1N_2$
- Std Dev $= \sigma = \mu_d^{1/2} \times S_d$
- Total Noise $= \{ \sigma^2 + (\omega/2^n)^2 + R^2\}^{1/2}$

Direct Fourier Reconstruction Scales $O(N^2)$

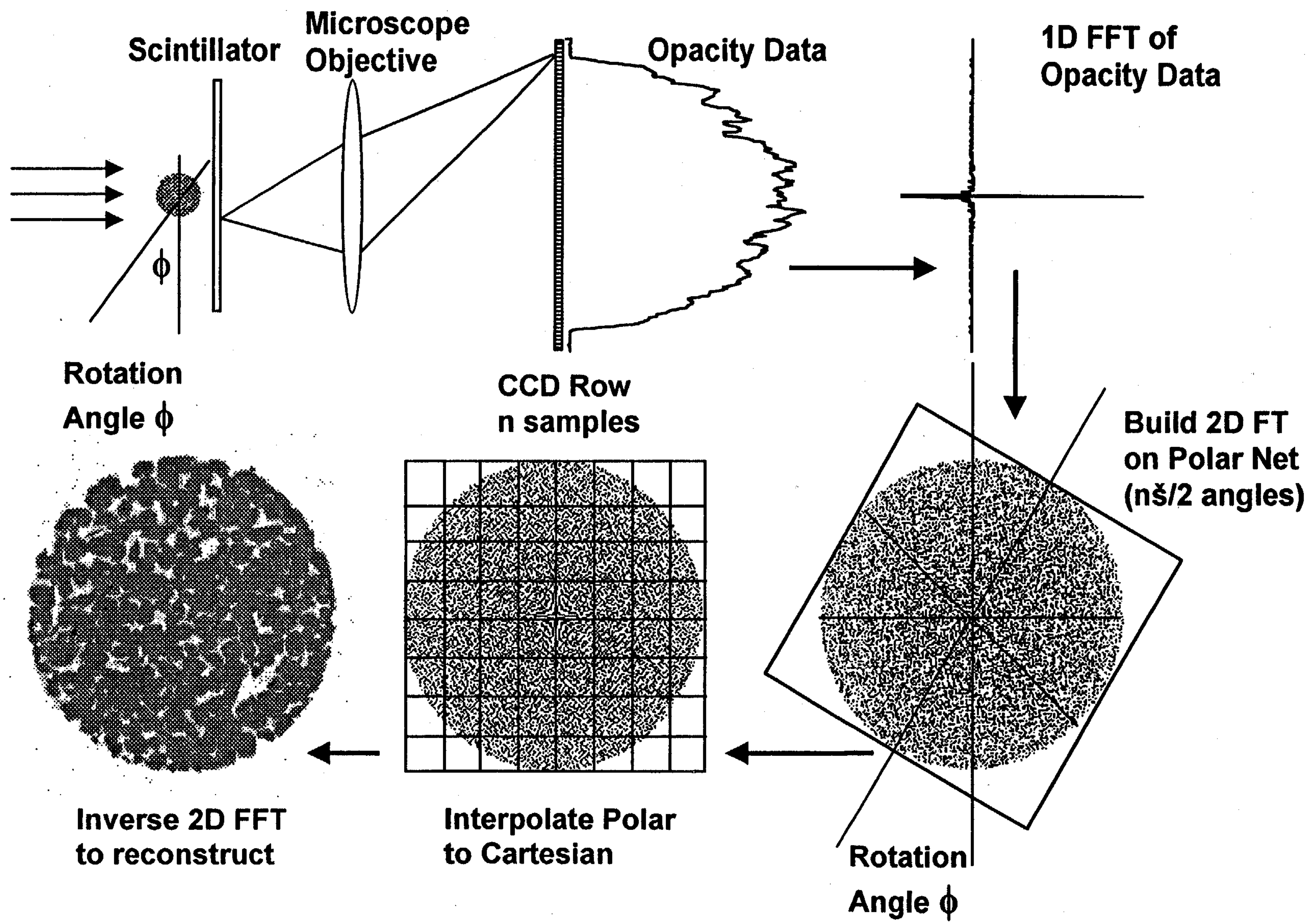

Microtomography: Then and Now

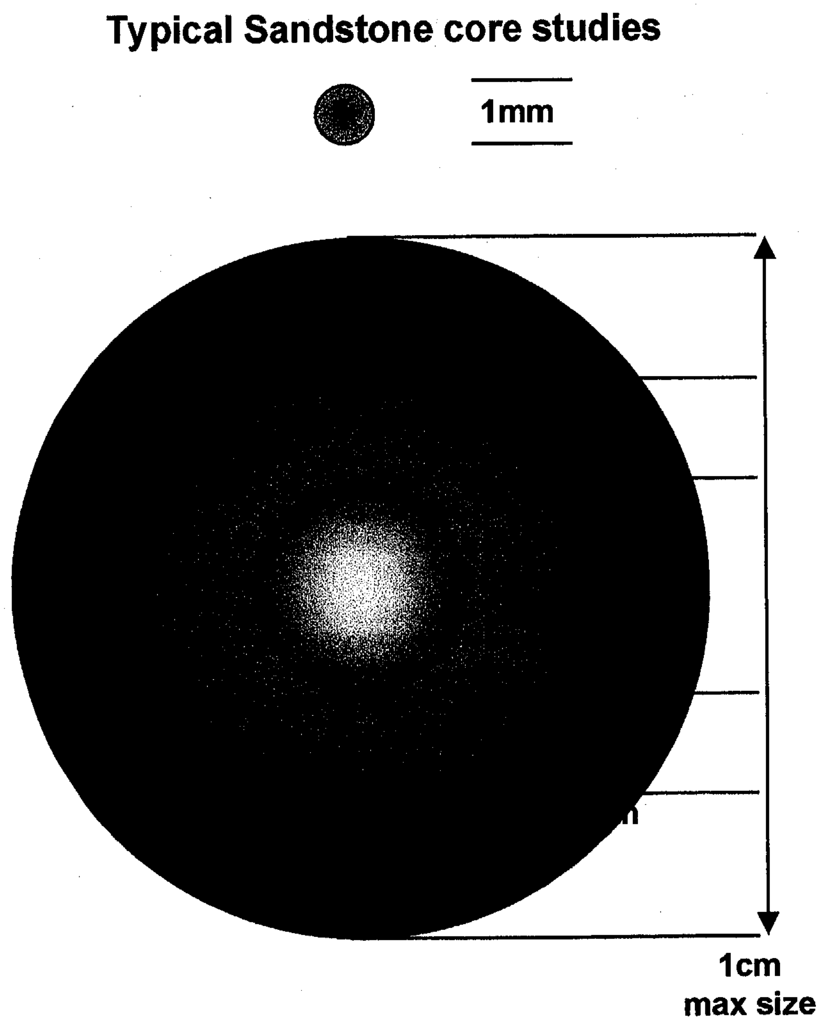

- **Then:(1987)**
  - Global reconstruction of 1mm Specimen 256^3 at 15μm resolution, 4hr scan time
  - Tools: none
- **Now:**
  - 3D chemical imaging (1991)
  - Speed enhancements < 1hr (1993)
  - Precision alignment (1993)
  - Systematic error suppression reconstruction (1995)
  - 1024^3 to 2 μm resolution (1996)
  - Tools:
    - + Segmentation
    - + Geometry
    - + Statistics
- **In the pipeline:**
  - Dynamic 3D imaging (1997)
  - Real time visualization(1998)

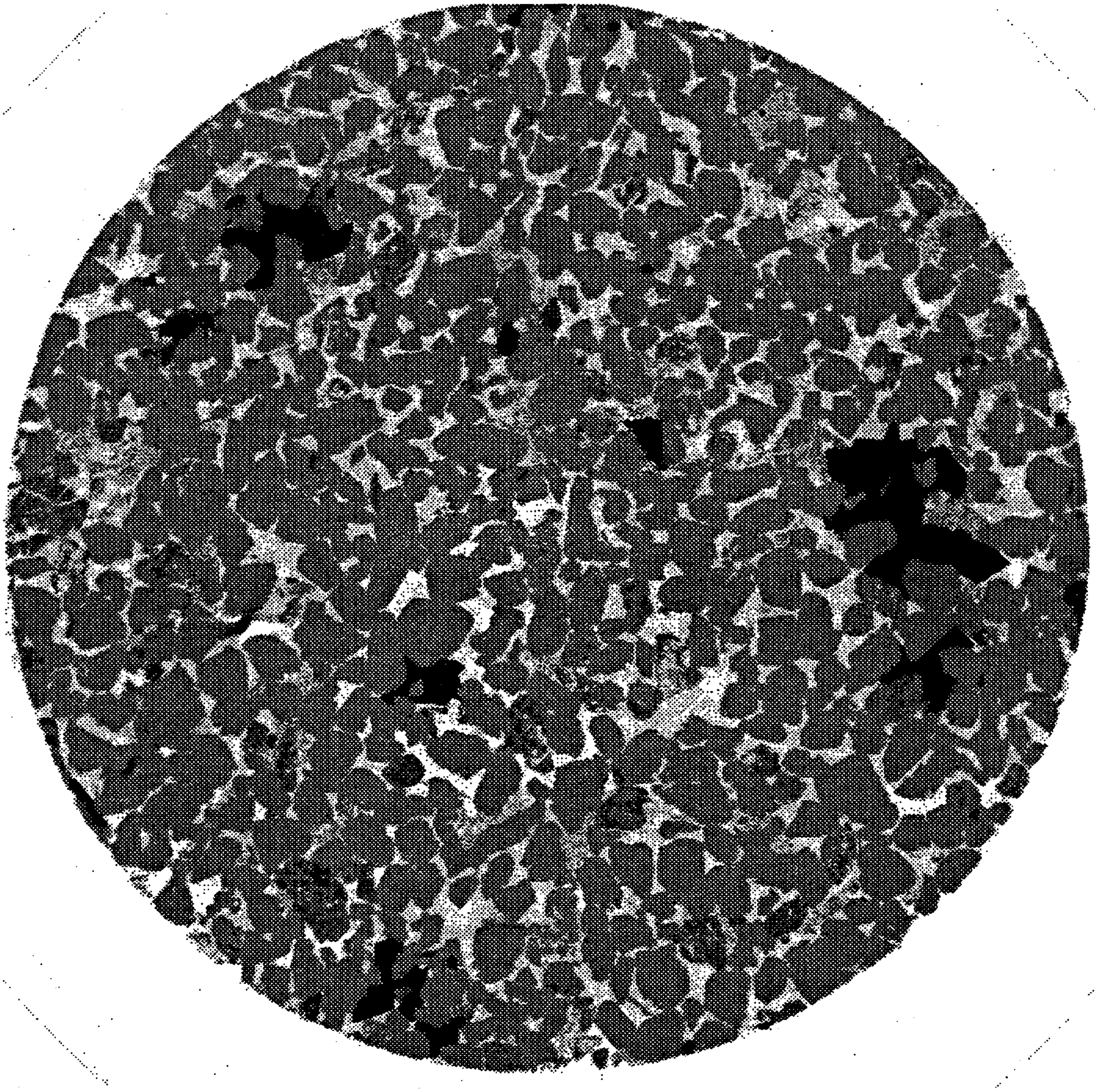

Berea Sandstone
4.5mm diameter, porosity = 21%
Imaged at 22 keV

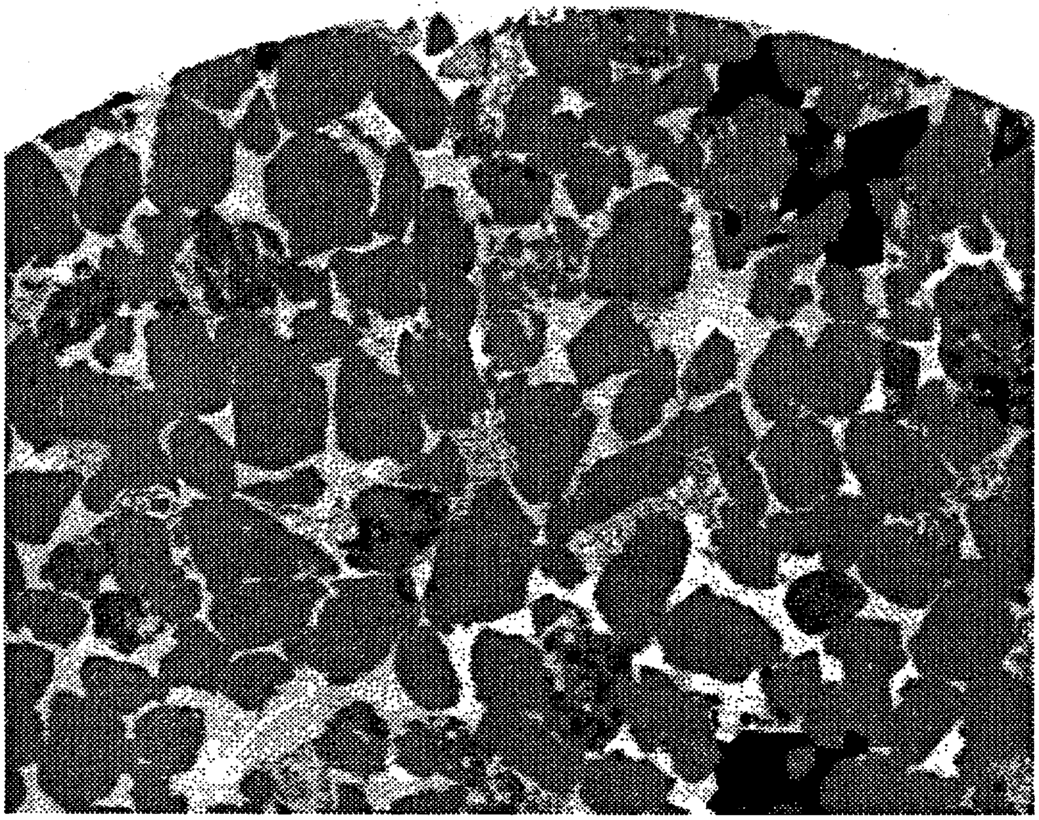

□ 100 µm (5.72µm/pixel)

Berea Sandstone
4.5mm diameter, porosity = 21%
Imaged at 22 keV

PORE BODY OF A FONTAINBLEAU SANDSTONE

- Topological Properties
  - Medial Axis Transform
  - Extract Network to Compute Absolute Permeability
- Statistical Properties
  - N point Probability Distribution N_1 = porosity
  - Lineal Path Function
  - Cumulative Pore Size Distribution
- Geometric Properties
  - Surface Area and Volume
  - Texture
  - Fractal Dimensions
  - Lattice-Boltzmann Simulation of Multi-phase Fluid Flow

X2-B Specifications

Beamline:	**White beamline with Single Si<111>monochomator in hutch tunable from 35 to 8keV**
Camera:	**Photometrics PXL, 1024CB/AR, 300K electrons 14 bits, 800kHz, 24 micron pixels**
Optics:	**2x , 4x, 10x, 20x high N.A. LD Plan Apochromats**
Scintillator:	**Polished single crystal CsI(Tl or Na)**
Throughput:	**Depends on resolution, x-ray energy, data size typically .5 hr for 6micron 512 cube at 17keV and 1.5 hr for 1024cube**
Recon:	**512cube, global 45 min, local 1.5hr 1024cube, global 3 hr, local coming soon**

Accept General users: **Yes with some restrictions.**

Application to Porous Media

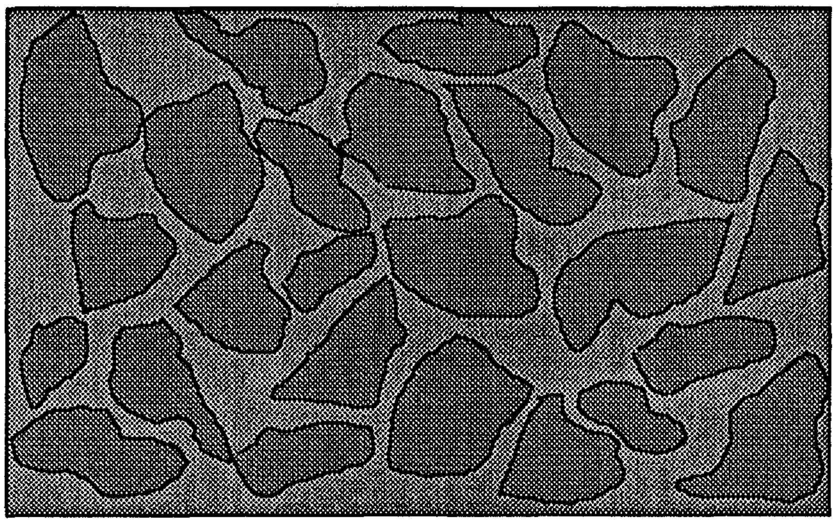

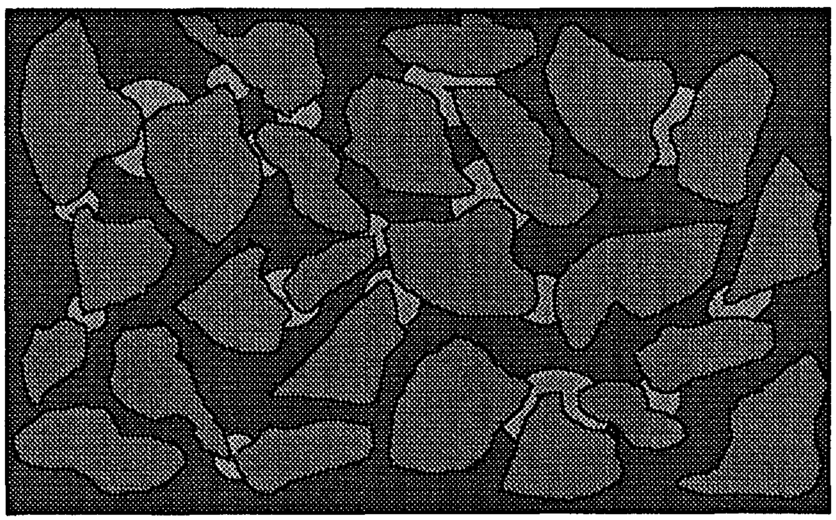

- Single fluid flow
  - Absolute permeability
    - $V = (k/\eta)\,\Delta P$
  - Related to geometry
- Multi fluid flow
  - Relative Permeability
    - Measured experimentally
  - Related to geometry, surface chemistry and history

CALCULATION of PERMEABILITY from μCT DATA*

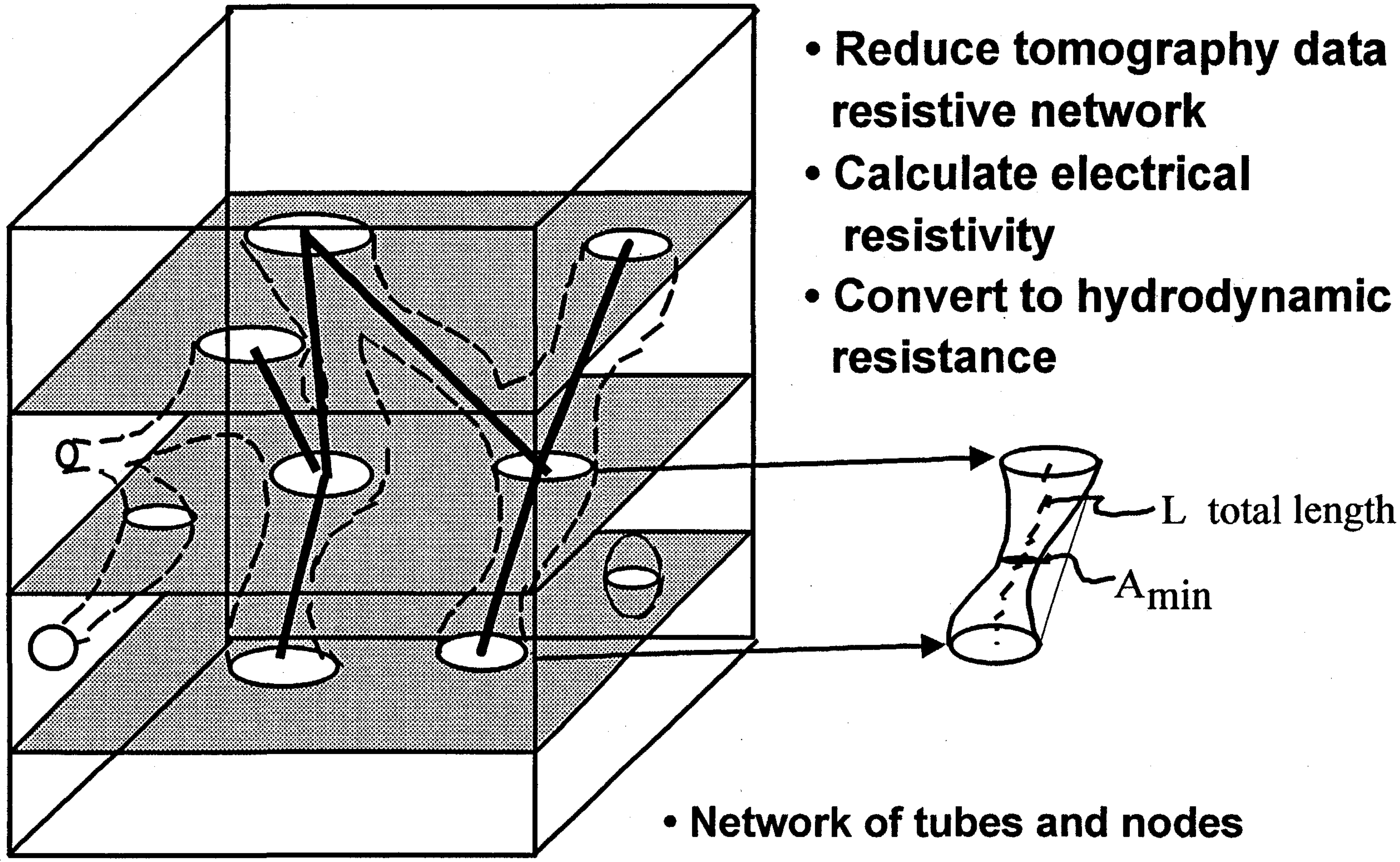

- Reduce tomography data to resistive network
- Calculate electrical resistivity
- Convert to hydrodynamic resistance

- Network of tubes and nodes

* M. Zhou 1995

Calculation vs Experiment for Fontainbleau* Sandstone

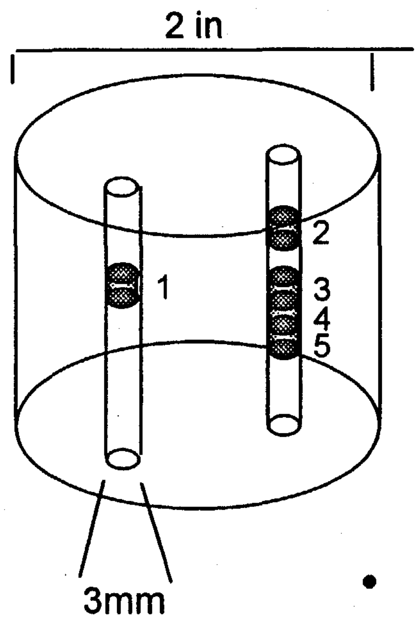

	Porosity		Formation Factor	Permeability K_o
Measured	14.8		22	1.3
Calculated	15.1	1	24	1.6
	12.8	2	34	.95
	12.8	3	33	.93
	12.8	4	36	.84
	13.3	5	33	1.0

- **Results for several Fontainbleau specimens**
  - excellent reproducibility within cylinders
  - variations consistent with natural variability of rock

*Specimen courtesy of Schlumberger-Doll Research

NMR AND ROCK PROPERTIES

- **MODEL FOR DATA INTERPRETATION**
  - Fluids in isolated pores
  - Pore size determines NMR relaxation time, T_2
  - Surface relaxivity connects NMR relaxation time to pore length

$$\frac{1}{T_2} = \rho_2\left(\frac{S}{V}\right)$$

- **REAL ROCKS**
  - Connected pores
  - Multi phase saturation
  - Distribution of NMR relaxation times, T_2, controlled by wettability

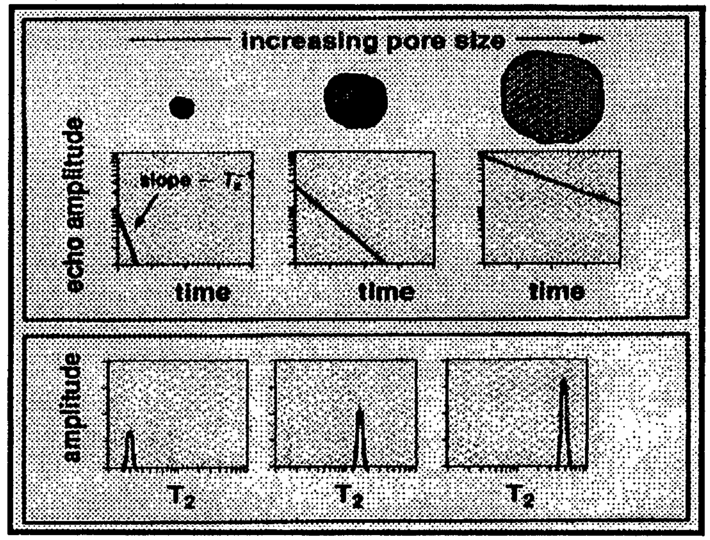

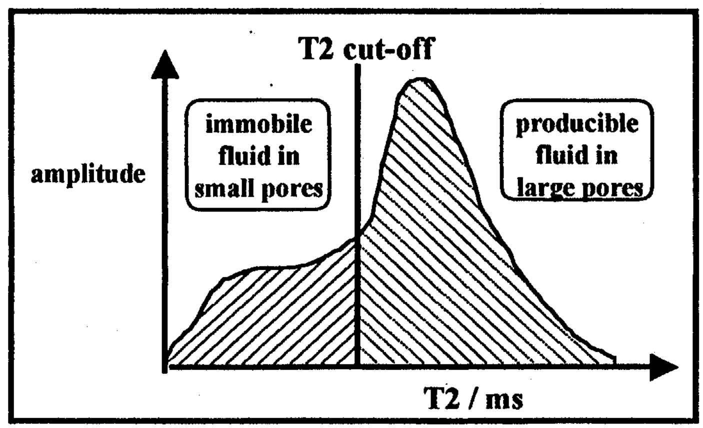

➡ NEED TO DETERMINE QUANTITATIVE PHYSICAL AND CHEMICAL CONTROLS ON NMR RELAXATION PARAMETERS

Mapping Relaxation Times in Fontainbleau Sandstone

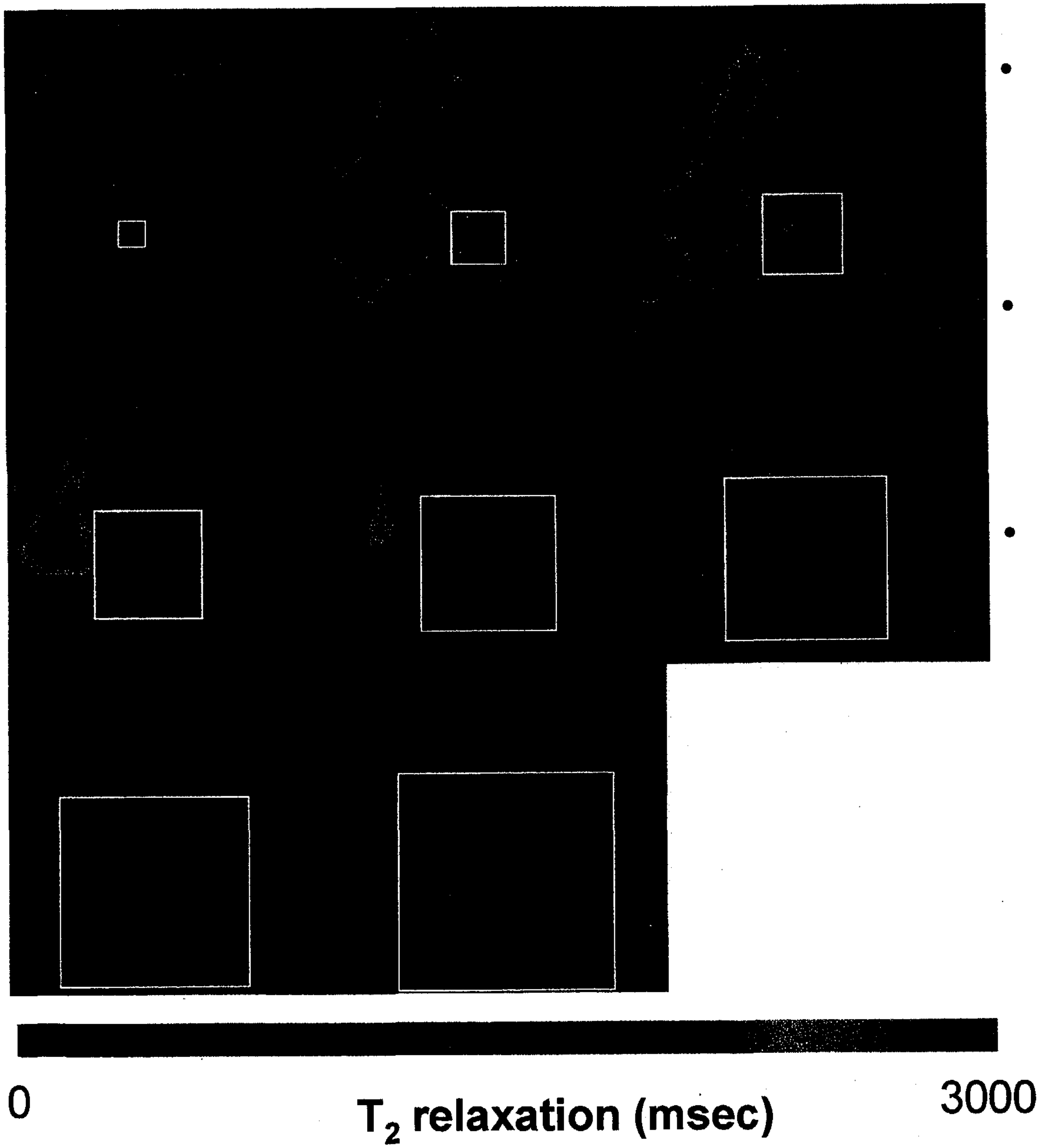

- Computational Technique:
  - Fast Relaxation model
  - Measure Local S/V
  - Box Size ~ $D_{(Brine)}/\rho_{(Brine,Rock)}$
- Low Diffusivity large ρ
  - Measures Local S/V
  - Dependent on local geometry
  - Many measurements needed
- High Diffusivity, small ρ
  - Probes entire volume
  - Measures Global S/V
  - Yields narrow T_2 distribution
  - Narrow distribution results in simple exponential decay

Relaxation Spectra for Two Sandstones

$D = 2.3 \mu m^2/sec$, $T_b = 3000$ msec

NMR Experiment gives 1000msec
Monte Carlo Simulation provides ρ = 15μm/sec,
Surface area overestimated by digitized media

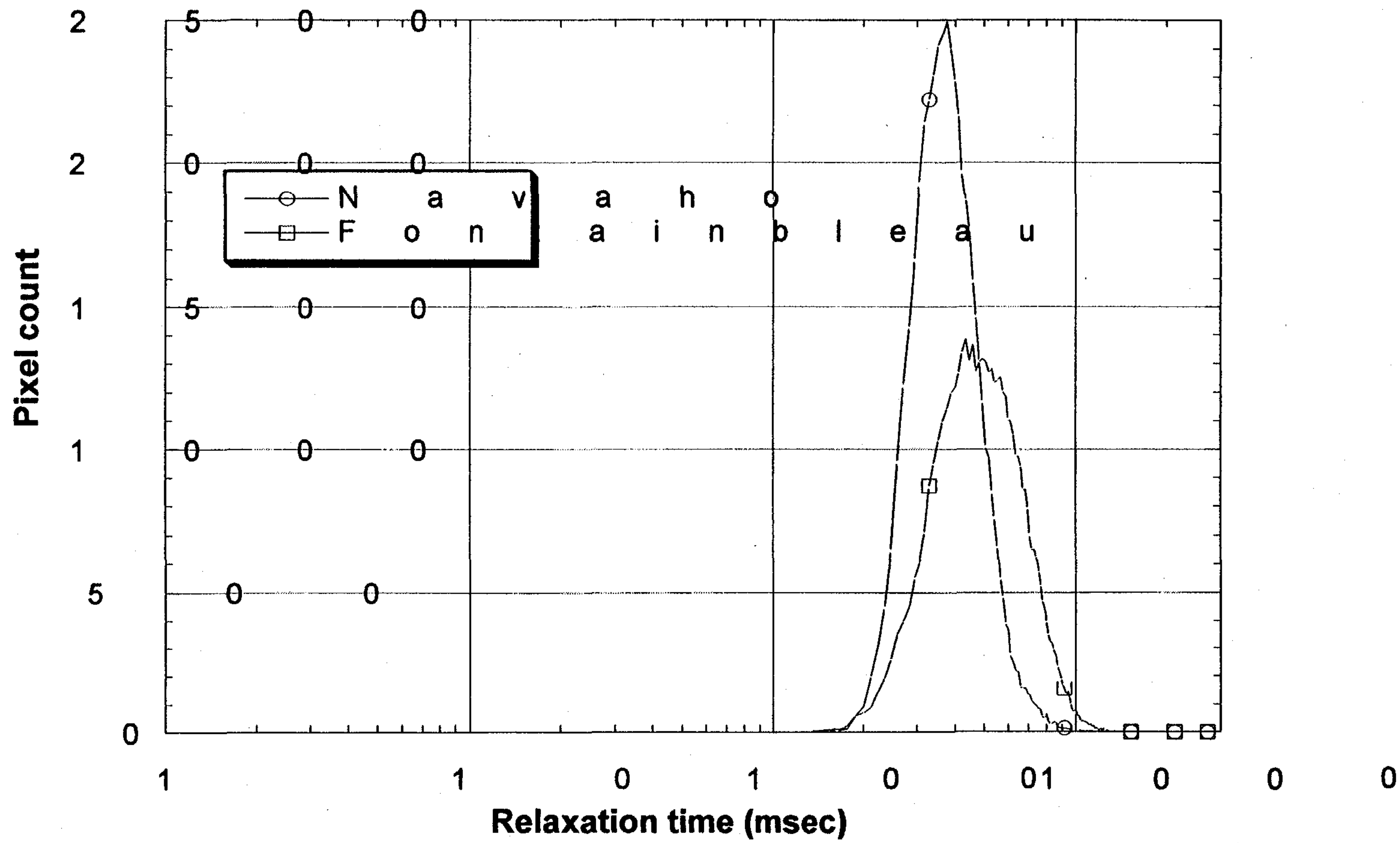

Magnetization Relaxation Spectra from Image Processing

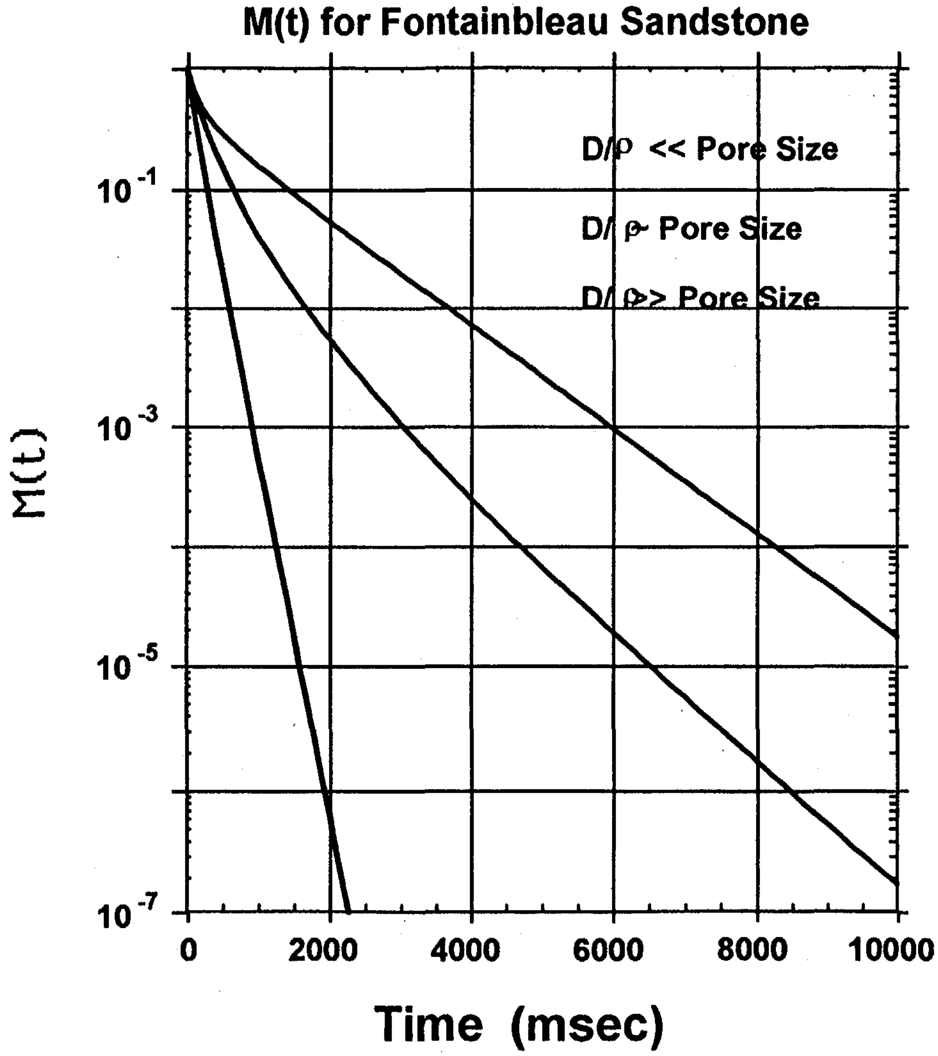

- Computed directly from vsrecord
  - $M(t) = M_i(0) \sum_{n=1}^{N} e^{-\left[\frac{1}{T2_{i(bulk)}} + \sum_{j=1, j \neq i}^{M} \frac{\rho_{ij} S_i}{V_i}\right] t}$
- Box << Pore Size
  - Short T_2 near Pore Wall
  - Bulk T_2 in Large Pores
- Box ~ Pore Size
  - Range of $T_2 < T_b$
- Box >> Pore Size
  - Single Value of T_2 Based on Global S/V

Multi-component Analysis

Brine saturation measured by absorption edge crossing

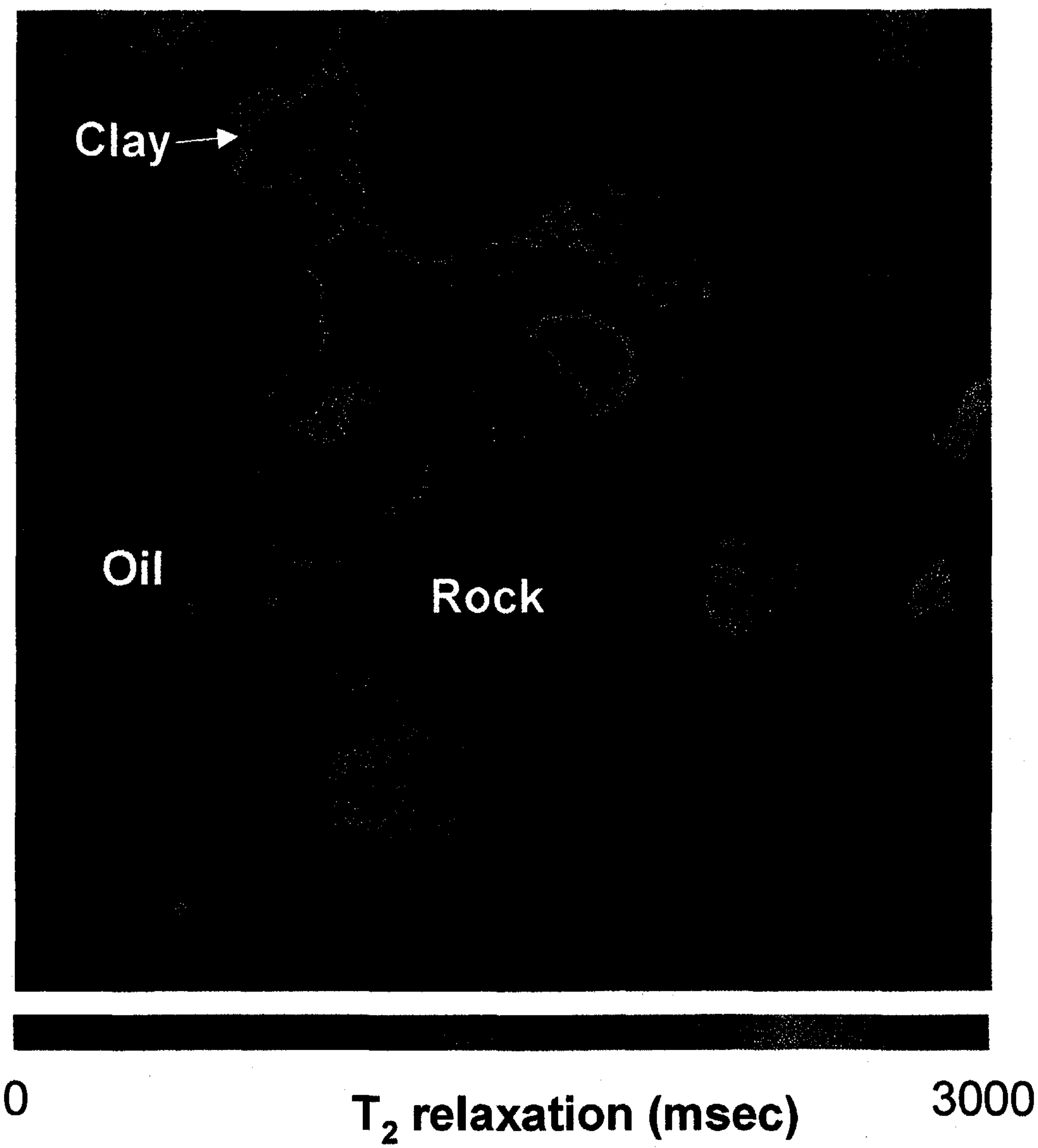

- **Physical parameters**
  - **Scale = 6 µm/pixel**
  - **D = 2.3 µm²/msec (~25°C)**
  - **T_b = 3000 msec (~25°C)**
  - **ρ_{rc} = 15 µm/sec**
  - **ρ_o = 0.3 µm/sec**
- **Fast relaxation on rock and clay surfaces**
- **Slow relaxation at brine-oil interface**
- **Non-contacting brine exhibits bulk relaxation**

T_2 DISTRIBUTION FROM M(t) INVERSION

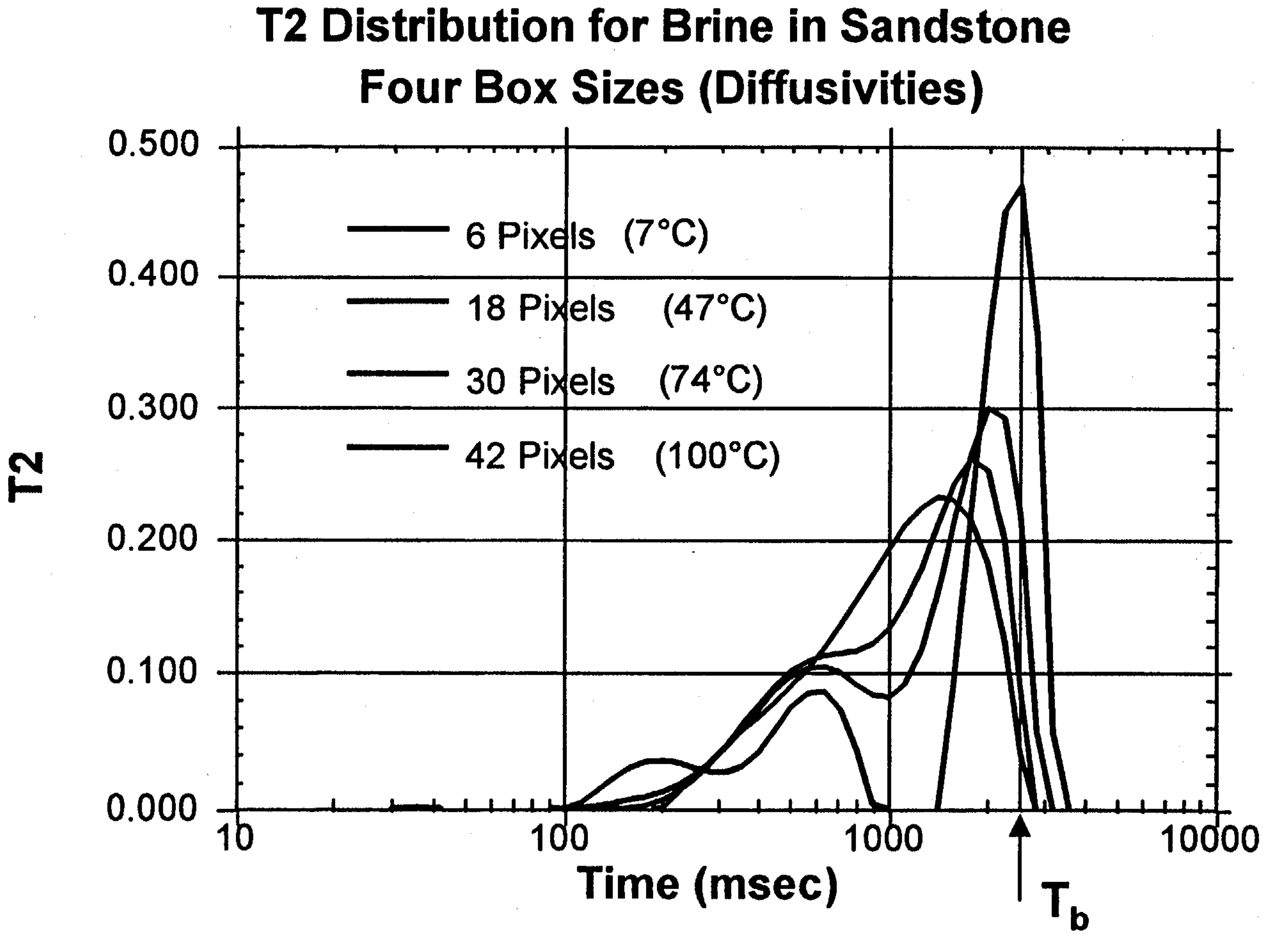

* M. Duran 1996

Part II

Per Spanne
European Synchrotron Radiation Facility (ESRF)

"Computer Microtomography Using X-rays from Third Generation Synchrotron X-ray"

Computed Microtomography Using Third Generation Synchrotron X-ray Sources

Per Spanne

European Synchrotron Radiation Facility

Grenoble, France

- The European Synchrotron Radiation Facility
- Instrumentation
- Phase contrast CMT
- Reconstruction using PVM
- Applications

European Synchrotron Radiation Facility

- Joint user facility for 12 European member countries
- 6 GeV electron storage ring
- 200 mA ring current
- CMT performed on beamline most suitable for detection task - mobile equipment

Some general source characterstics

- 30-200 microns source size
- 35-150 m source to object distance
- For monochromatised beam this results in high spatial coherence
- Interference patterns from samples up to 10-50 microns
- Refraction angles on the order of microrad

Detector systems: Basic components

- Scintillator
- Light optics adapted to required spatial resolution, effective pixelsize >.6 microns
- Mirror at 45 degrees
- ESRF CCD based camera, FRELON
- Camera control by SUN Ultra workstation

Scintillators

- Among several tested $Y_3Al_5O_{12}$:Ce showed best spatial resolution
- 5 microns sensitive layer on 1 mm substrate
- 5 mm diameter disc
- DQE = 0.024 at 14 keV

- Spatial distribution of deposited energy not limiting spatial resolution for YAG
- Pixel size limited at 0.8 microns resulting in spatial resolution of 1.6 microns

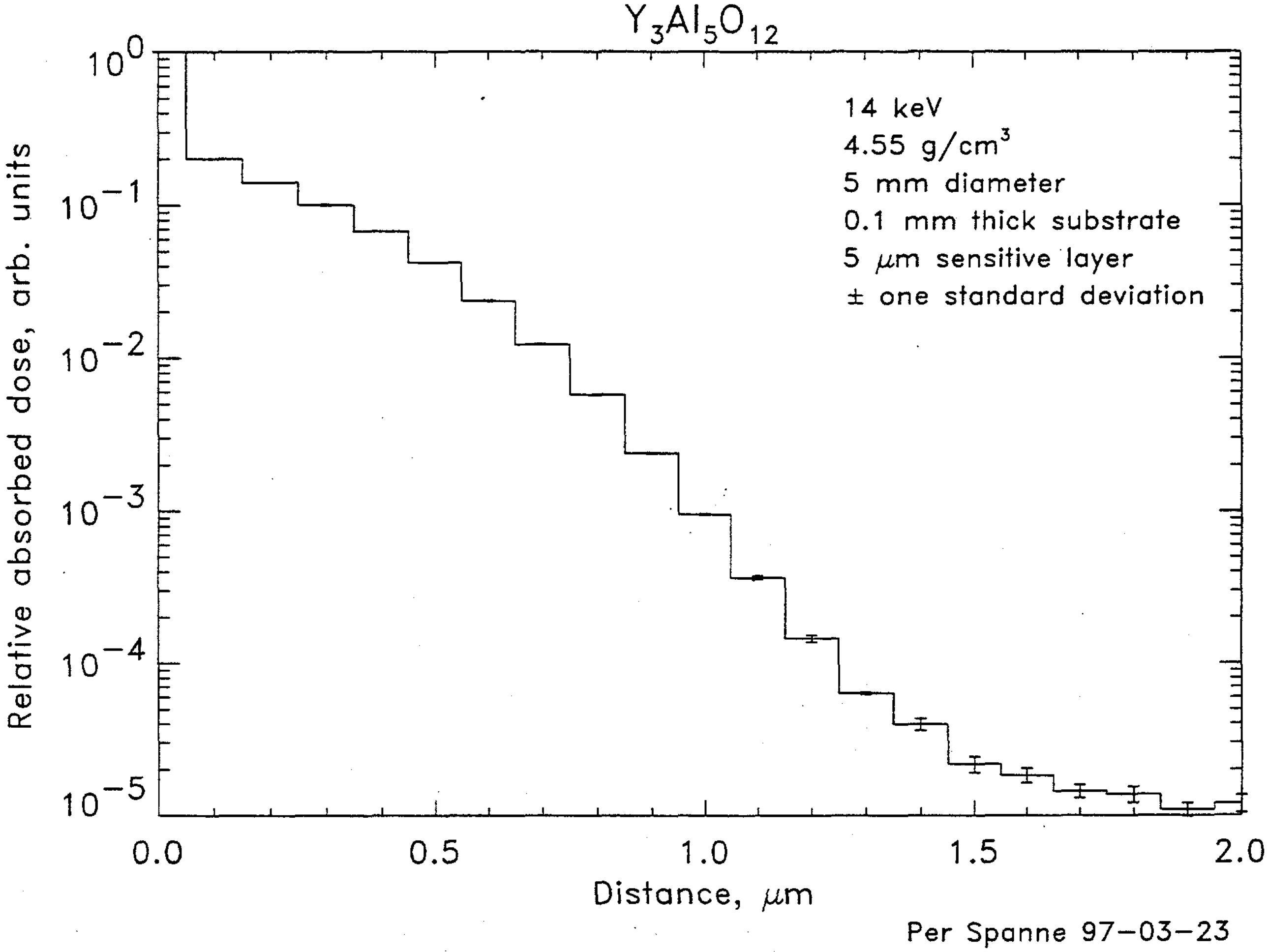
$Y_3Al_5O_{12}$
14 keV
4.55 g/cm³
5 mm diameter
0.1 mm thick substrate
5 μm sensitive layer
± one standard deviation
Relative absorbed dose, arb. units
10^0
10^{-1}
10^{-2}
10^{-3}
10^{-4}
10^{-5}
0.0
0.5
1.0
1.5
2.0
Distance, μm
Per Spanne 97-03-23

Optics for CMT detector

- Intermediate resolution - 5-10 microns. 2 lenses and 45 degree mirror
- High resolution - submicron pixelsize achieved using x20-40 microscope objectives
- Eyepiece to match field of view to size of CCD chip, corrects chromatic abberations

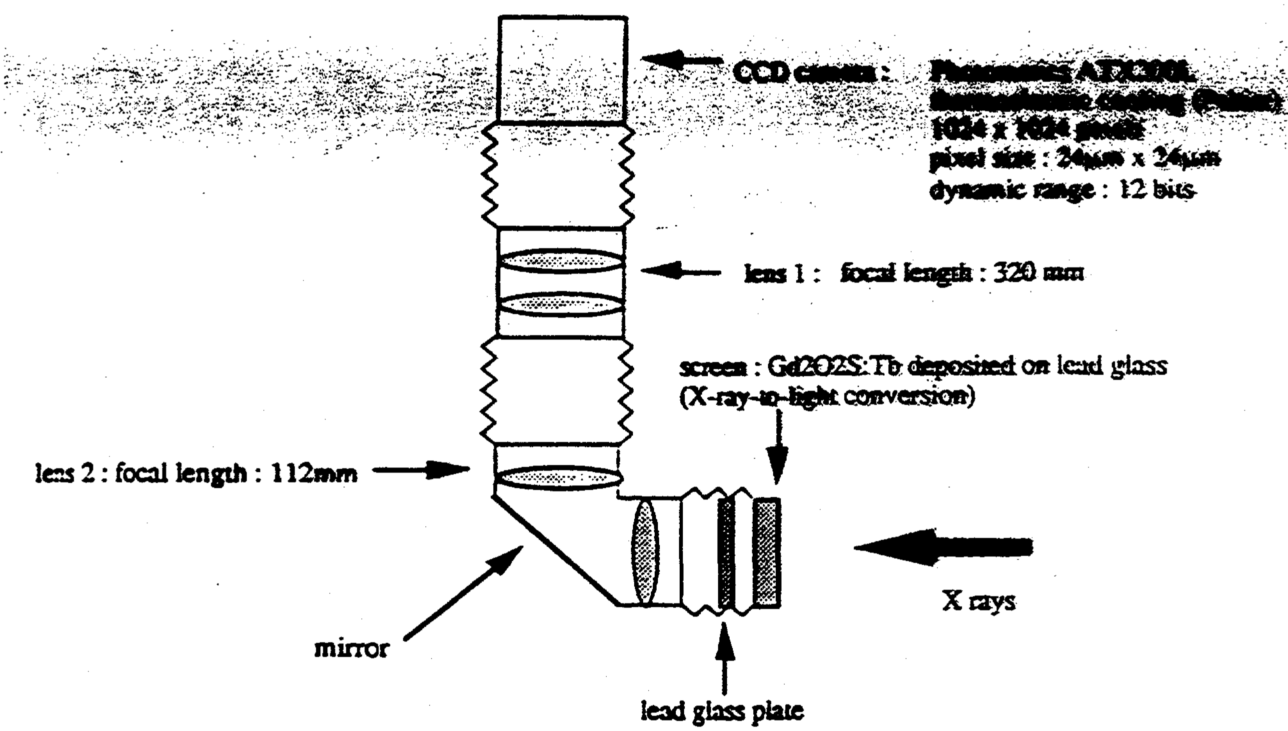

CCD based area detector

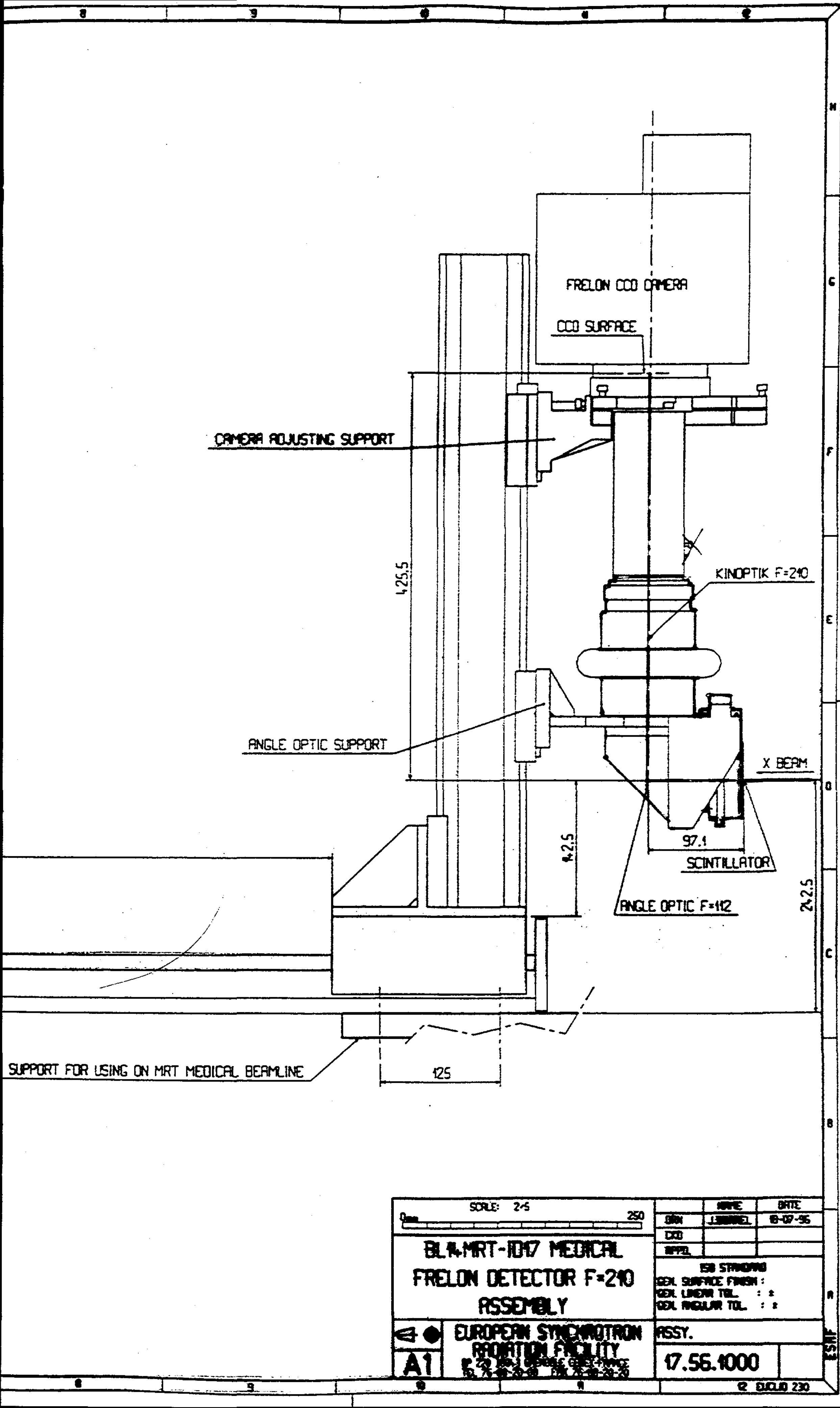
FRELON CCD CAMERA
CCD SURFACE
CAMERA ADJUSTING SUPPORT
425.5
KINOPTIK F=210
ANGLE OPTIC SUPPORT
X BEAM
42.5
97.1
SCINTILLATOR
ANGLE OPTIC F=112
242.5
SUPPORT FOR USING ON MRT MEDICAL BEAMLINE
125
SCALE: 2:5
250
NAME
DATE
DRN
CKD
APPD.
BL14-MRT-ID17 MEDICAL
FRELON DETECTOR F=210
ASSEMBLY
ISO STANDARD
GEN. SURFACE FINISH :
GEN. LINEAR TOL. : ±
GEN. ANGULAR TOL. : ±
EUROPEAN SYNCHROTRON
RADIATION FACILITY
A1
ASSY.
17.56.1000
ESRF
EUCLID 230

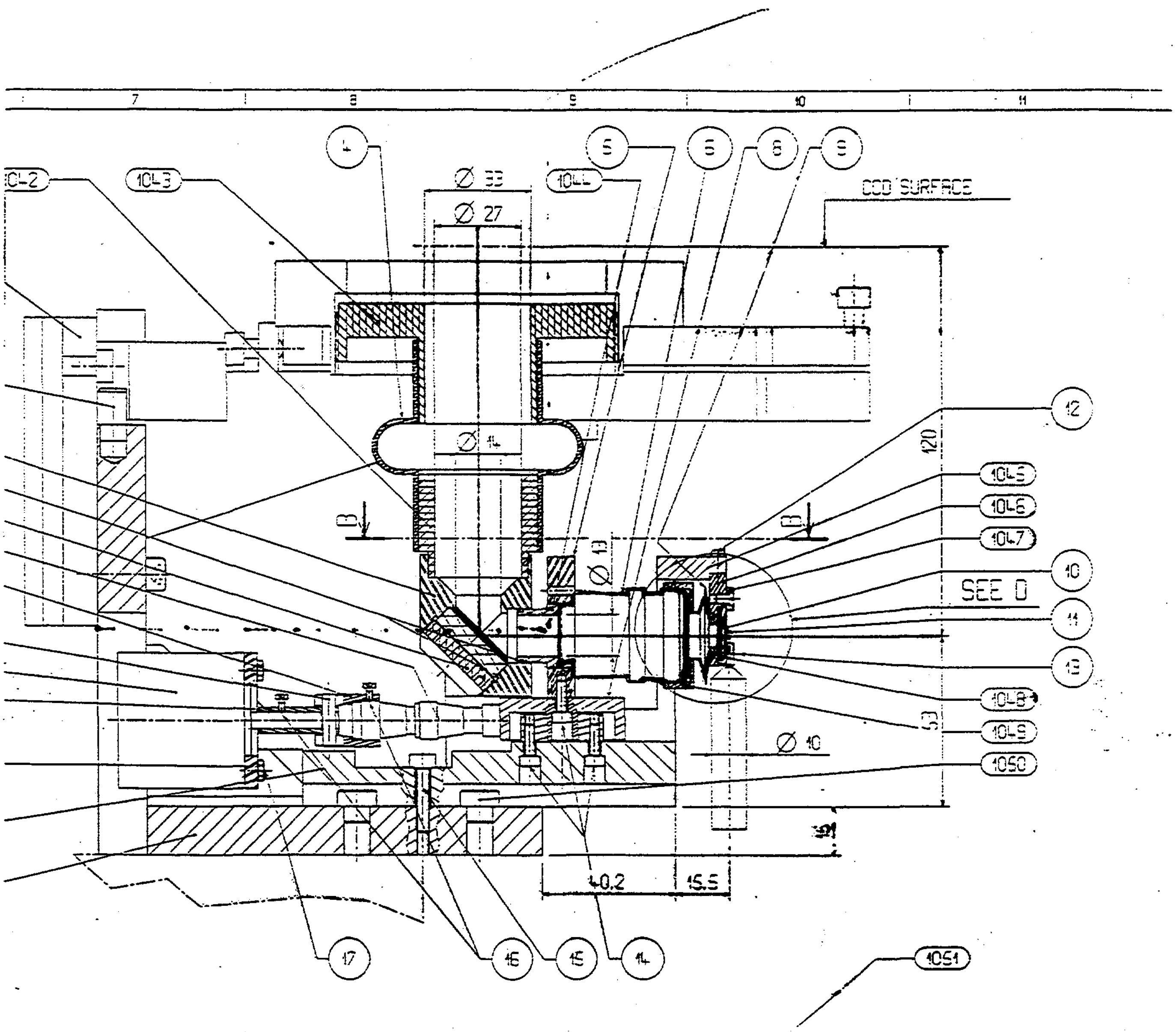

7
8
9
10
11
4
5
6
8
9
1043
1044
Ø 33
Ø 27
Ø 14
Ø 13
Ø 10
120
12
1045
1046
1047
10
SEE D
11
13
1048
1049
1050
40.2
15.5
17
16
15
14
1051

Reconstruction today:

SNARK filtered backprojection

Parallel processing using PVM

Now 16 computers

Average of 36 s per 1024^2 slice

10^9 voxels in 10 h

SNARK Fourier techniques 3 times faster

Future improvements :

Implementation and parallellisation of the linogram method will increase speed by a factor of 8 as compared to filtered backprojection with equal image quality

Alternative algorithm can perhaps give another factor of 2

Phase contrast CMT techniques

- Analyser crystal after sample
- Bonse-Hart interferometer
- Backpropagation
- In-line holography setup

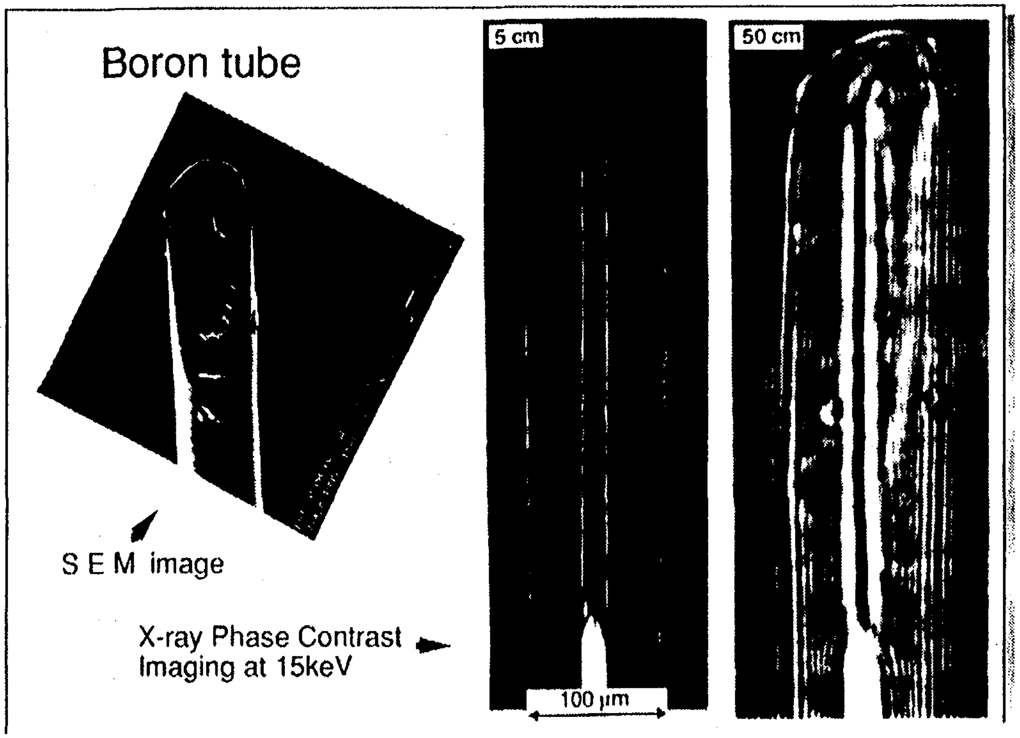

Fig.3: Image in scanning electron microscope and experimentally obtained X-ray phase contrast images of the boron 100 μm fibre with 15 μm Tungsten core recorded at 15 keV at two distances (5 and 50 cm).

55
fine
dete
The
pha
sho
cont

A. Snigirev et. al

C. Raven, A. Snigirev, I. Snigireva, A. Suvorov, P. Spanne

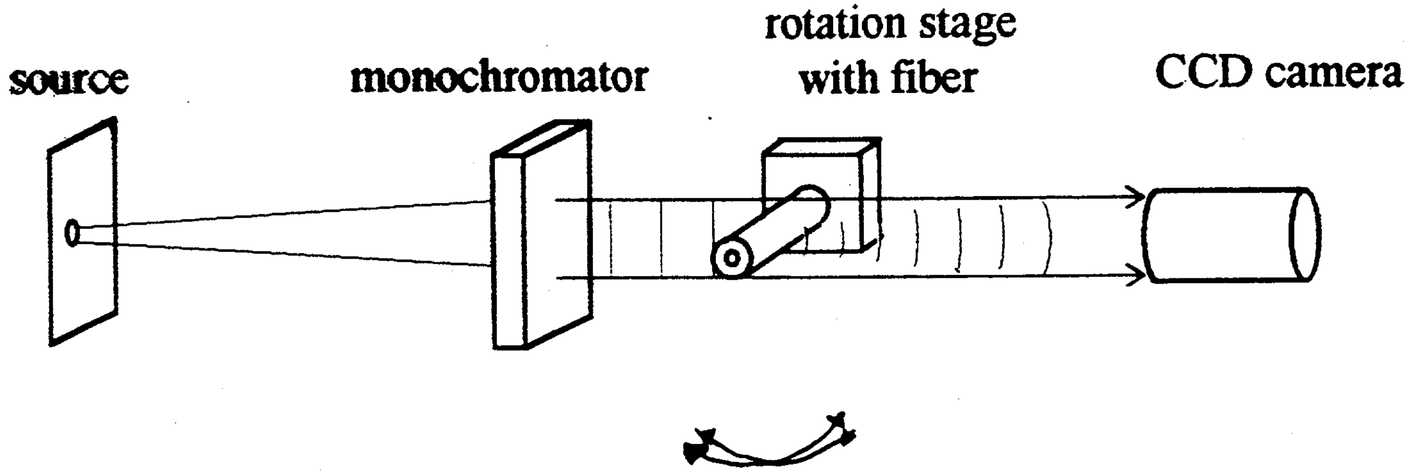

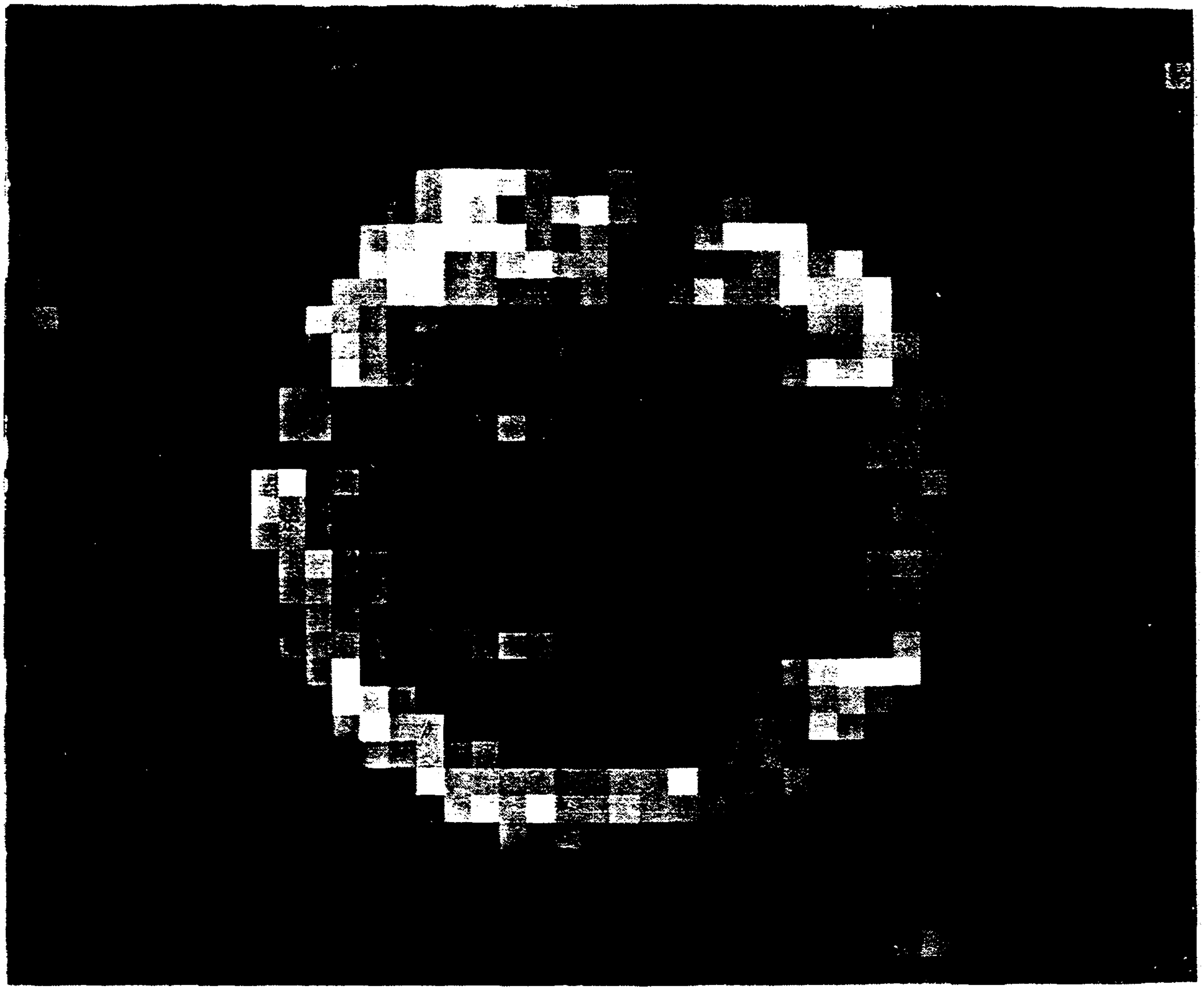

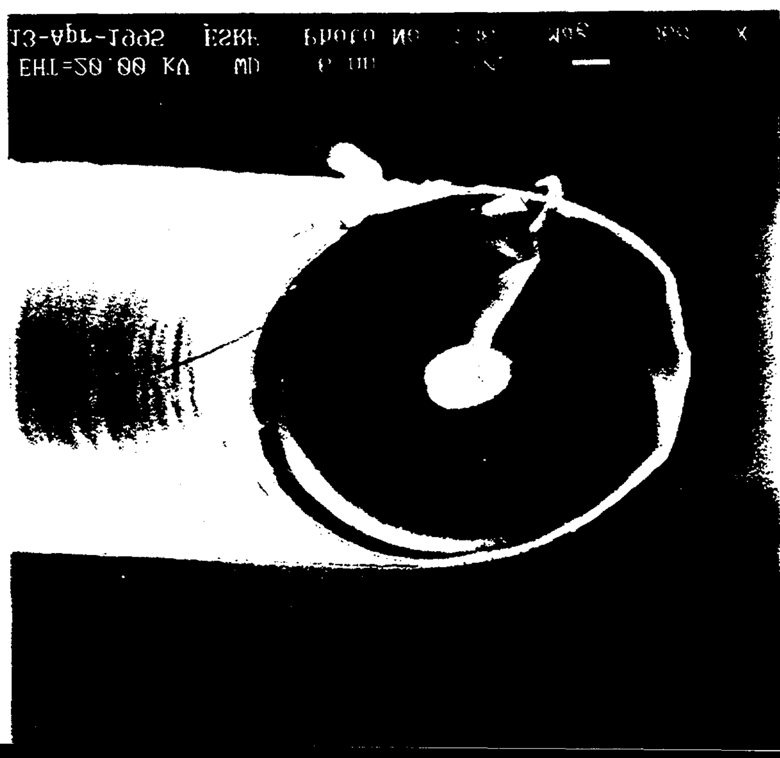

Outline mode CMT advantages

- Monochromator only optical element needed
- Absorption CT algorithms can be used
- Space for sample not a constraint
- Sample can be keep under normal temperature and pressure

Outline CMT mode advantages

- Use of high photon energy makes possible visualization of low Z details in high Z materials

Outline mode CMT disadvantages

- Only borders between regions with different refractive indices imaged - edge enhancement
- Qualitative

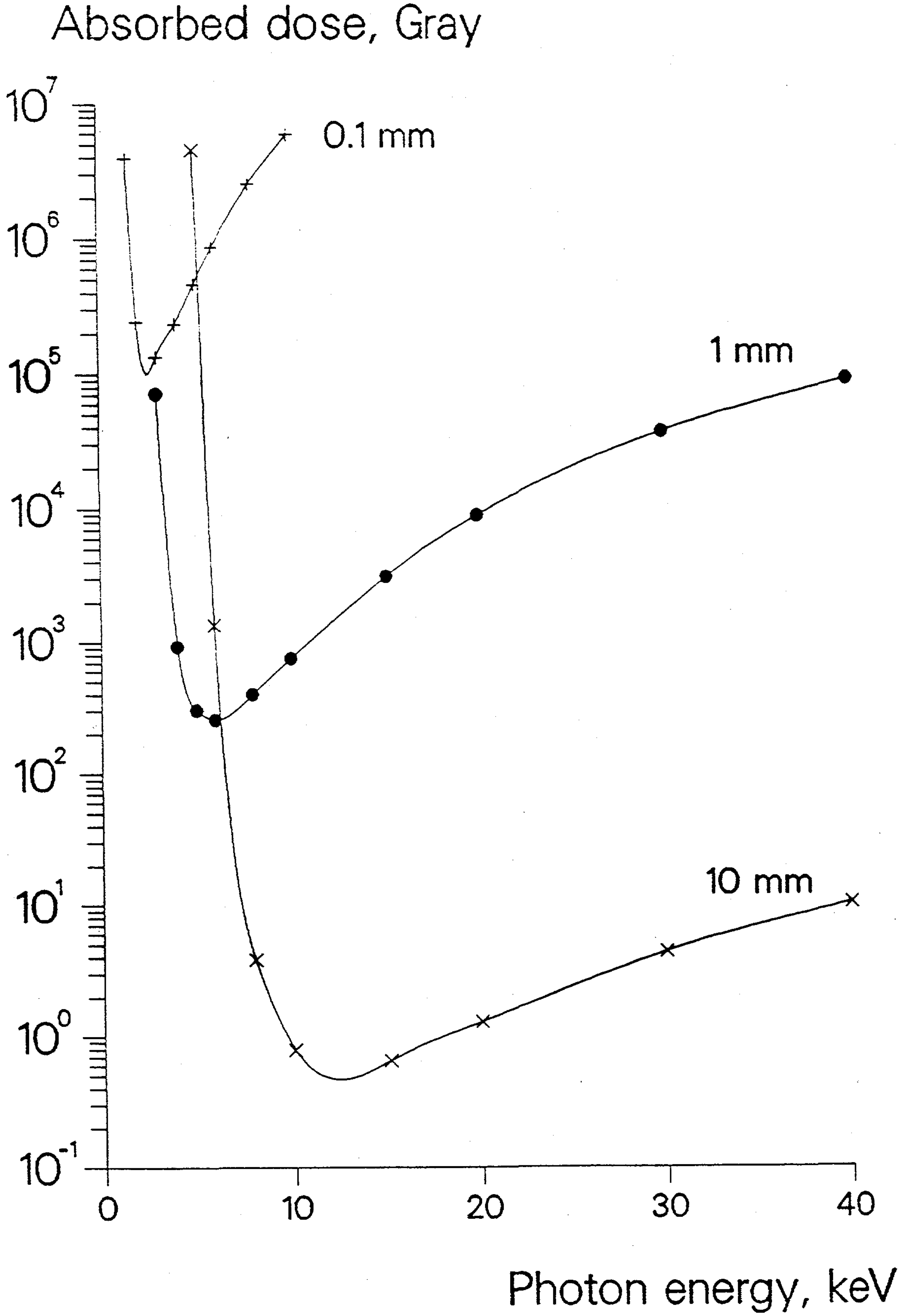

Absorbed dose, Gray
10^7
10^6
10^5
10^4
10^3
10^2
10^1
10^0
10^{-1}
0.1 mm
1 mm
10 mm
0
10
20
30
40
Photon energy, keV

Acknowledgements

- Imaging group:
- U. Kleuker
- M. Pateyron-Salome
- F. Peyrin
- Micro-FID group:
- C. Raven
- A. Snigirev
- I. Snigireva
- Detector group:
- J.P. Moy
- A. Koch
-
- Topography group:
- J. Baruchel
- P. Cloetens

Part III

Chris Jacobsen
SUNY Stony Brook

"Approaches to Soft X-ray Nanotomography"

Stony Brook ALS/LBNL APS/ANL X-1A NCSU NSLS/BNL Lucent Bell Labs

X-ray microscopy at Stony Brook

State University of New York at STONY BROOK Department of Physics and Astronomy

- State University of New York at Stony Brook:
  - Faculty: Chris Jacobsen and Janos Kirz
  - Technical support: Sue Wirick
  - Postdocs: Jörg Maser
  - Graduate students: Michael Feser, Jianwe Miao, Ulrich Neuhäusler, Angelika Osanna, Aaron Stein, Stefan Vogt, Steve Wang, Barry Winn

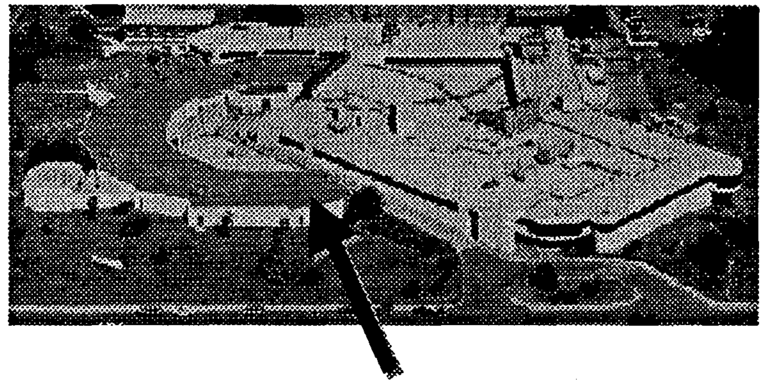

X-1A beamline, National Synchrotron Light Source, Brookhaven National Laboratory

Support from:
•Office of Health and Environmental Research, Department of Energy
•Electrical and Communications Division and Division of Biological Infrastructure, National Science Foundation

Birth of cell biology electron microscopy

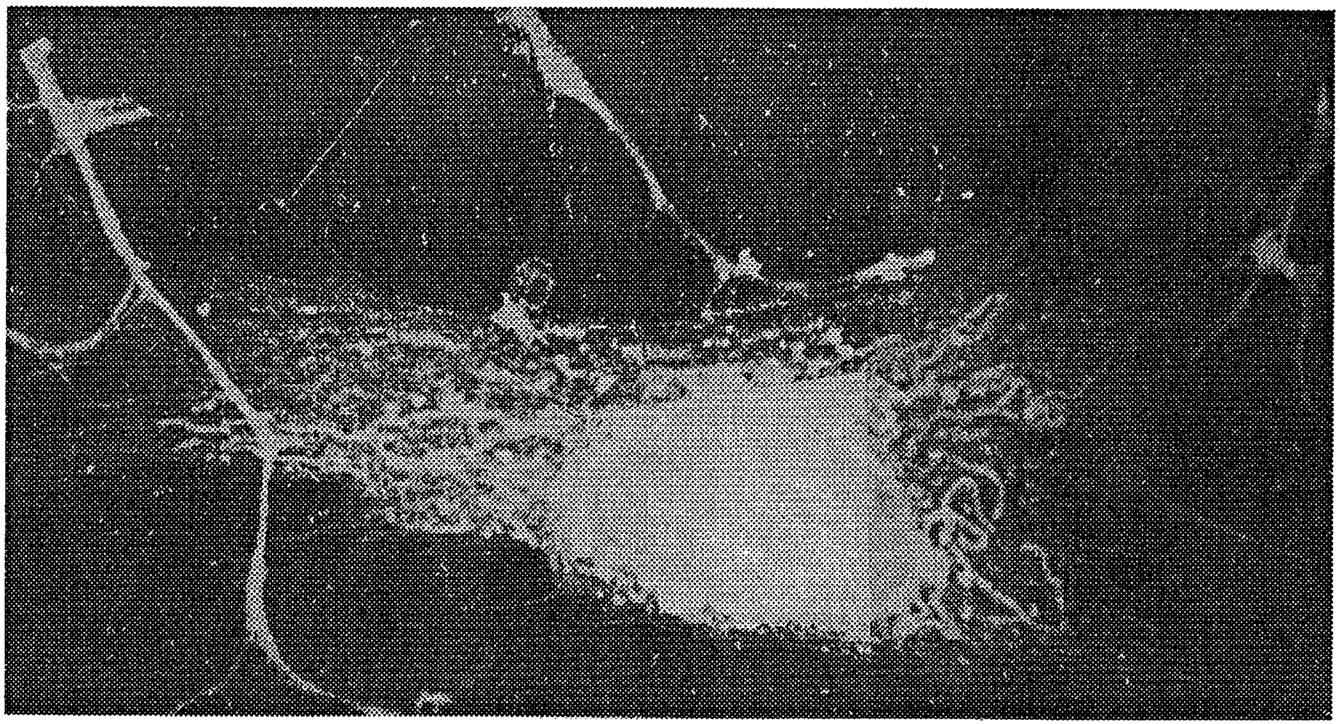

K. Porter, A. Claude, and E. Fullam, *J. Exp. Med.* **81**, 233-246 (1945), as reproduced on cover of *Mol. Bio. Cell* **8**(4), April 1997.

Soft x-rays for imaging organic specimens

- Small λ: better resolution than optical microscopes. Confocal: ~200 nm. Near-field: ~20 nm but only within 50 nm of tip.
- Energy resolution: <0.1 eV
- Well-matched to single cell dimensions
- Good intrinsic contrast (especially for hydrated samples)

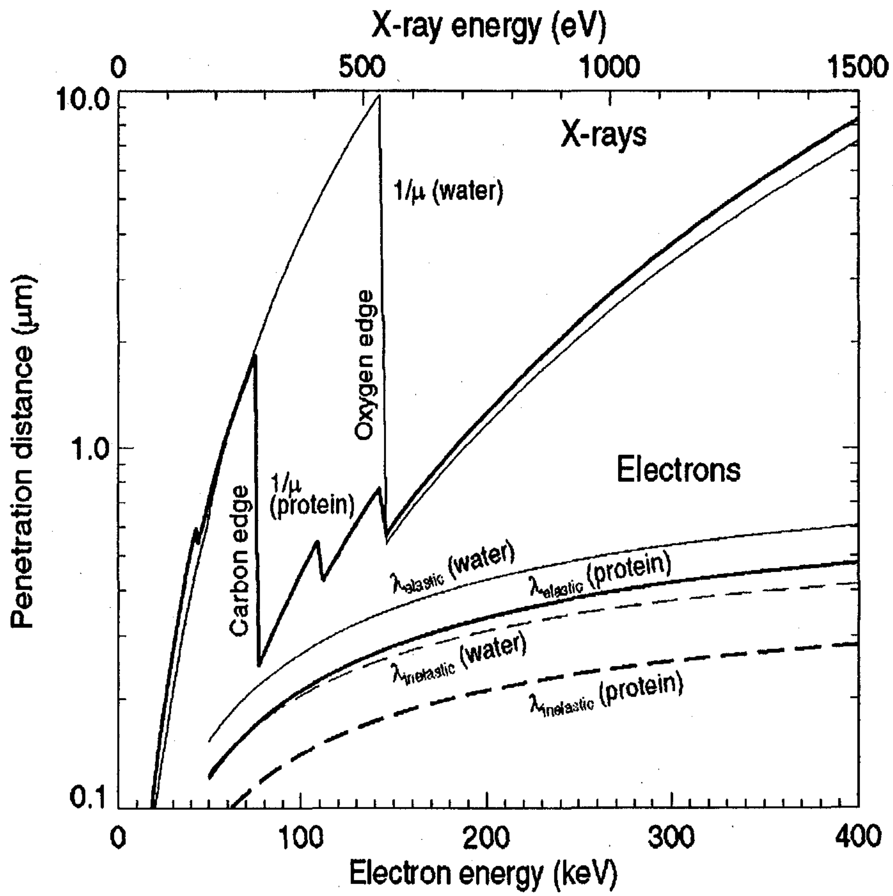

Chris Jacobsen

Soft x ray optical interactions

- At ~0.2-2 keV:

absorption

>> coherent scattering

>> incoherent scattering

- **No multiple scattering** with thick specimens

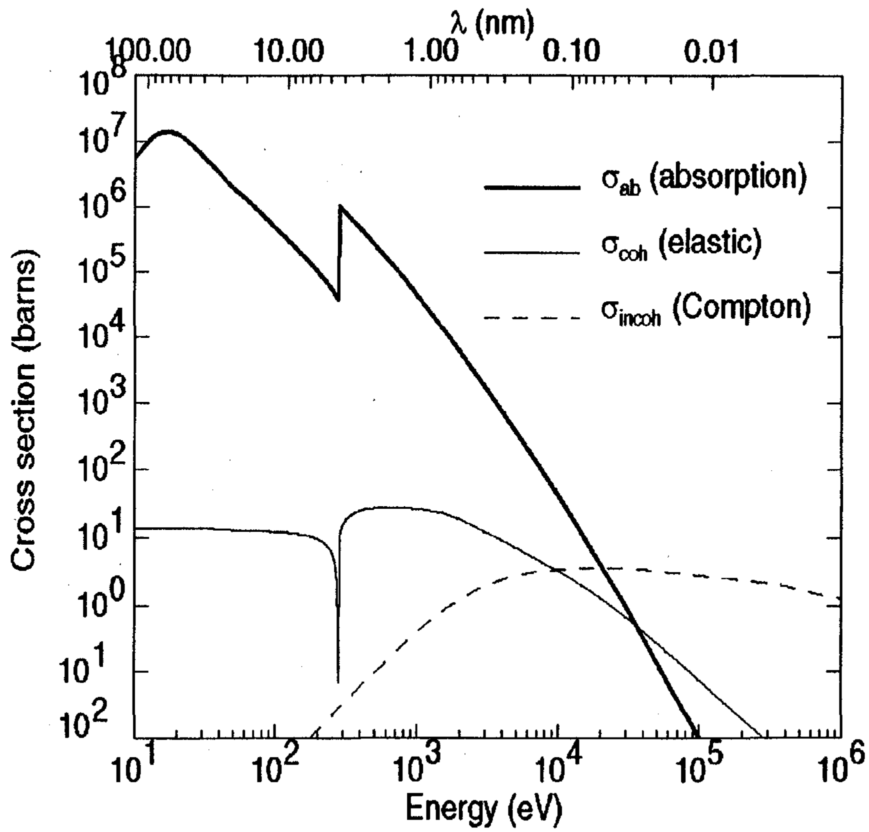

Carbon

Chris Jacobsen

Stony Brook ALS/LBNL APS/ANL X-1A NCSU NSLS/BNL Lucent Bell Labs

Electron categories

State University of New York at STONY BROOK Department of Physics and Astronomy

- For 200 keV electrons in ice
- Phase contrast: want mixing of single scattered and unscattered electrons

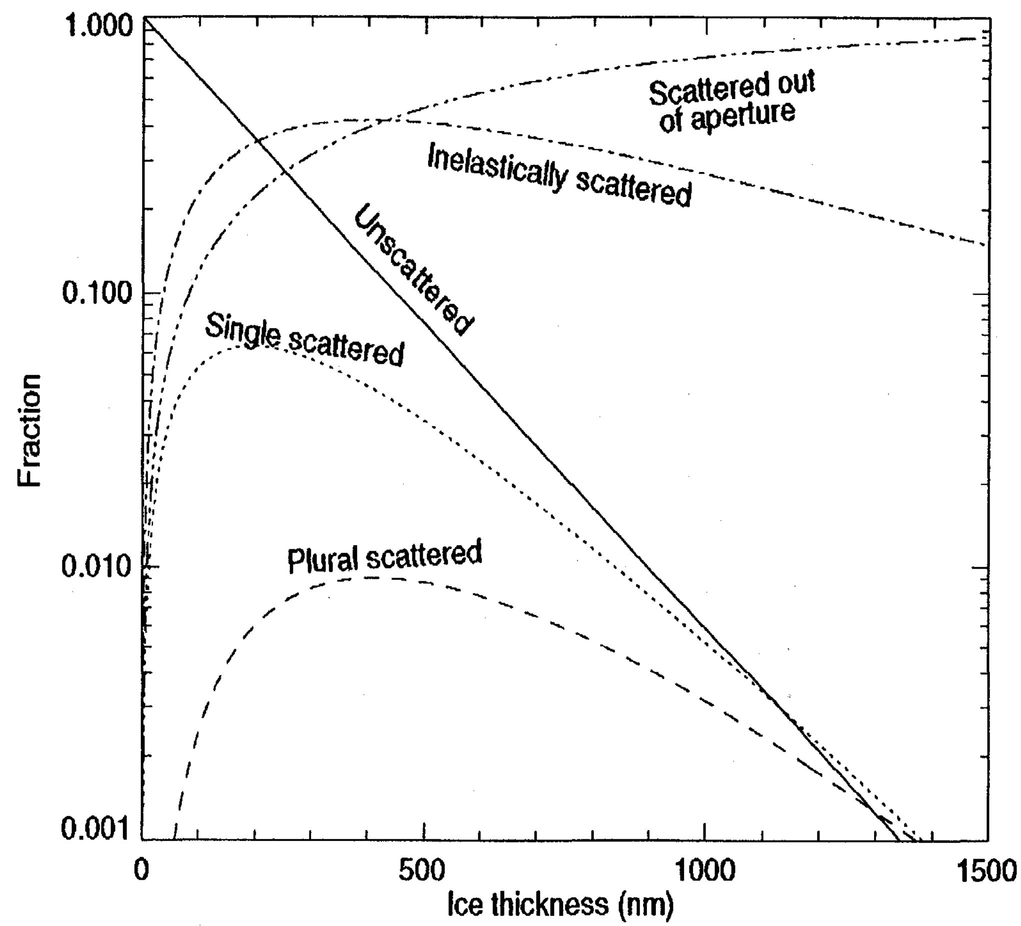

Chris Jacobsen

Stony Brook ALS/LBNL APS/ANL X-1A NCSU NSLS/BNL Lucent Bell Labs

State University of New York at STONY BROOK Department of Physics and Astronomy

Dose comparison with cryo electron microscopy

- Electrons: ~100 nm thin sections, virus suspensions, membrane proteins
- X rays: up to several μm thick, spectromicroscopy

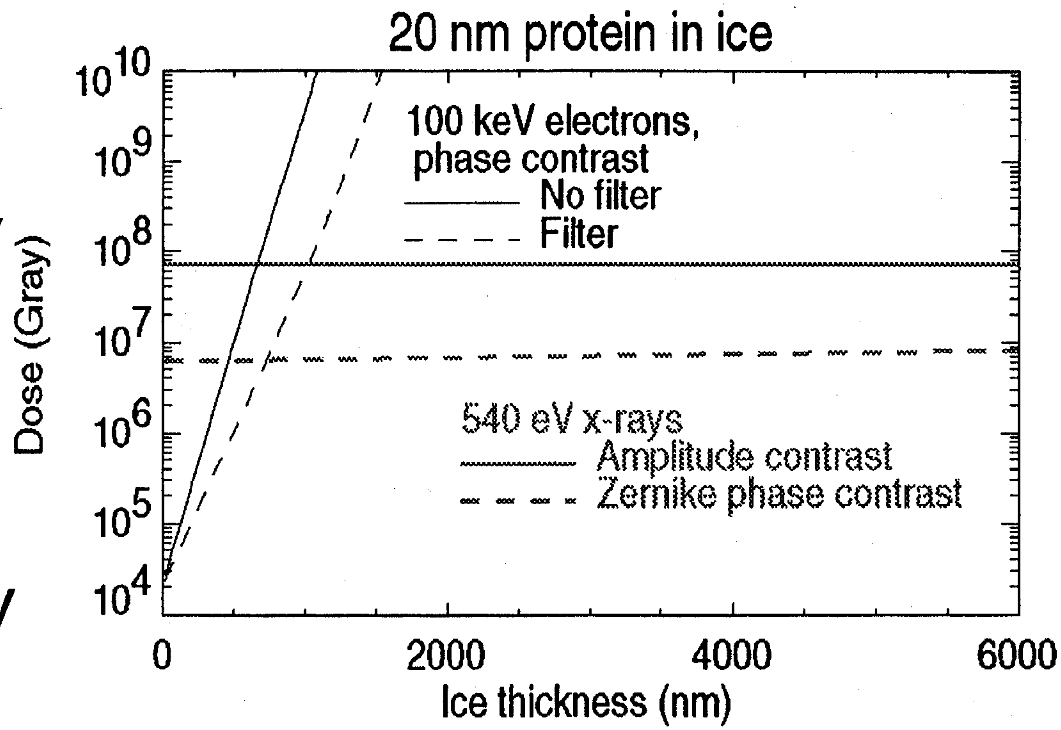

Chris Jacobsen

Stony Brook ALS/LBNL APS/ANL X-1A NCSU NSLS/BNL Lucent Bell Labs

How many x-ray photons are needed?

State University of New York at STONY BROOK
Department of Physics and Astronomy

- Require statistical significance of signal difference between feature-present and feature-absent pixels.
- For 5:1 SNR with contrast *C*, photons per pixel needed: $N \geq \frac{25}{C^2}$

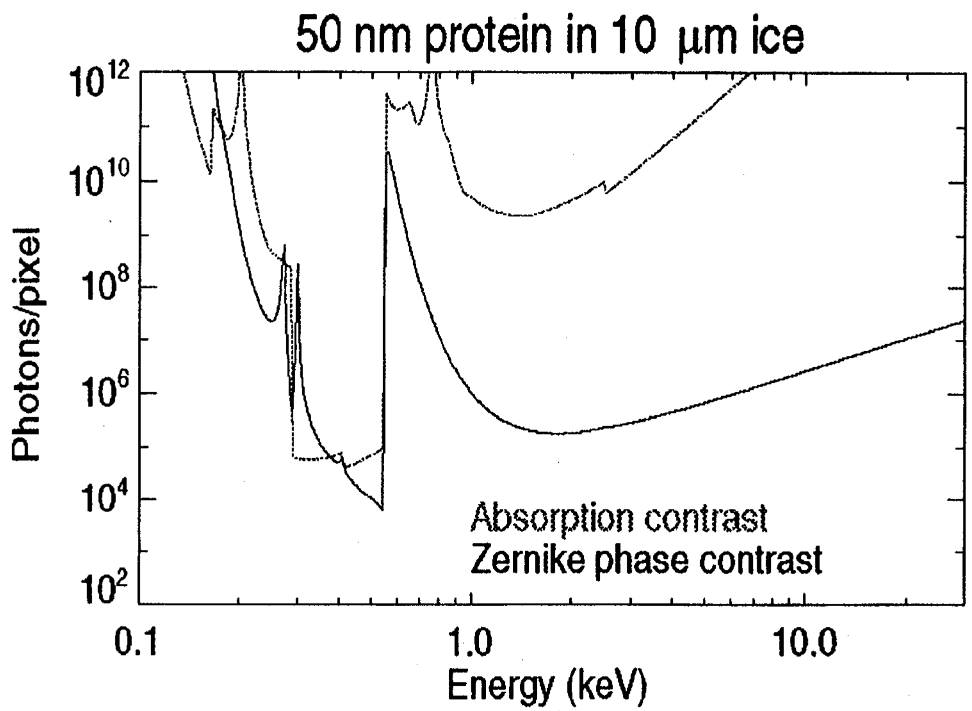

Chris Jacobsen

Stony Brook ALS/LBNL APS/ANL X-1A NCSU NSLS/BNL Lucent Bell Labs

NSLS X-1: near 3rd generation

State University of New York at STONY BROOK Department of Physics and Astronomy

- For soft x rays, NSLS X-1 is nearly a third generation source

NSLS soft x-ray undulator brightness

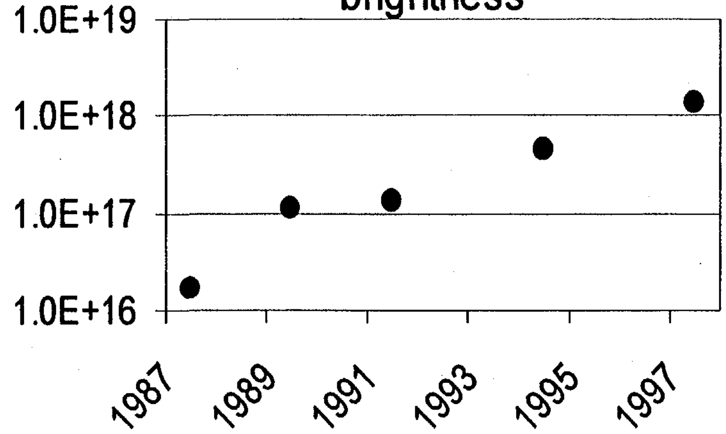

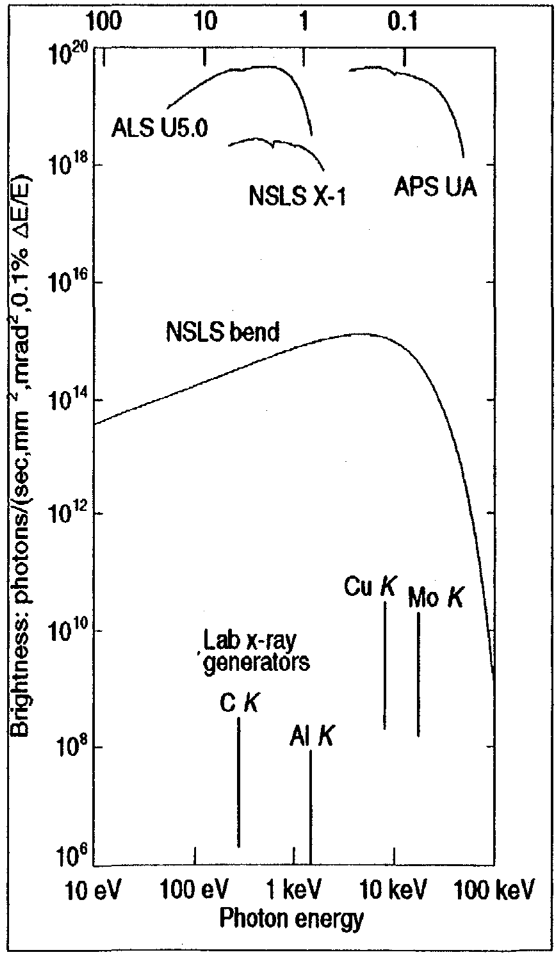

Stony Brook ALS/LBNL APS/ANL X-1A NCSU NSLS/BNL Lucent Bell Labs

NSLS X-1 undulator

State University of New York at STONY BROOK Department of Physics and Astronomy

- Brightness within ~10× 3rd generation sources
- Horizontal emittance gives broad harmonics: take spectra without scanning undulator gap

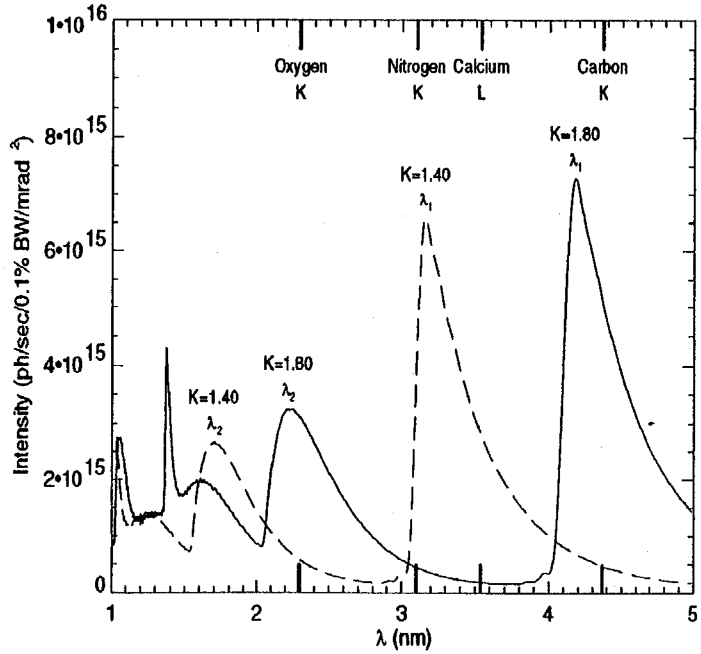

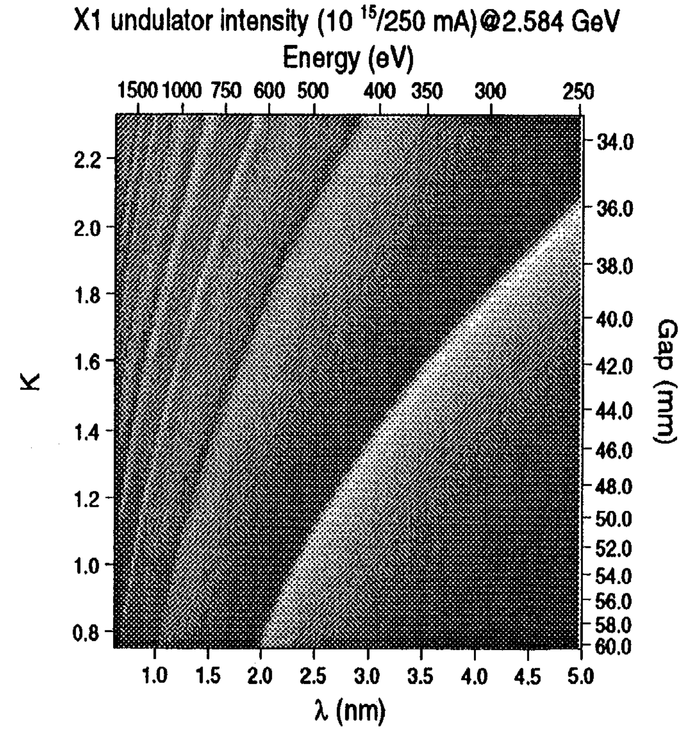

Chris Jacobsen

Sharing multiple modes

- Scanning microscopes require coherent illumination to get maximum resolution
- Phase space of a mode is λ. X-1 undulator puts out ~50 modes in horizontal direction
- Using one mode near the peak of the horizontal distribution still lets lots of incoherent modes get by (X-1B)

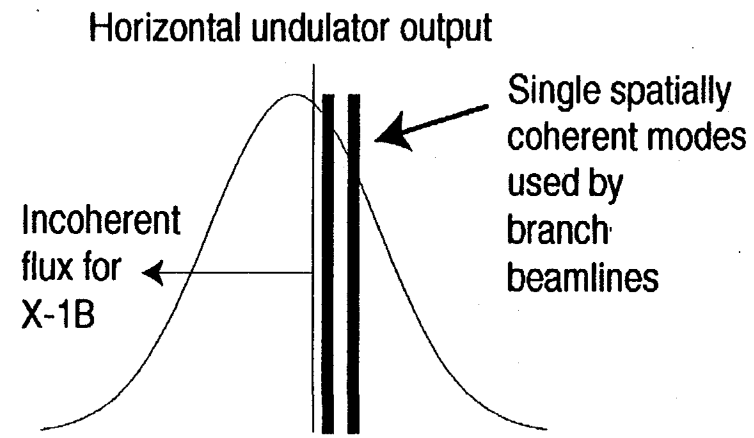

Stony Brook ALS/LBNL APS/ANL X-1A NCSU NSLS/BNL Lucent Bell Labs

The X-1A beamline

State University of New York at STONY BROOK
Department of Physics and Astronomy

- Beamline upgrade: July 1996 - February 1997
- Separate monochromators for two end stations
- Higher spectral resolution for spectromicroscopy: up to $\frac{E}{\Delta E} \approx 5000$
- Better transport of coherent beam

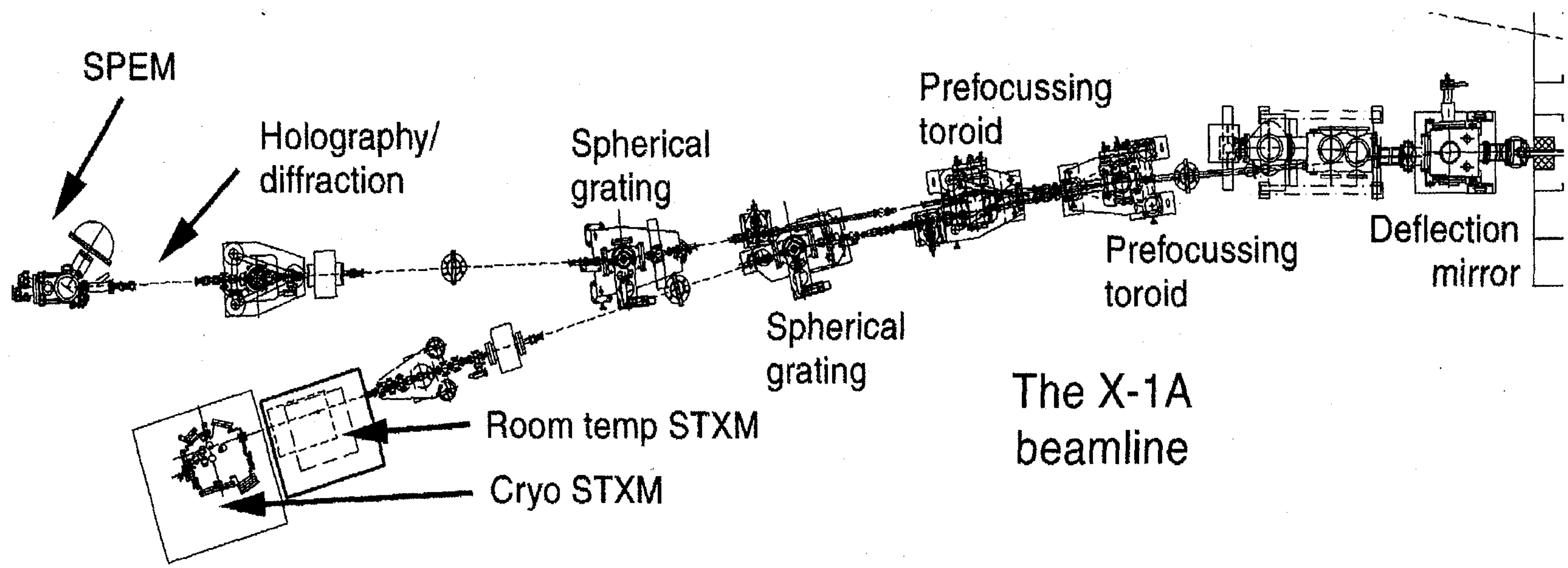

The X-1A beamline

Chris Jacobsen

Specimen heating: timescales

There are two choices:

1. Image so quickly that one has all the data before radiation damage and thermal effects have altered the specimen
2. Image slowly enough for heat conduction to work, and make the specimen as resistant as possible to radiation damage

Specimen heating: how fast is fast?

- 10^6 Gray=10^6 J/kg=4×10^6 cal/g is needed for high resolution imaging: would vaporize sample!
- J. C. Solem, *J. Opt. Soc. Am. B* **3**, 1551 (1986), and R. London *et al.*, *Proc. SPIE* **1741**, 333 (1992): hydrodynamic blurring will become significant at the 10 nm level for timescales longer than around a nanosecond

Stony Brook ALS/LBNL APS/ANL X-1A NCSU NSLS/BNL Lucent Bell Labs

Specimen heating: how slow is slow?

State University of New York at STONY BROOK Department of Physics and Astronomy

- Temperature rise with heated radius r_1 and reservoir radius r_2:

$$+2\ln\frac{r_1}{r_2}$$

- Heat rise is lower with point illumination than with full field illumination

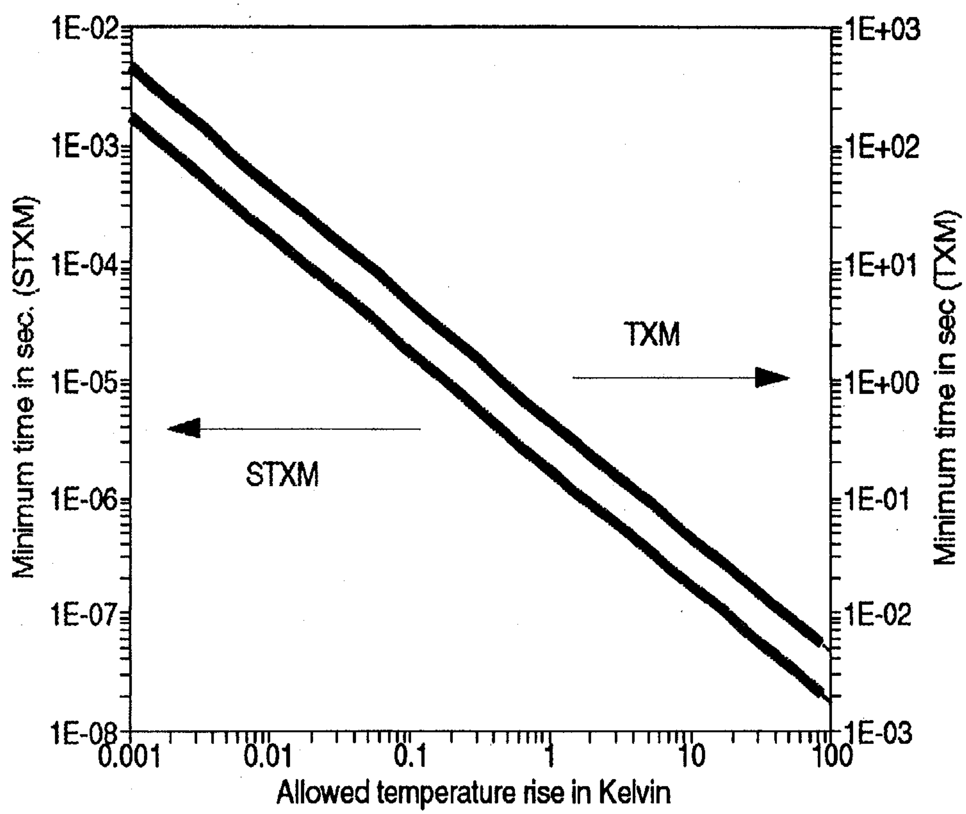

Chris Jacobsen

Stony Brook ALS/LBNL APS/ANL X-1A NCSU NSLS/BNL Lucent Bell Labs

How to focus x rays?

State University of New York at STONY BROOK Department of Physics and Astronomy

- *Grazing incidence* critical angle for mirror reflection:

$$\cos\theta_c = 1-\delta \text{ or } \theta_c \approx \sqrt{2\delta}$$

- Multilayer mirrors: work well at approx. $\lambda \geq 10$ nm
- Refraction: only for high energy x rays where $\delta >> \beta$ (Fresnel lenses, Snigirev lens). MTF rolloff from absorption, especially at lower energies...
- Diffraction: requires small grating period (e.g., electron beam lithography)

Fresnel zone plates

- Diffractive optics: radially varied grating spacing
- Largest diffraction angle is given by outermost (finest) zone width δ_{r_N} as
  $$= \lambda / 2\delta_{r_N}$$
- Rayleigh resolution is then
  $$_t = 0.61\lambda / \theta = 1.22\delta_{r_N}$$
- Zones must be positioned to ~1/3 width over diameter (10 nm in 100 μm, or 1:10^4)

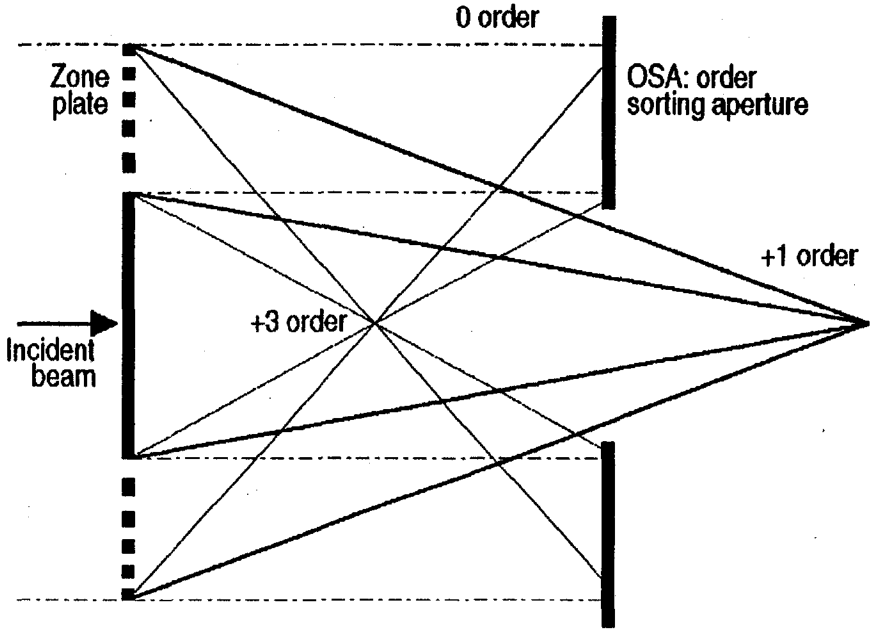

Central stop and order sorting aperture (OSA) to isolate first order focus

Chris Jacobsen

Fresnel zone plates for soft x-ray microscopy

- Stony Brook: Steve Spector (now at Bell Labs), Aaron Stein, and Chris Jacobsen
- Lucent Technologies Bell Labs: Don Tennant

Lucent Technologies
Bell Labs Innovations

- Technology driver for finest structures, plus tie-in to EUV and Scalpel lithography
- Use of commercial machine: JEOL JBX-6000FS
  - 500 pA into 7 nm spot
  - Can stitch 80 μm fields at 5-10 nm placement (have done 160 μm fields)
  - Rewrote software for improved writing of arcs (zone plate zones)

Stony Brook ALS/LBNL APS/ANL X-1A NCSU NSLS/BNL Lucent Bell Labs

JEOL JBX-6000FS

State University of New York at STONY BROOK Department of Physics and Astronomy

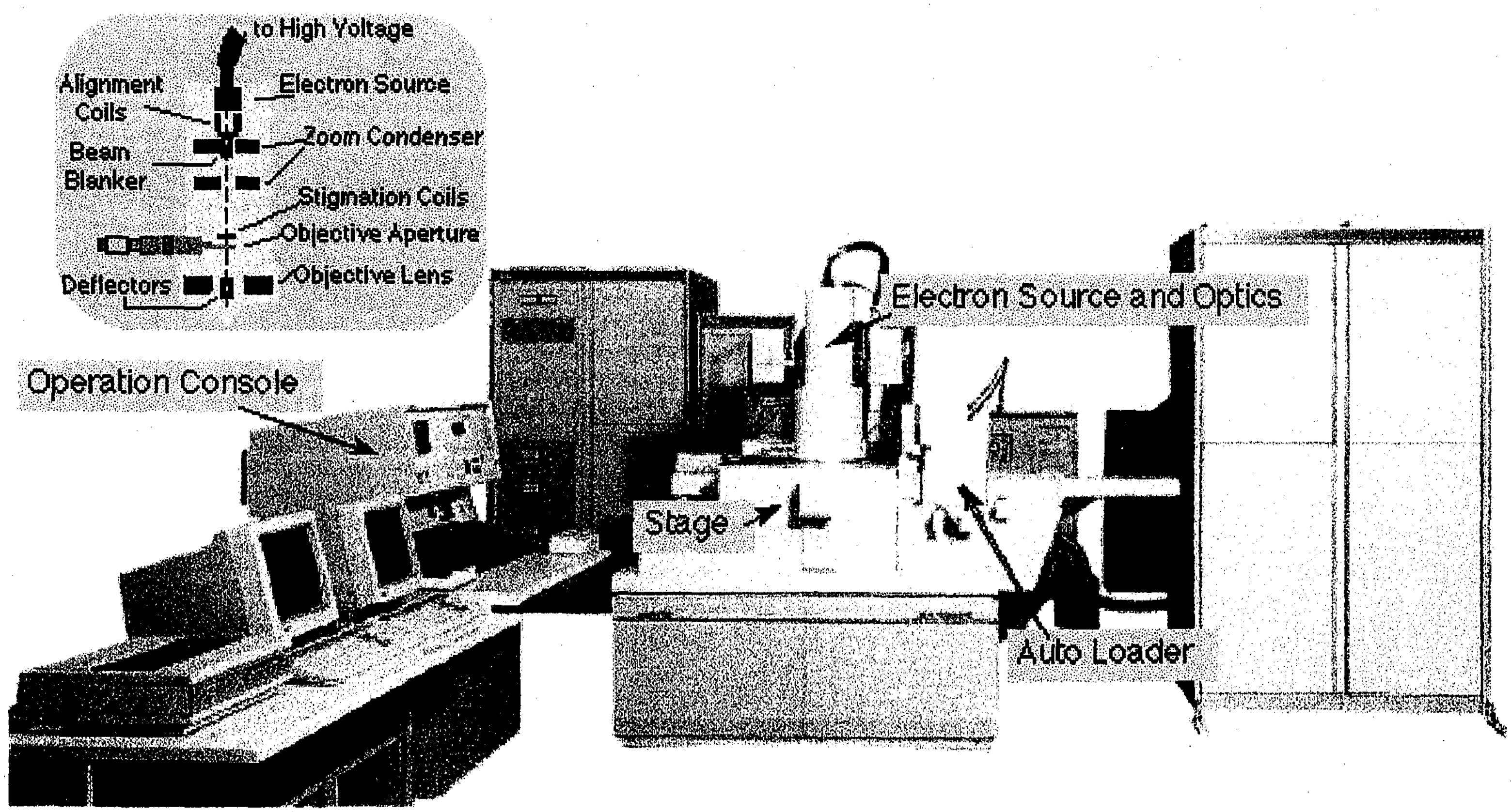

Chris Jacobsen

Stony Brook
ALS/LBNL
APS/ANL
X-1A
NCSU
NSLS/BNL
Lucent Bell Labs

Germanium zone plates

State University of New York at STONY BROOK
Department of Physics and Astronomy

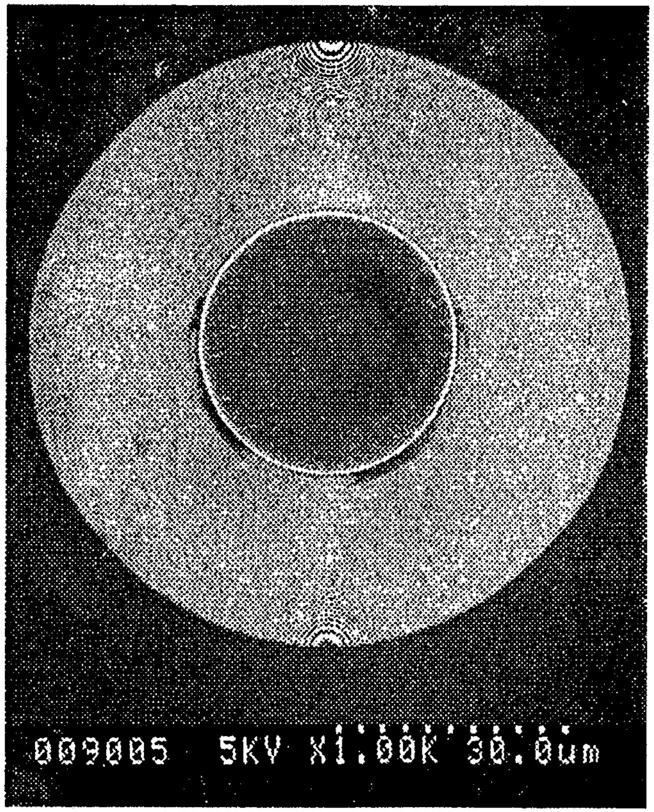

Entire 80 μm diameter ZP with central stop

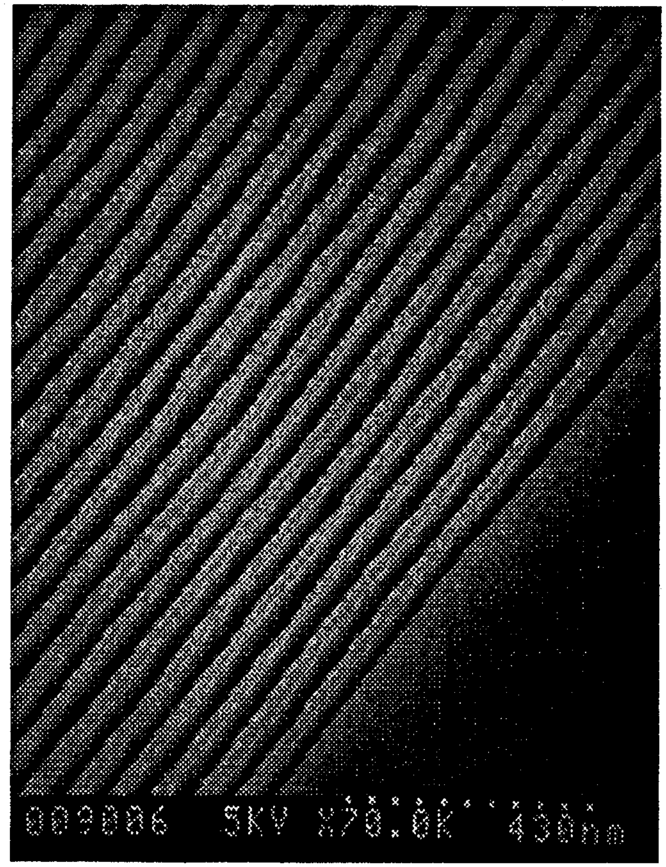

30 nm outermost zones

Chris Jacobsen

Nickel zone plates

State University of New York at Stony Brook
Department of Physics and Astronomy

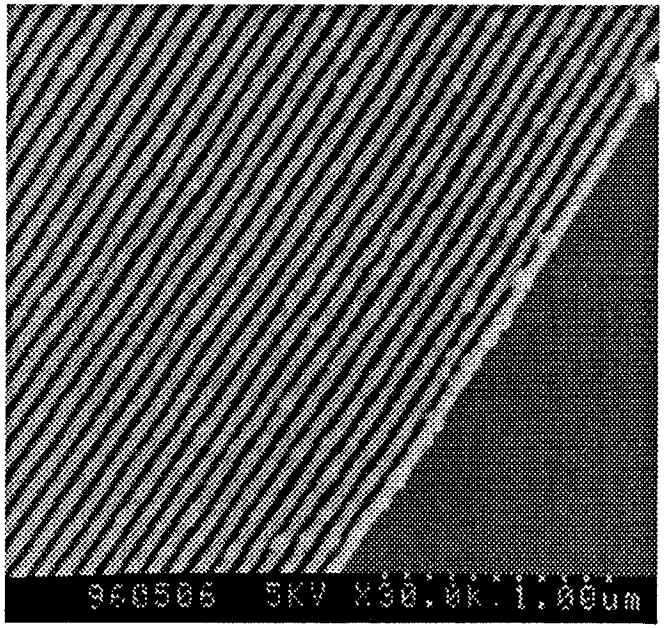

40 nm zones in 110 nm Ni

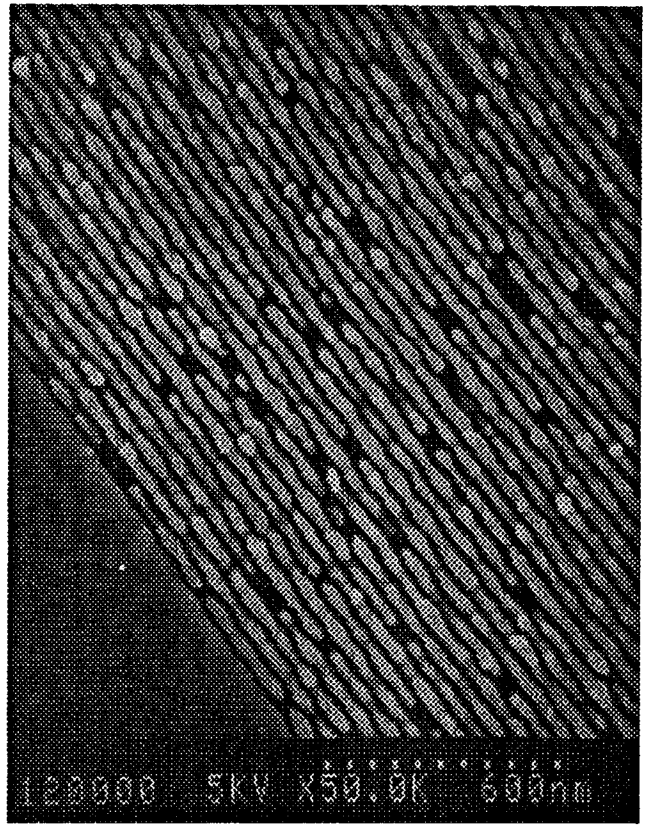

20 nm zones in 60 nm Ni

Stony Brook ALS/LBNL APS/ANL X-1A NCSU NSLS/BNL Lucent Bell Labs

Zone plate microscopes

State University of New York at STONY BROOK Department of Physics and Astronomy

Transmission x-ray microscope (TXM)

- Incoherent illumination; therefore fast, high resolution imaging (bending magnet; pixels in parallel)
- Low spectral resolution at present:

$$\frac{E}{\Delta E} \approx 300$$

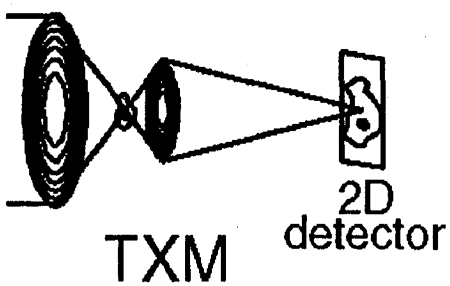

Incoherent illumination

Scanning transmisson x-ray microscope (STXM)

- Coherent illumination; works best with an undulator, and not as fast (pixels in serial)
- More modalities, lower dose, better suited to conventional grating monochromator

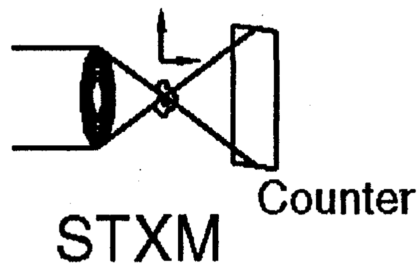

Coherent illumination

Chris Jacobsen

Coherent and incoherent imaging

- Coherent imaging: all photons must be within a phase space area of less than

  $$2\text{N.A.})(2\delta) = 2.44\lambda$$

- At right: MTF contours for source size *p*=(full angle)*(full width)/λ
- Incoherent imaging: multiply that phase space by number of pixels in image: e.g., 1024^2

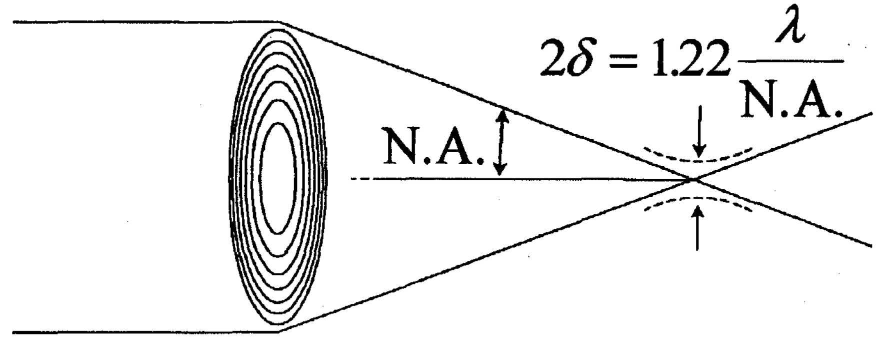

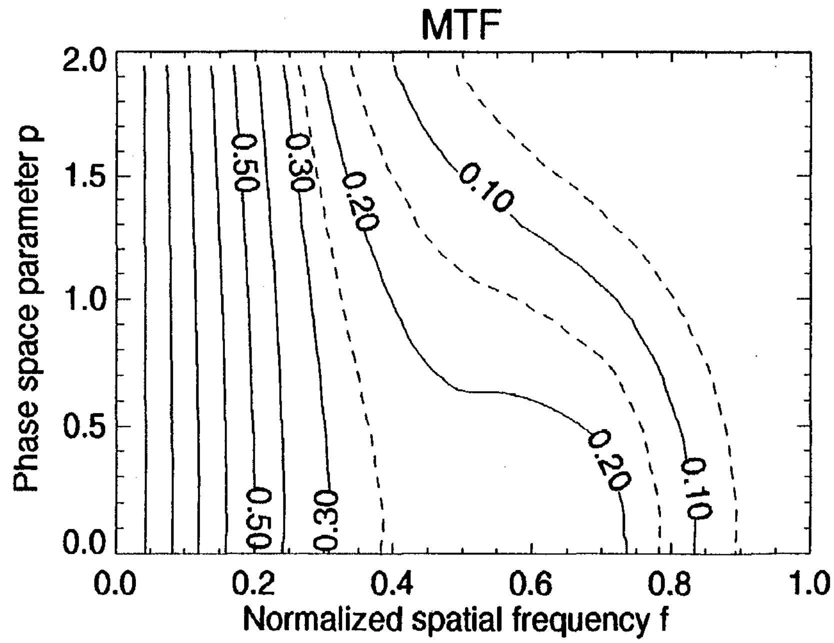

Chris Jacobsen

Stony Brook
ALS/LBNL
APS/ANL
X-1A
NCSU
NSLS/BNL
Lucent Bell Labs

The Stony Brook STXM

State University of New York at
STONY BROOK
Department of Physics and Astronomy

- Stepping motors for large scan range
- Piezos for fine scans
- Spectra from ~0.2 μm spots

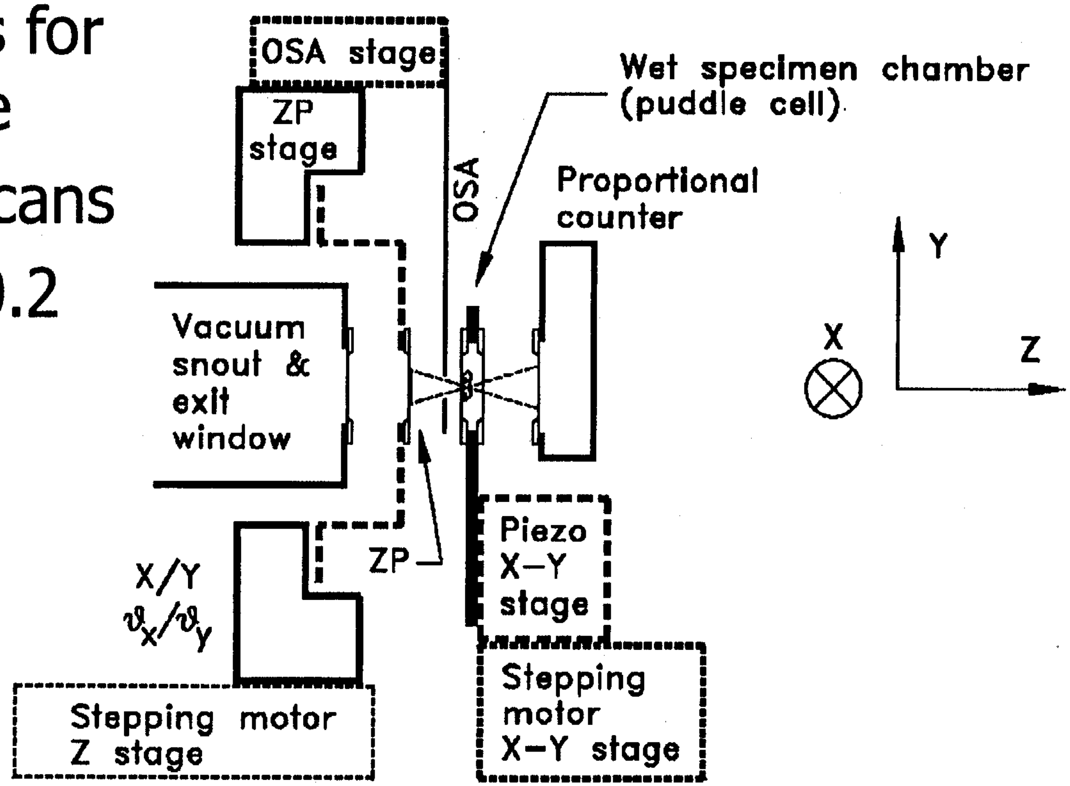

Stony Brook ALS/LBNL APS/ANL X-1A NCSU NSLS/BNL Lucent Bell Labs

Science with STXM

State University of New York at STONY BROOK Department of Physics and Astronomy

- Dry, sectioned specimens with clearly separated phases
  - Polymers - Ade (NCSU) and industrial collaborators
- Dry specimens with mixed phases
  - Geochemistry - coal and wood - Cody and collaborators (Carnegie Instutute)
  - Geochemistry - interplanetary dust particles and meteorite sections - Flynn (Plattsburgh)
  - Bone and osteoporosis - Buckley (King's College, London)
- Wet specimens with mixed phases
  - Sperm and fertility - Balhorn (LLNL; now done wet)
  - Cell biology and nuclear structure - Berrios (Stony Brook) and Spector (Cold Spring Harbor Lab)
  - Soil colloids - Thieme (Göttingen)
  - Soil microorganisms - Shulze and Stodt (Purdue U.)

Chris Jacobsen

Sperm

- X. Zhang, R. Balhorn, J. Mazrimas, and J. Kirz, *J. Structural Biology* **116**, 335 (1996)
- DNA packing in sperm mediated by protamine I and protamine II; fraction of protamine II can vary from 0% to 67% among several species
- Bulk measurements: compromised by immature or arrested spermatids
- Conclusion: protamine II replaces protamine I, rather than binding to protamine I complex

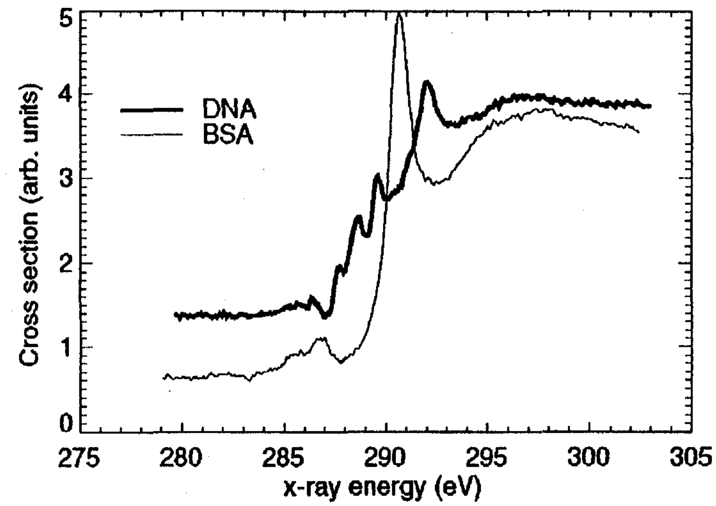

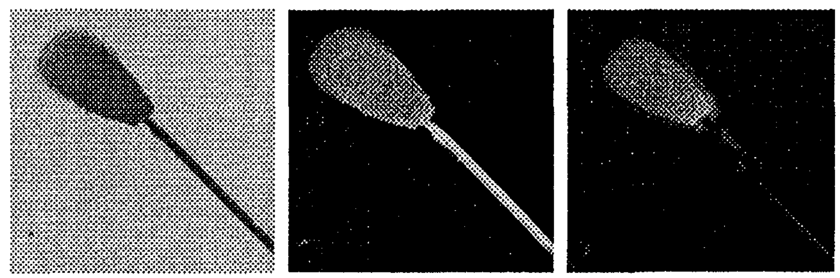

Image @ λ=4.268 nm
2 μm Bull sperm

Protein map

DNA map

Chris Jacobsen

The microdiffraction plane

- H. Chapman, C. Jacobsen, and S. Williams, *Ultramicroscopy* **62**, 191 (1996)
- Use of CCD camera to look at microdiffraction plane

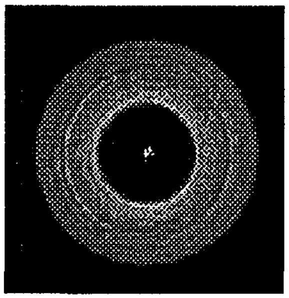

Object: empty

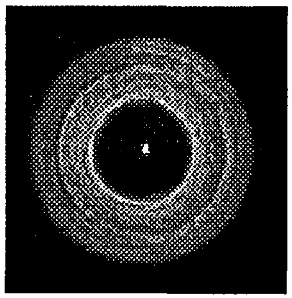

Object: 30 nm Au spheres

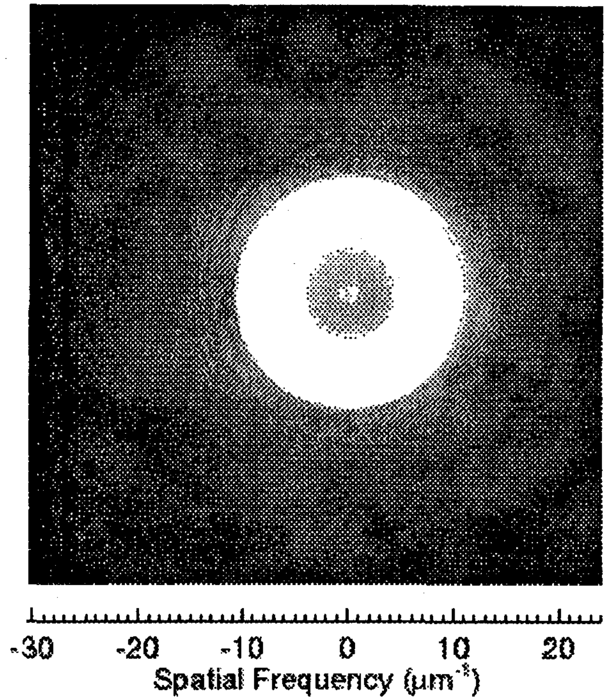

Object: 30 nm Au spheres, logarithmic intensity scale

Stony Brook ALS/LBNL APS/ANL X-1A NCSU NSLS/BNL Lucent Bell Labs

Dark field microscopy

State University of New York at STONY BROOK Department of Physics and Astronomy

- Use absorbing stop (disk or wire) to block out low-scatter-angle beam
- Like annular dark field in STEM

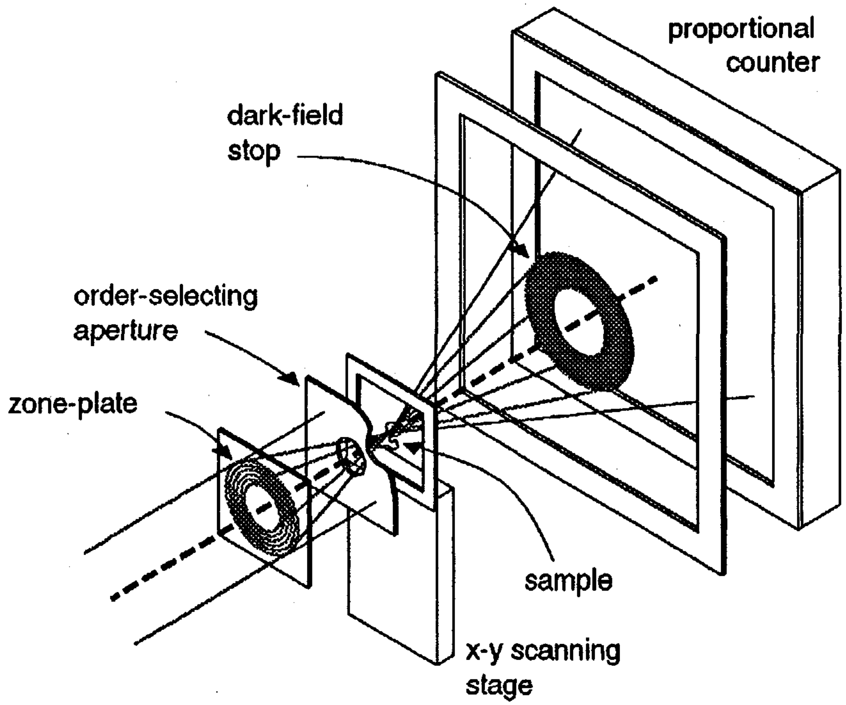

Chris Jacobsen

Stony Brook ALS/LBNL APS/ANL X-1A NCSU NSLS/BNL Lucent Bell Labs

Dark field: gold labels

State University of New York at STONY BROOK
Department of Physics and Astronomy

- H. Chapman, J. Fu, C. Jacobsen, and S. Williams, *J. Microscopy Soc. Am* **2**, 53 (1996).
- Antibody labeling for tubulin with 10 nm gold, then silver enhanced to 5 nm (K. Hedberg, U. Oregon)
- Unique ability to see through intact nucleus
- Present efforts: labeling of nuclear structures (Vogt, Berrios, and Jacobsen, StonyBrook)

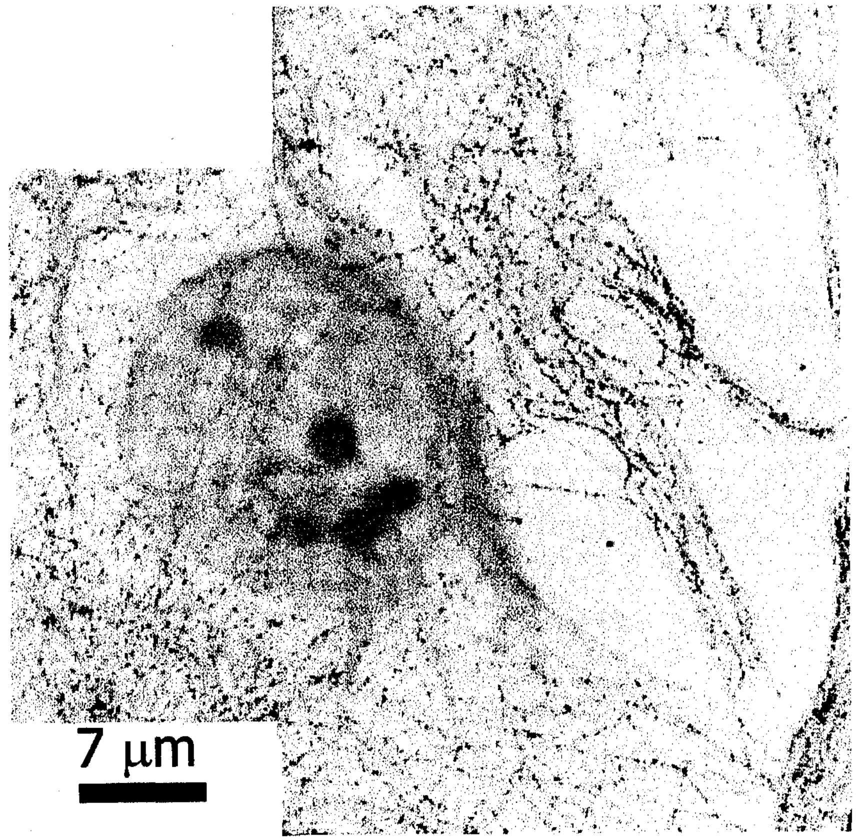

Grey: bright field
Red: dark field superimposed

Chris Jacobsen

Stony Brook
ALS/LBNL
APS/ANL
X-1A
NCSU
NSLS/BNL
Lucent Bell Labs

Cryo microscopy

State University of New York at
STONY BROOK
Department of Physics and Astronomy

- Freeze specimen at 10^4-10^5 K/sec
- Gives "glassy" state of ice - no ice crystalization
- Must maintain specimen at below 140 K
- Improved tolerance of radiation damage:
  - *G* factor (bonds broken per 100 eV) reduced ~2x
  - Free radicals are locked in matrix and unable to diffuse
- EM experience: specimen can tolerate ~10^8 Gray (1 Gray=100 rad=1 J/kg)
- Göttingen/BESSY TXM experience (G. Schneider *et al.*): doses to 10^{10} Gray

Stony Brook ALS/LBNL APS/ANL X-1A NCSU NSLS/BNL Lucent Bell Labs

cryoSTXM

State University of New York at STONY BROOK Department of Physics and Astronomy

- J. Maser, Y. Wang, A. Osanna, C. Jacobsen, J. Kirz, plus S. Spector and J. Warnking
- TEM-type sample mount: airlock, specimen cooled to 110 K with LN_2 dewar
- System at 10^{-7} torr pressure
- Spectroscopy
- Tomography: designed to allow for ±60° tilt
- First tests have used δ_{rN}=60 nm zone plate for "easy" working distances

Stony Brook
ALS/LBNL
APS/ANL
X-1A
NCSU
NSLS/BNL
Lucent Bell Labs

The cryoSTXM

State University of New York at
STONY BROOK
Department of Physics and Astronomy

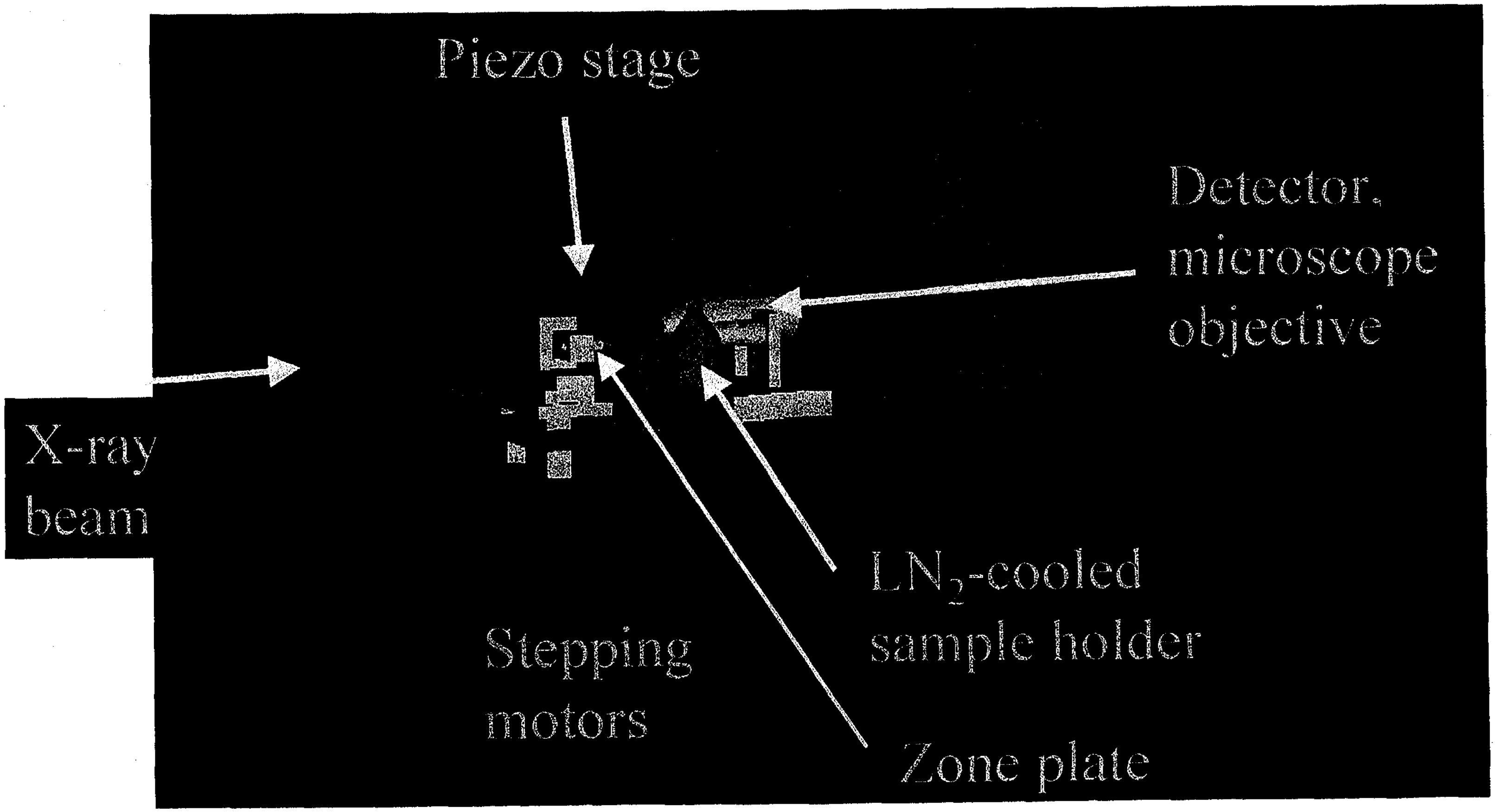

Chris Jacobsen

Stony Brook ALS/LBNL APS/ANL X-1A NCSU NSLS/BNL Lucent Bell Labs

cryoSTXM

State University of New York at STONY BROOK Department of Physics and Astronomy

- J. Maser, Y. Wang, A. Osanna, C. Jacobsen, J. Kirz, plus S. Spector and J. Warnking
- TEM-type sample mount: airlock, specimen cooled to 110 K with LN_2 dewar
- System at 10^{-7} torr pressure
- Spectroscopy
- Tomography: designed to allow for ±60° tilt
- First tests have used δ_{rN}=60 nm zone plate for "easy" working distances

Spatial Resolution

- Image of a test pattern using a zone plate with D = 160 μm, dr_n = 60 nm
- Spatial frequencies of up to 12.5μm^{-1} are detected (cutoff frequency: f_c = [illegible])

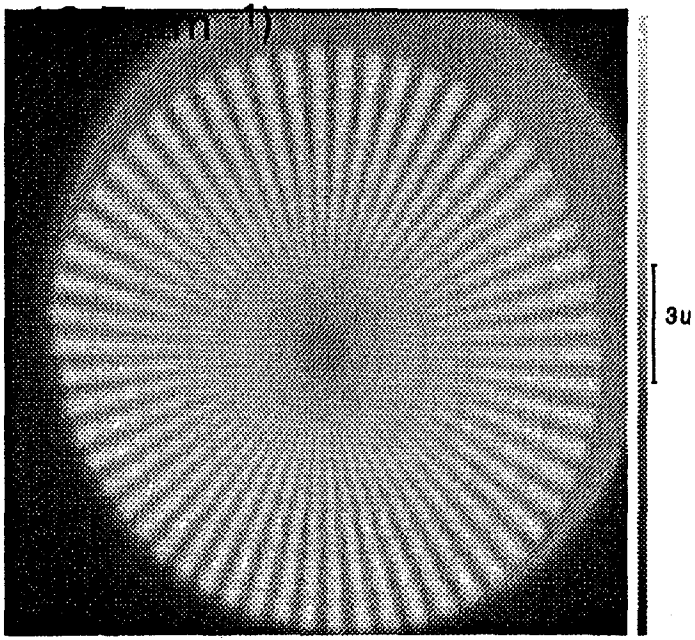

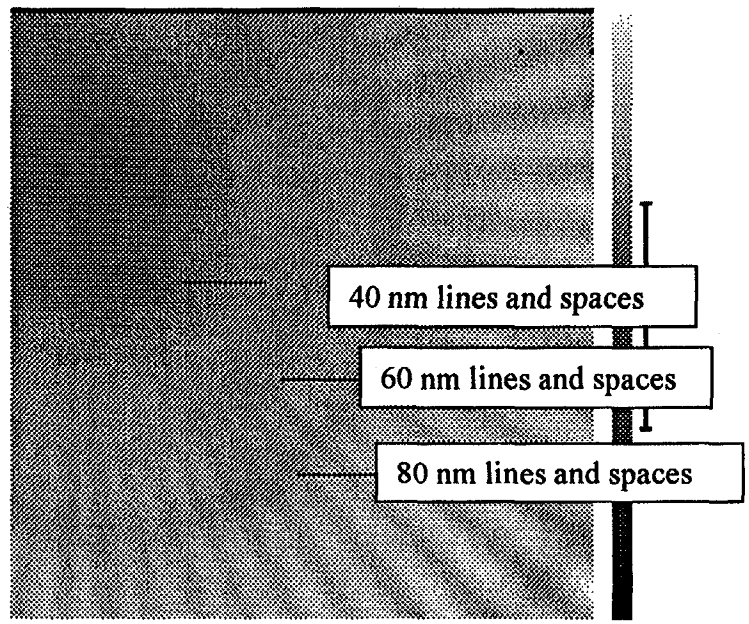

Test pattern and zone plate made by Steve Spector

Stony Brook ALS/LBNL APS/ANL X-1A NCSU NSLS/BNL Lucent Bell Labs

First tests: 3T3 fibroblasts

State University of New York at STONY BROOK Department of Physics and Astronomy

- Cultured on formvar-coated gold TEM grids
- Plunge-frozen while live into liquid ethane(LN_2-cooled)
- View in cryoSTXM within 15 minutes of plunging

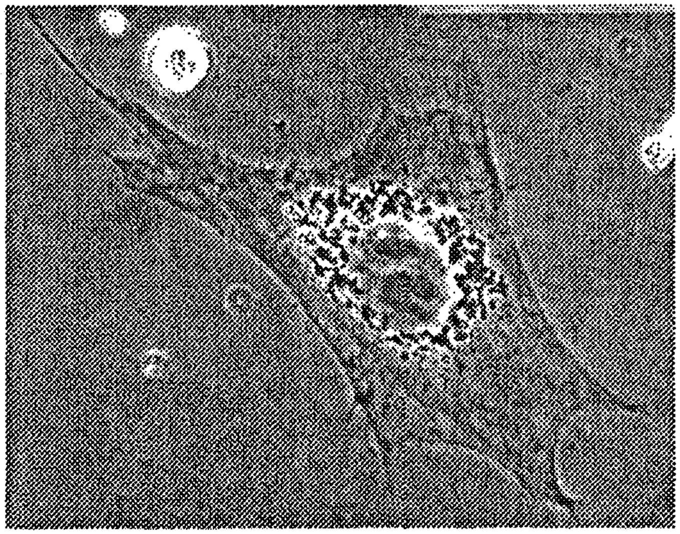

Visible light micrograph before freezing (40x phase contrast objective)

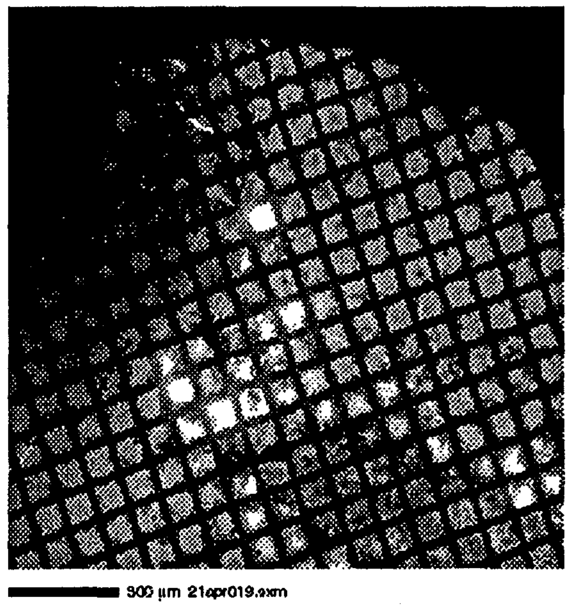

Large area scan after freezing (cryoSTXM)

Chris Jacobsen

Stony Brook ALS/LBNL APS/ANL X-1A NCSU NSLS/BNL Lucent Bell Labs

Frozen hydrated 3T3 fibroblasts

State University of New York at STONY BROOK Department of Physics and Astronomy

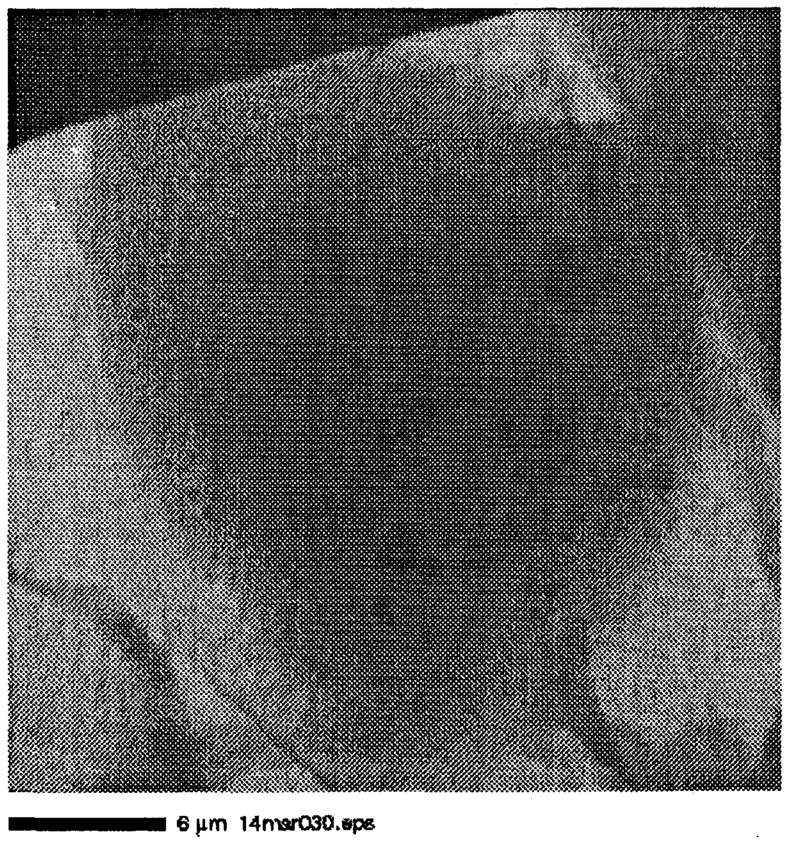

Chris Jacobsen

Stony Brook ALS/LBNL APS/ANL X-1A NCSU NSLS/BNL Lucent Bell Labs

Radiation damage resistance in cryo

State University of New York at STONY BROOK Department of Physics and Astronomy

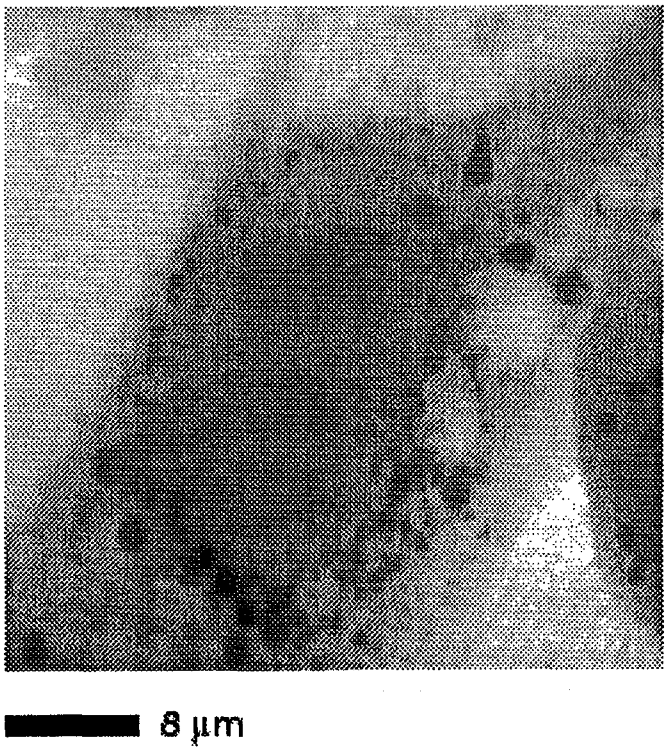

Frozen hydrated image *after* exposing several regions to ~10^{10} Gray

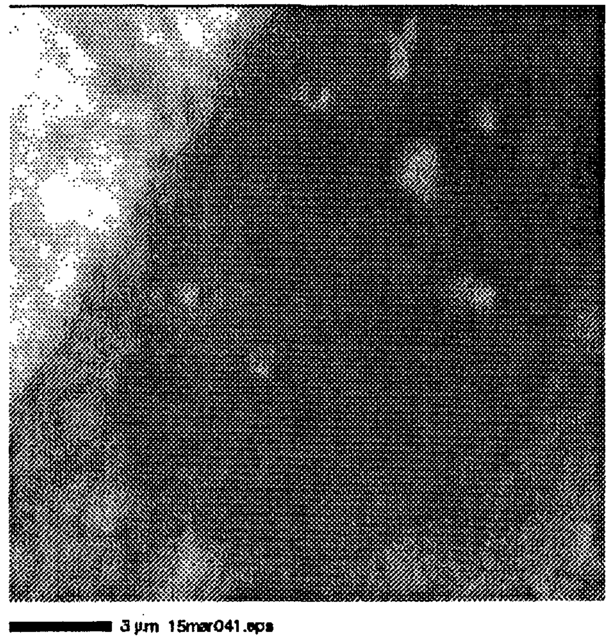

After warmup in microscope (eventually freeze-dried): holes indicate irradiated regions!

Chris Jacobsen

Stony Brook ALS/LBNL APS/ANL X-1A NCSU NSLS/BNL Lucent Bell Labs

Radiation damage: effects on spectra

State University of New York at STONY BROOK Department of Physics and Astronomy

- Cryo protects overall electron density (images)
- Cryo stops free radical diffusion
- Cryo reduces (*G* factor) but does not eliminate bond breaking

Human sperm

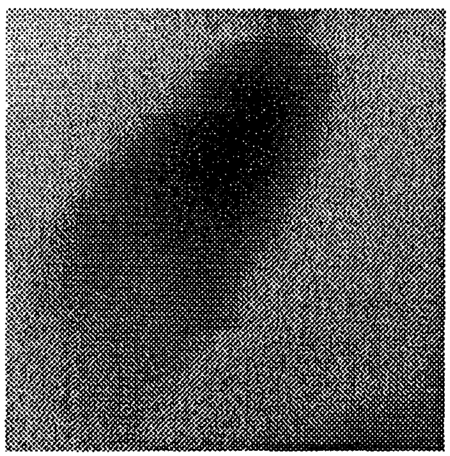

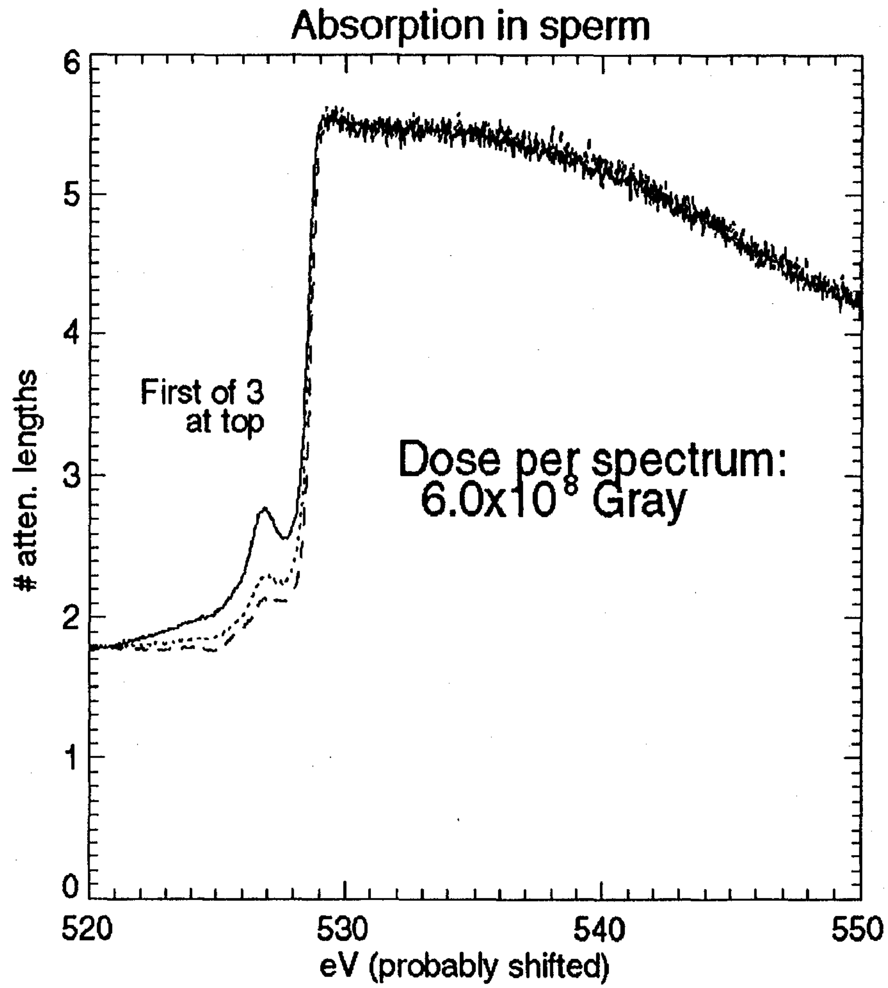

Chris Jacobsen

Stony Brook
ALS/LBNL
APS/ANL
-1A
NCSU
NSLS/BNL
Lucent Bell Labs

Effects of fixation

State University of New York at
STONY BROOK
Department of Physics and Astronomy

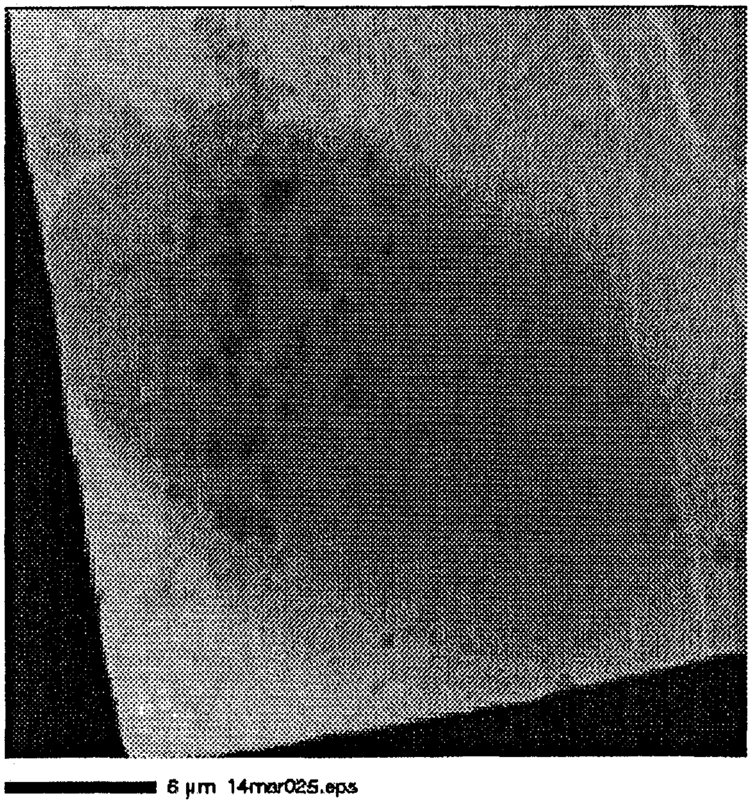

Unfixed, frozen hydrated

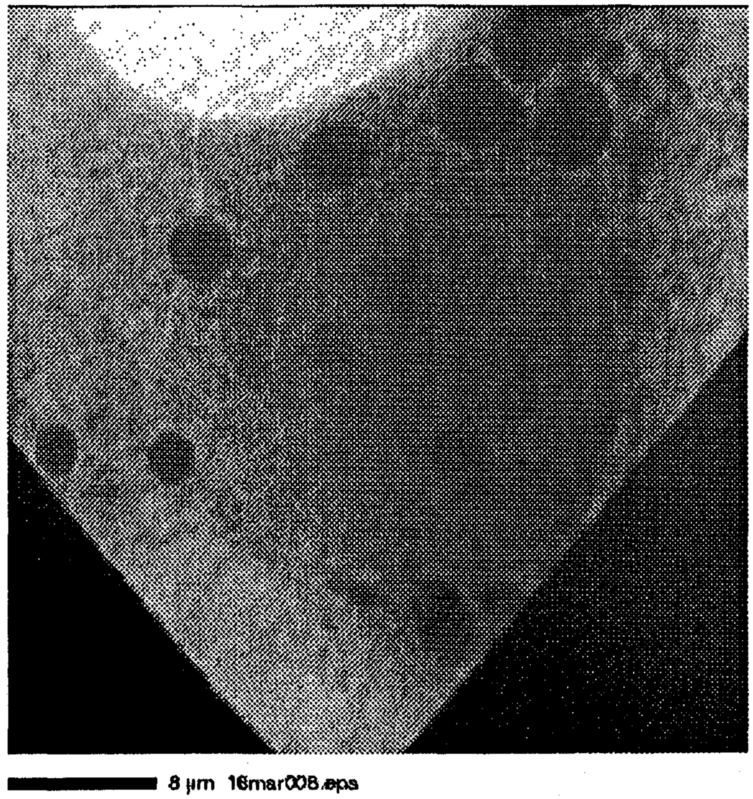

Fixed in paraformaldehyde, then frozen hydrated

Chris Jacobsen

Thick samples: tomography!

- Must resolve overlap of information.
- Want to get significant contrast from a voxel: pushes one to lower x-ray energies as voxel size is decreased
- At low energies, get diffraction blurring $\sim\sqrt{\lambda \cdot d}$ where *d* is distance between sample and detector
- Conclusion: cannot use "classical" approach of parallel ray tomography

Tomography in a microscope

- Need a linear mapping from recorded image to column density in line integral
- This is *true* for absorption, fluorescence
  - simple addition of signal
  - can deconvolve focal series to get in-focus projection
- This is *not true* for phase contrast
  - sin(θ) is not simply additive unless θ is small (multiples of 2π - phase unwrapping)
  - cannot deconvolve with incoherent illumination (phase problem)

Stony Brook ALS/LBNL APS/ANL X-1A NCSU NSLS/BNL Lucent Bell Labs

How to do soft x-ray tomography?

State University of New York at STONY BROOK Department of Physics and Astronomy

- Cannot use parallel beam: diffraction blurring goes as

$$\sqrt{\lambda \cdot d}$$

  from wavelength λ over thickness d. Difficult to get below 100 nm resolution.
- One approach: rotate sample through depth of field of a microscope to collect projections. Brightfield incoherent imaging: can only use absorption contrast, and must remain within depth of focus
- Alternative approach: record complex wavefield which exits sample (a hologram). Gives absorption and phase contrast, lets one deal with samples which extend beyond depth of field. Successful with visible light, microwaves, seismic waves: diffraction tomography (A. Devaney)

Diffraction-limited imaging of 3D objects

- Resolution cutoff (*not* Rayleigh resolution): maximum diffraction angle θ from outer zone width δ_{rN}
  - Transverse: $t = \frac{\lambda}{4\theta} = \frac{\delta_{r_N}}{2}$
  - Longitudinal: $l = \frac{\lambda}{\theta^2} = 4\delta_{r_N}\left(\frac{\delta_{r_N}}{\lambda}\right)$
- Examples:
  - At 540 eV with δ_{rN}=50 nm: $l = 4.4\ \mu m$
  - At 8 keV with δ_{rN}=200 nm: $l = 1.03$ mm

Stony Brook ALS/LBNL APS/ANL X-1A NCSU NSLS/BNL Lucent Bell Labs

Incoherent imaging: 3D resolution

State University of New York at STONY BROOK Department of Physics and Astronomy

- At 540 eV (λ=2.4 nm), with δ_{rN} zone plate with 50% central stop:

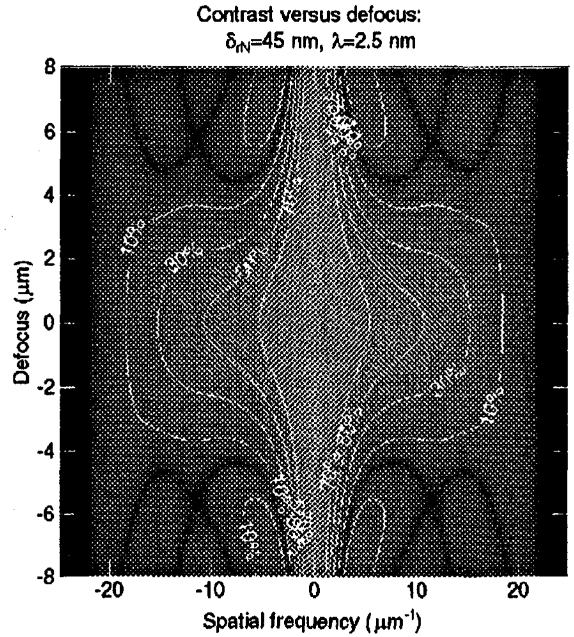

Modulation transfer function

⇐Focus⇒

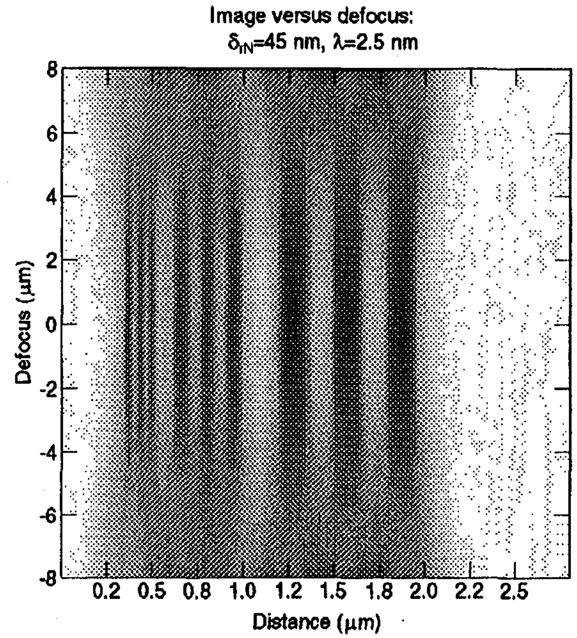

Simulated image of 33, 70, 140 nm bars and spaces

Chris Jacobsen

Projections via microscopy

- Demonstrated at λ =2.5 nm using scanning transmission x-ray microscopy: Haddad *et al.*, *Science* **266**, 1213 (1994). Specimen: two-plane microfabricated test pattern. ~100 nm 3D resolution
- Demonstrated at λ =2.5 nm using transmission x-ray microscopy: J. Lehr, Universität Göttingen (to be published in *Optik*). Specimen: mineral sheath of soil bacteria. ~60 nm 3D resolution.
- Only works for absorption contrast

Stony Brook ALS/LBNL APS/ANL X-1A NCSU NSLS/BNL Lucent Bell Labs

CryoSTXM: first steps towards tomography

State University of New York at STONY BROOK Department of Physics and Astronomy

- Paraformaldehyde-fixed, then frozen hydrated 3T3 fibroblast
- Images at 5° tilt intervals over a 30° tilt range
- 3D image reconstructed by Steve Wang using an ART algorithm
- Slices at 1 micron spacing through reconstruction

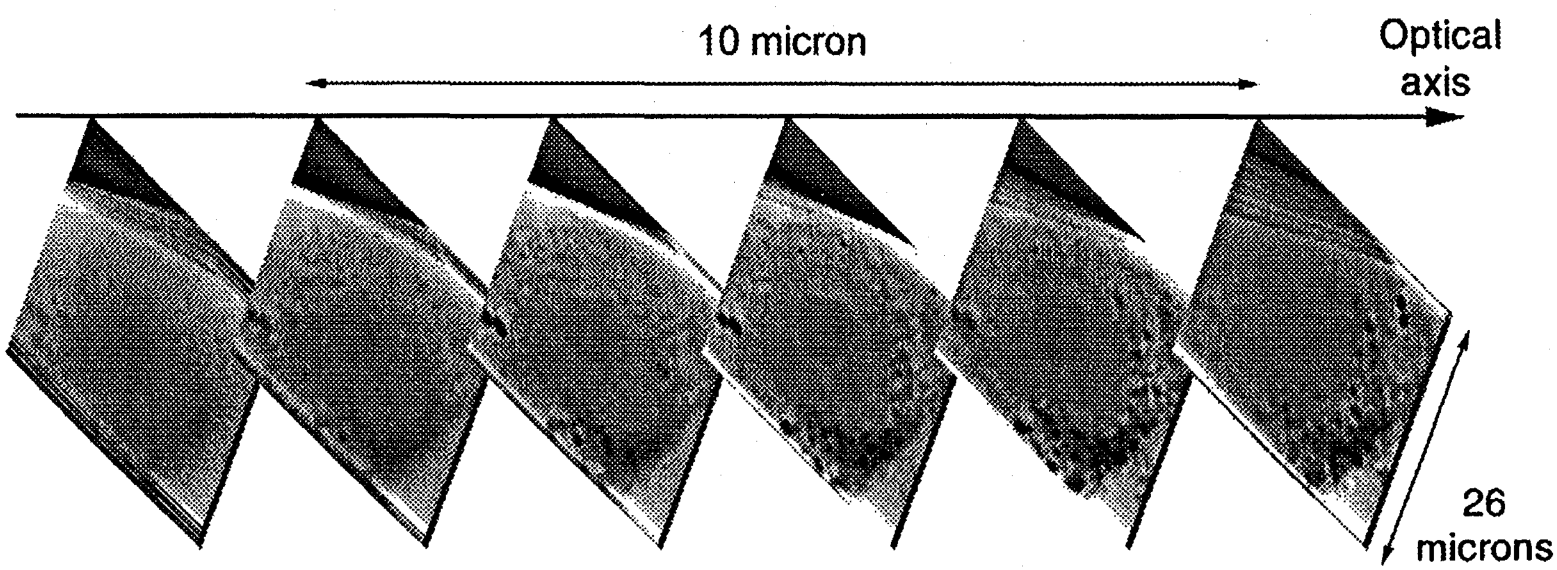

Chris Jacobsen

Dose fractionation

- To acquire 100 projections for a 3D reconstruction, you do *not* need to expose the specimen to 100× the 2D image dose.
- R. Hegerl and W. Hoppe, *Zeitschrift für Naturforschung* **31 a**, 1717 (1976)

  A three-dimensional reconstruction requires the same integral dose as a conventional two-dimensional micrograph provided that the level of significance and the resolution are identical.
- Assumes low contrast object; only noise is photon statistics; perfect registration/alignment of projections; no change to object

Dose fractionation: simulations

- Computational simulations by McEwen, Downing, and Glaeser in *Ultramicroscopy* **60**, 357 (1995)
  - One can use cross-correlation to register the projections in low-statistics images
  - Dose fractionation is valid for "less weak" objects such as biological specimens imaged with soft x rays.

Depth of focus versus resolution

- Again: depth of focus decreases as square of improved transverse resolution

Transverse: $t = \frac{\lambda}{4\theta} = \frac{\delta_{r_N}}{2}$

Longitudinal: $l = \frac{\lambda}{\theta^2} = 4\delta_{r_N}\left(\frac{\delta_{r_N}}{\lambda}\right)$

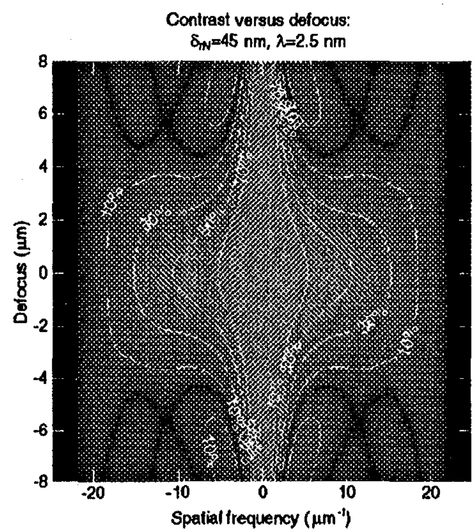

45 nm zone plate

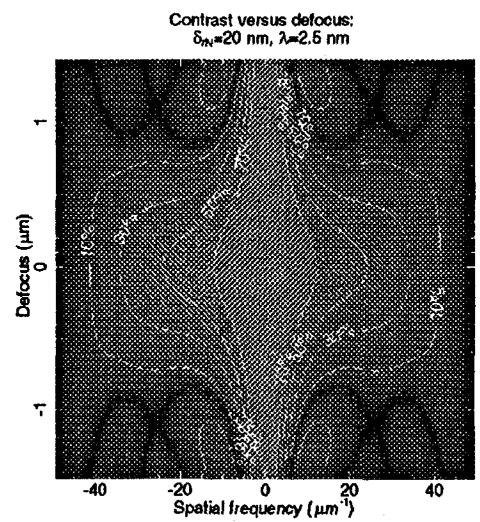

20 nm zone plate

Chris Jacobsen

Diffraction tomography

- Well established in visible light, microwave, seismic imaging (e.g., T. Devaney)
- Record in-line holograms at each rotation. Backpropagate wavefield through object.
- Each backpropagated plane includes both in-focus data, and artifacts (e.g., twin-image fringes). In 3D reconstruction, data will constructively superimpose, while artifacts will tend to cancel each other out.
- Allows one to handle absorption and phase

How to do diffraction tomography?

- Record wavefield downstream from specimen (hologram).
  - Phase at object is encoded as intensity
  - Allows for phase contrast (two holograms help with phases)
  - Allows for backpropagation through specimen
- Transfer this wavefield to electronic detector:

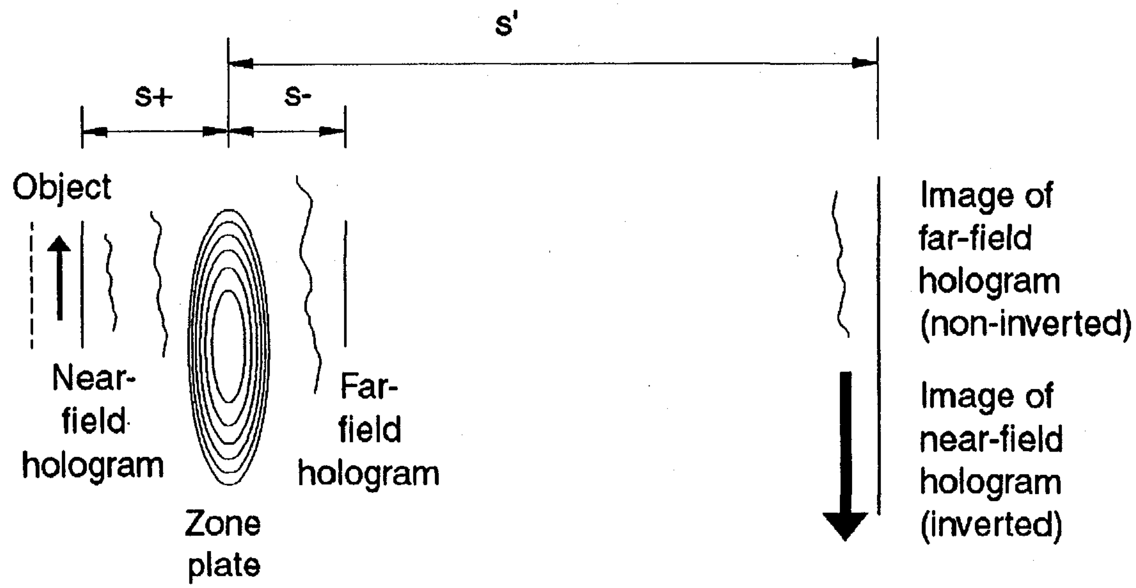

Chris Jacobsen

Stony Brook ALS/LBNL APS/ANL X-1A NCSU NSLS/BNL Lucent Bell Labs

Soft x-ray diffraction tomography: first steps

State University of New York at STONY BROOK Department of Physics and Astronomy

- Dried spiral bacteria
- S. Lindaas and M. Howells (LBL) and J. Miao and C. Jacobsen (Stony Brook)

Left: near-field hologram (almost in focus)

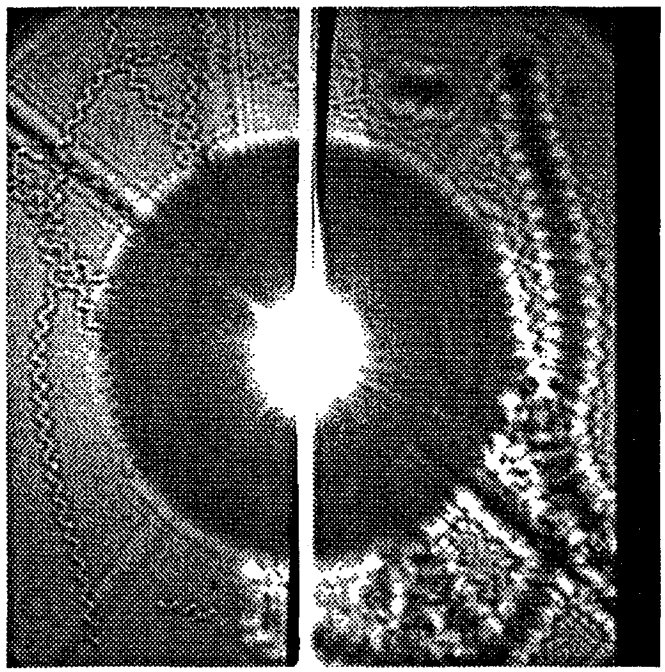

Right: far-field hologram (far from focus)

Stony Brook ALS/LBNL APS/ANL -1A NCSU NSLS/BNL Lucent Bell Labs

LN_2 plunge

State University of New York at STONY BROOK Department of Physics and Astronomy

- Severe ice crystal damage occurs because freezing is too slow

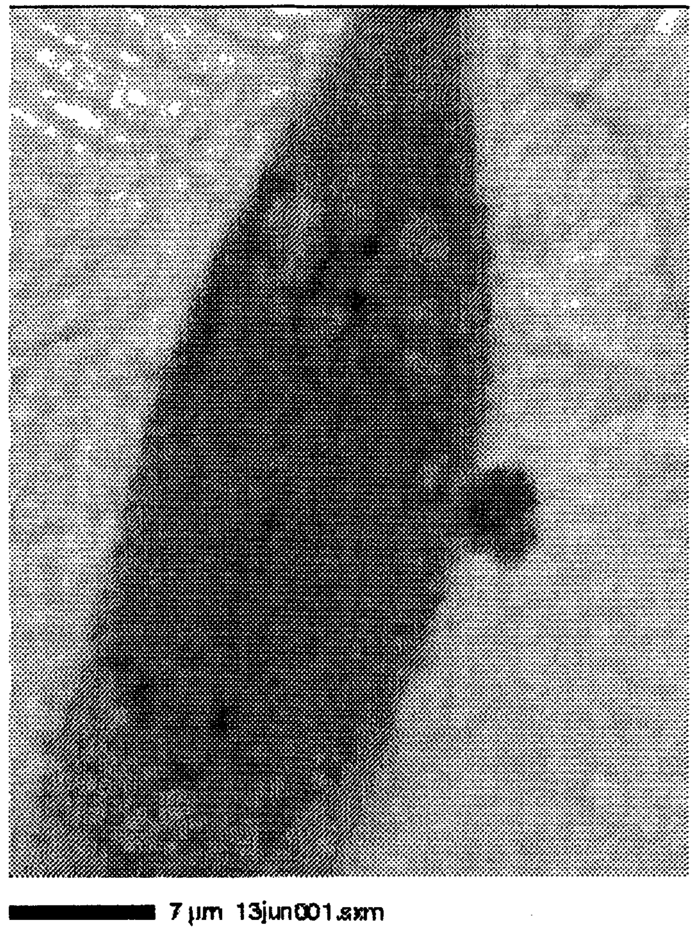

Chris Jacobsen

Part IV

Avraham Dilmanian
Zhong Zhong
Brookhaven National Laboratory (BNL)

"Diffraction Enhanced Tomography"

Diffraction Enhanced CT

Zhong Zhong, Ph.D., NSLS
and
Avraham Dilmanian, Ph.D., Medical Dept.

BNL

nsls

CSRRI

Center for Synchrotron Radiation Research and Instrumentation
Illinois Institute of Technology

Mammography X-ray Refraction Imaging using Monochromatic Synchrotron Radiation - *Collaborators*

• D. Chapman	IIT/CSRRI
• W. Thomlinson	NSLS / BNL
• F. Arfelli	NSLS / INFN di Trieste
• N. Gmur	NSLS / BNL
• R. Menk	INFN di Trieste
• R.E. Johnson	UNC Chapel Hill
• D. Washburn	UNC Chapel Hill
• E. Pisano	UNC Chapel Hill
• B. Burns	UNC Chapel Hill
• D. Sayers	NCSU Raleigh
• D. Peplow	NCSU Raleigh
• I. Ivanov	IIT / CSRRI
• T. Irving	IIT / CSRRI

Normal Radiography

- Normal Radiography: $I_n = I_R + I_D + I_C + I_I$
  - I_C and I_I: Coherent and incoherent scattering
  - I_D: Small angle diffraction (~ 1 mrad)
  - I_R: Transmitted beam undergone refraction

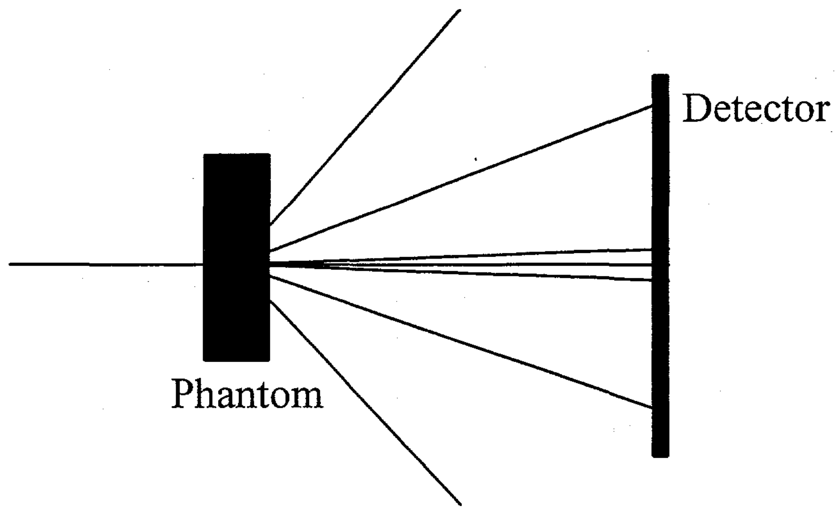

- Synchrotron in-line scan: $I_n = I_D + I_R$ (better)

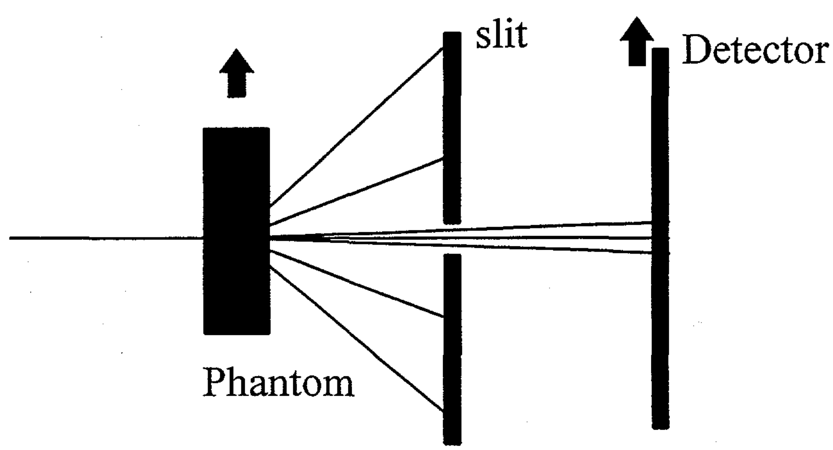

What an analyzer does?

$$I \approx I_r R(\theta_B + \theta) = I_R\left(R_0 + \frac{dR}{d\theta}\right)\Delta\theta$$

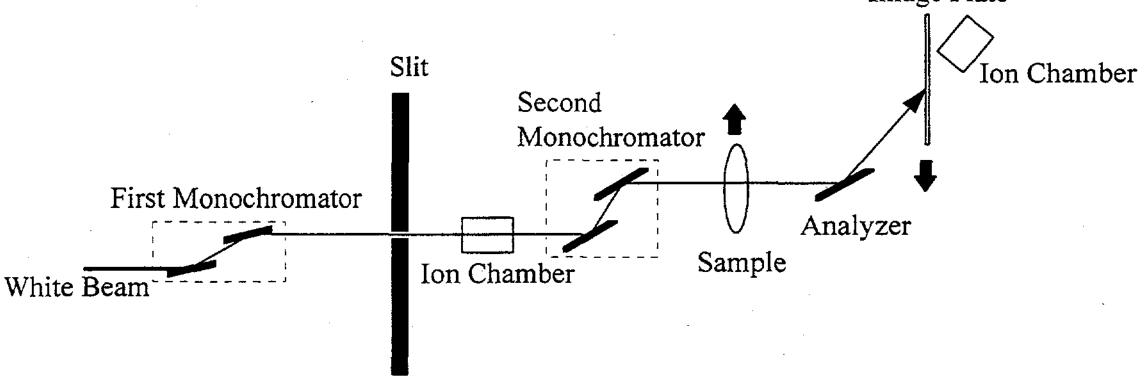

Two sides of rocking curve:

$$I_L = I_R[R(\theta_L) + \frac{dR}{d\theta}(\theta_L)\Delta\theta_z]$$

$$I_H = I_R[R(\theta_H) + \frac{dR}{d\theta}(\theta_H)\Delta\theta_z]$$

Solve them to get I_R and $\Delta\theta_z$ on a pixel to pixel basis

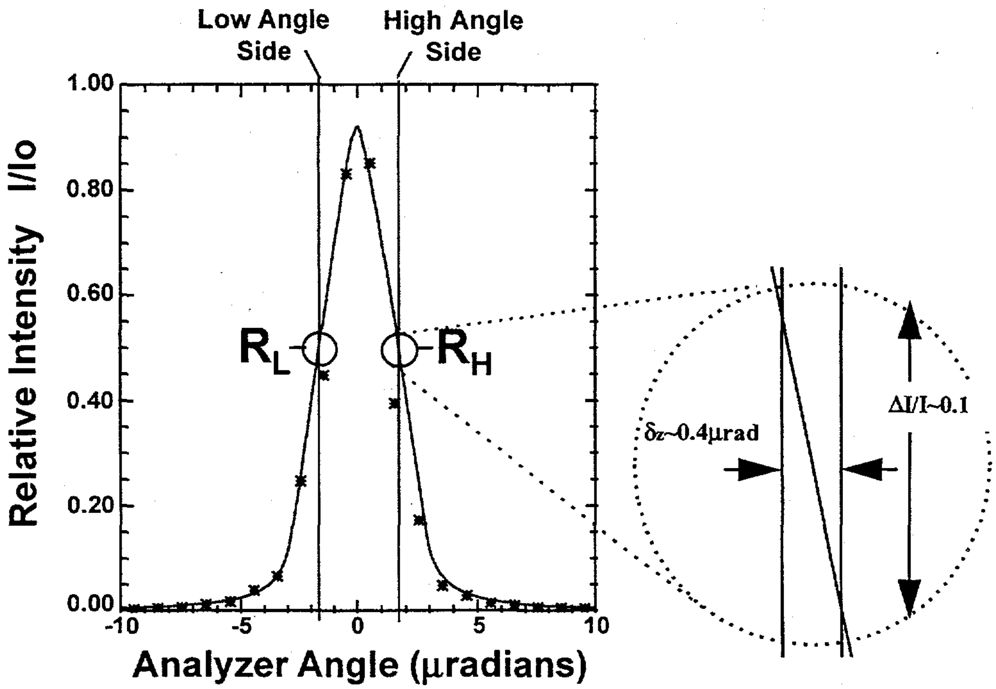

Two things not available in normal radiography

- Refraction angle (edge detection)

$$\Delta\theta = \frac{1}{n}\frac{dn}{dz}\Delta l$$

- Apparent absorption free from small angle diffraction:
  - Differentiate materials of similar density and chemical composition but different structure, e.g. fat and tissue

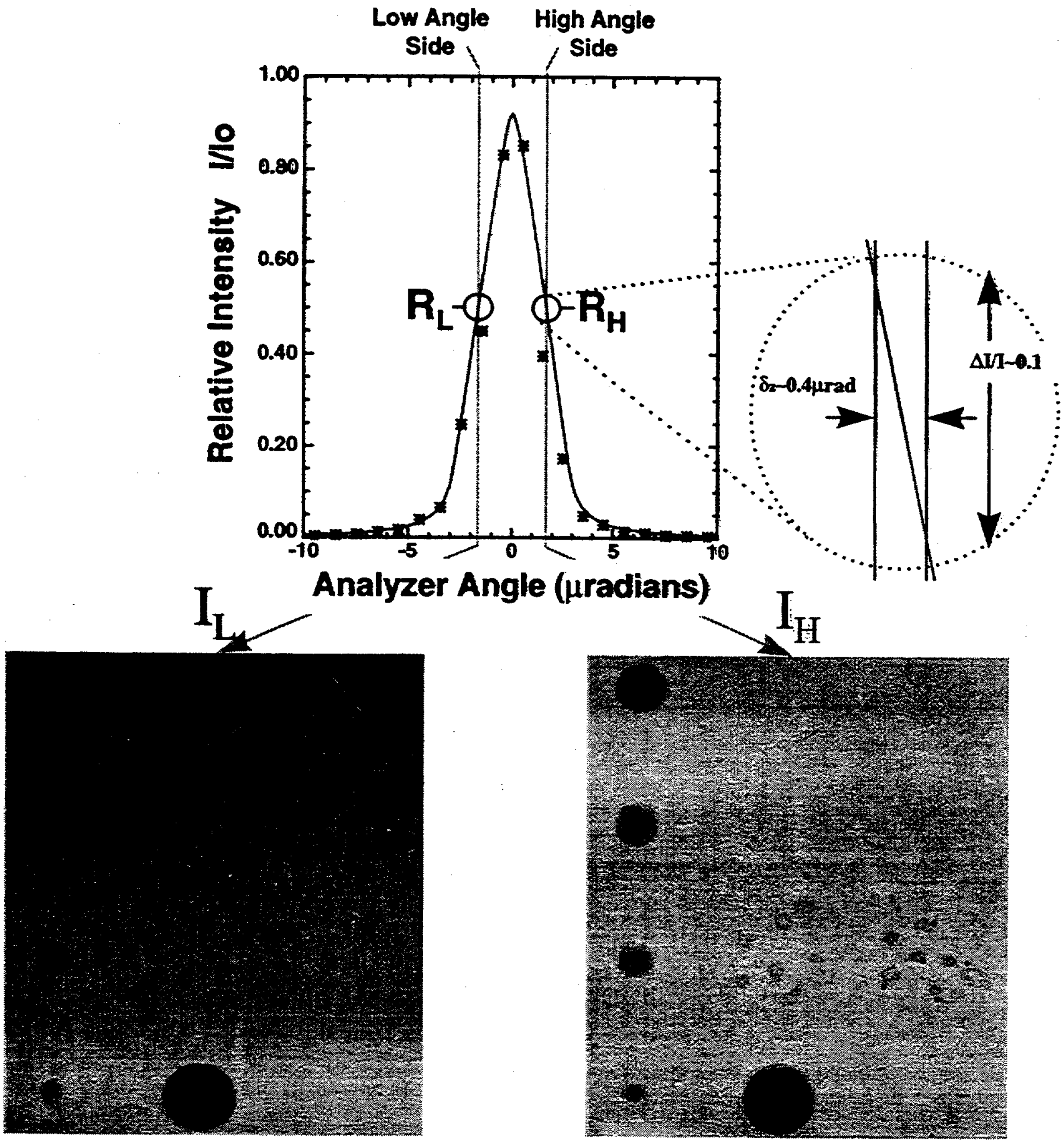

Low Angle Side
High Angle Side
1.00
0.80
0.60
0.40
0.20
0.00
Relative Intensity I/Io
R_L
R_H
-10
-5
0
5
10
Analyzer Angle (μradians)
δz~0.4μrad
ΔI/I~0.1
I_L
I_H

Figure 1.

Where did the absorption contrast come from??

CSRRI Center for Synchrotron Radiation Research and Instrumentation Illinois Institute of Technology

- Excess contrast is due to lack of scatter, including small angle scattering (down to the microradian level)
- The figure below is a "rocking curve" of an image line through the tumor simulations
- Note
  - the lack of intensity in the simulation at the curve peak
  - the excess intensity in the wings of the curve
- Extinction Contrast

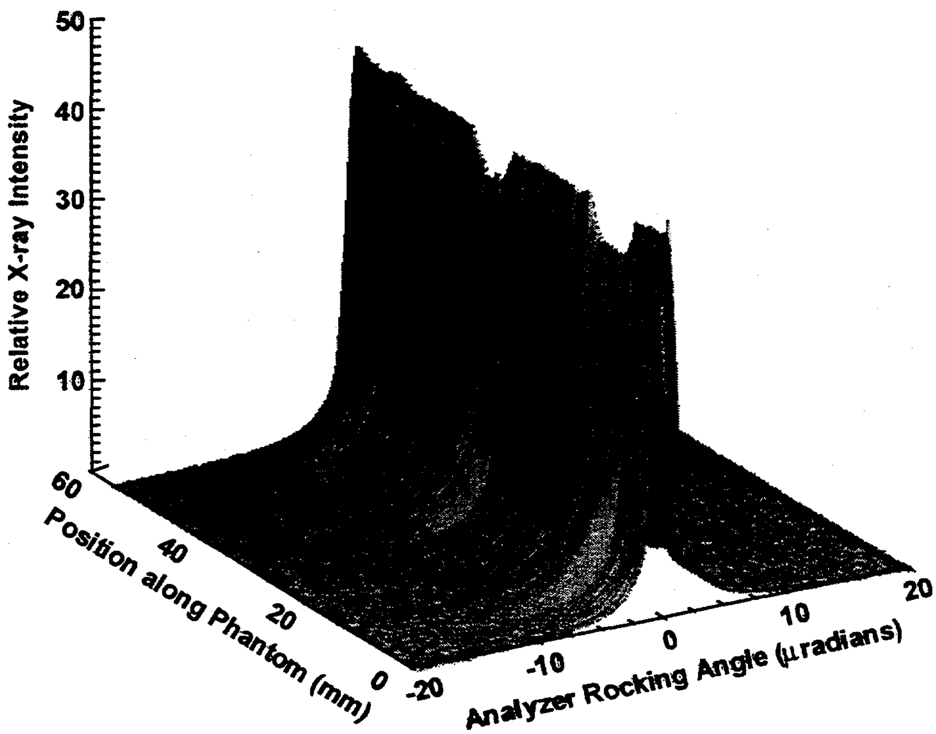

Sources of Contrast with DEI

nsls

CSRRI
Center for Synchrotron Radiation Research and Instrumentation
Illinois Institute of Technology

- Normal Absorption - same as from conventional radiography
- Refraction Contrast - sensitive to refractive index gradients at the imaging energy
  - Edge enhancement without computer processing the image…much less noise introduced
  - Will be enhanced near absorption edges of elements within the material
- Extinction Contrast - sensitive to the order within the material
  - Example -
    - practically all of the contrast seen in the ACR tumor simulations is due to extinction
    - wax in the vicinity of the calcifications has the structurally altered - slight ordering present
  - Raises possiblility of structural imaging similar to conventional topography except in what would be considered a disordered system
  - Images can be taken "off peak" to obtain optimal contrast depending of system.

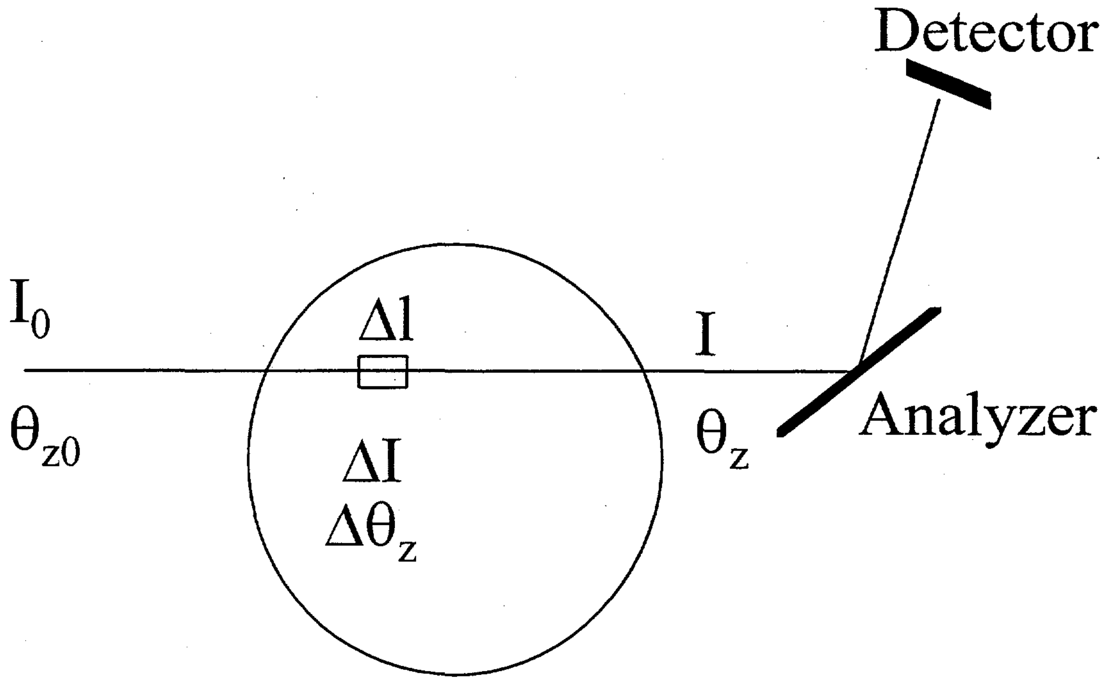

$$I_L = I_R[R(\theta_L) + \frac{dR}{d\theta}(\theta_L)\Delta\theta_z]$$

$$I_H = I_R[R(\theta_H) + \frac{dR}{d\theta}(\theta_H)\Delta\theta_z]$$

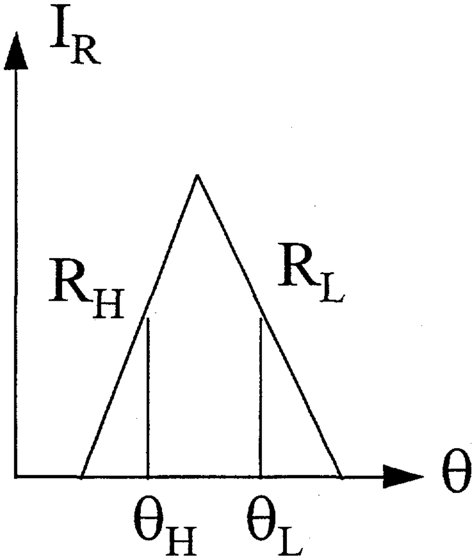

Projection data obtained at two opposite points on the rocking curve

$$\Delta I = -\mu\Delta l - \gamma_{ext}\Delta l$$

where

$\mu\Delta l$ is the attenuation (does not include small - angle scattering)

$\gamma_{ext}\Delta l$ is the extinction

$$\Delta\theta z = \frac{1}{\mathrm{n}}\frac{\partial n}{\partial z}\Delta l$$

where n is the index of refraction and $\frac{\partial n}{\partial z}$ is the out - of - plane gradient

$$I = I_0 \exp[-\int_0^L \mu(l)dl - \int_0^L \gamma_{ext}(l)dl]$$

$$I = I_0 \exp(-\Sigma(\mu+\gamma)\Delta l)$$

$$\ln(\frac{I}{I_0}) = -\Sigma(\mu+\gamma)\Delta l$$

and

$$\theta_z = \theta_{z0} + \int_0^L \frac{1}{n(L)}\frac{\partial n(l)}{\partial z}dl$$

In summary

$$I_{\mathrm{Detected}} = f(I,\theta z)$$

$$I_R = \frac{I_L \frac{dR}{d\theta}(\theta_H) - I_H \frac{dR}{d\theta}(\theta_L)}{R(\theta_L)\frac{dR}{d\theta}(\theta_H) - R(\theta_H)\frac{dR}{d\theta}(\theta_L)}$$

$$\Delta\theta_Z = \frac{-I_L R(\theta_H) + I_H R(\theta_L)}{I_L \frac{dR}{d\theta}(\theta_H) - I_H \frac{dR}{d\theta}(\theta_L)}$$

- We now have two sets of projection data: I_R and $\Delta\theta_z$.
- We backproject each one separately. $\ln(I_0/I_R)$ gives us the extinction image. $\Delta\theta_z$ gives us the refraction image.

DEI CT: Plans at NSLS

- Microtomography: using the detector system of Dr. Peter Siddons at X27A
- Tomography: using the MECT system at X17B2

Diffraction-Enhanced CT: Tissue Characterization

- The refraction image will probably reveal interfaces, and act as an edge-enhancing tool.
- The extinction image will probably show contrast between different tissue types: e.g. fat and muscle.

MECT

Staff:

Avraham Dilmanian, Ph.D.
Xiao Ye Wu, Ph.D.
Xiaoling Huang, graduate student
Baorui Ren, graduate student

BNL Collaborators:

Daniel Slatkin, Ph.D.
William Thomlinson, Ph.D.
Zhong Zhong, Ph.D.

Illinois Institute of Technology:

Dean Chapman, Ph.D.

State University of New York, Stony Brook:

Terry Button, Ph.D., Medical Physicist
Fabio Giron, M.D., Vascular Surgeon
Michael Petersen, M.D., Vascular Surgeon
Clemente Roque, M.D., Neuroradiologist
Karen Gadol, M.D., Radiologist

Industry:

Analogic Corporation, Peabody, MA
Science Research Laboratory, Somerville, MA

Multiple Energy Computed Tomography (MECT)

A synchrotron-based monochromatic CT for human studies

Rationale:

1. To establish the performance of a monochromatic CT

2. To examine its usefulness in radiology

3. To examine the prospects for developing a compact, clinical version of the system

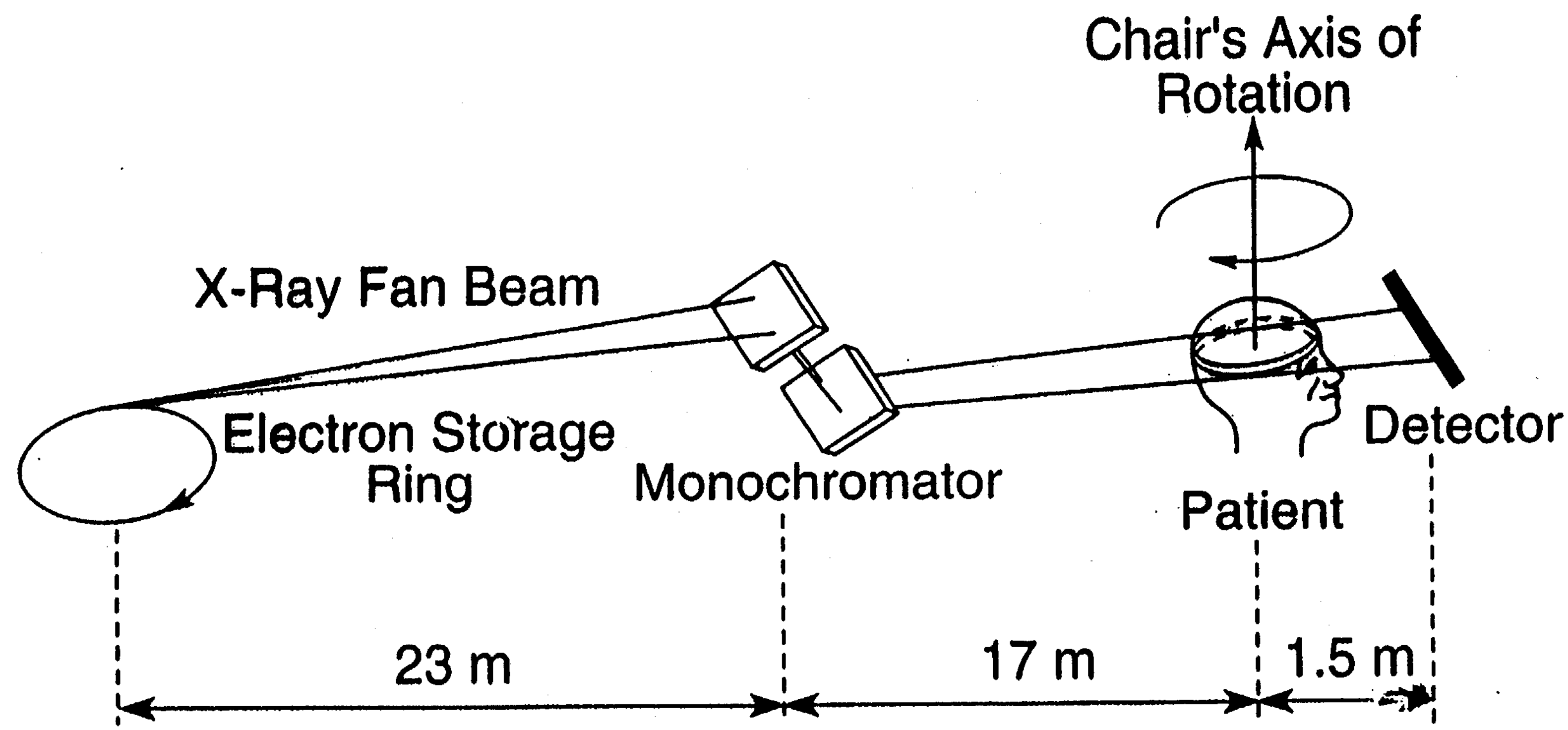

Chair's Axis of
Rotation
X-Ray Fan Beam
Electron Storage
Ring
Monochromator
Patient
Detector
23 m
17 m
1.5 m

The relationship between carotid plaque composition, plaque morphology, and neurologic symptoms

J.M. Seeger, E. Barratt, G.A. Lawson, and N. Klingman, Department of Surgery, University of Florida, Gainesville, FL 32610

J. Surg. Res. 1995, 58:330-336

Variations in plaque composition could make carotid artery plaques prone to ulceration, subintimal hemorrhage, plaque progression, or embolization and, thus, increase the risk of ipsilateral ischemic neurologic events. Seventy-eight carotid endarterectomy specimens from 74 patients (38 symptomatic and 36 asymptomatic) were analyzed. Prior to analysis, 43 of the 78 plaques were divided into sections based on disease severity and examined by light microscopy for surface ulceration and subintimal hemorrhage. Extracted lipid, cholesterol, collagen, and calcium content were determined in all 78 plaques and compared to clinical presentation and/or morphologic observations. Plaques removed from symptomatic patients contained more extracted lipid and cholesterol than those from asymptomatic patients. In addition, compared to the remainder of the plaque, the most stenotic portion of the plaque contained more cholesterol, more calcium, and less collagen. Finally, irrespective of clinical presentation, ...

Diffraction-Enhanced Computed Tomography

The following Laboratory Directed Research and Development (LDRD) grant was obtained in September 1996 for two years. It was entitled "X-ray Schlieren Computed Tomography", L.D. Chapman, F.A. Dilmanian (P.I.), B.A. Dowd, D.P. Siddons, and W.C. Thomlinson.

Part V

Betsy Dowd
Brookhaven National Laboratory (BNL)

"X-ray Computed Microtomography Applications at the NSLS"

History of XCMT by BNL

- Mid-1980's: The first CMT measurements were performed at BNL by Per Spanne (presently at ESRF) and Mark Rivers (Univ. of Chicago)
  - First generation scanning technique with single detector
  - Achieved resolution on the order of a few microns
  - Various sandstones and catalysts analyzed

- 1994: A third generation CMT measurement was taken by Mark Rivers and Peter Eng of Univ. of Chicago
  - A cooled Charge-Coupled Device (CCD) provided a two dimensional detector for faster acquisition: multiple slices imaged simultaneously
  - Various scintillators for converting X-Ray to visible photons were tried: best results obtained with a YAG type scintillator

Current Status

- A third-generation CMT scheme has been developed and tested at Beamline X27C at the Light Source during the past 2 years under an Advanced Computational Technology Initiative (ACTI). Participants of the ACTI are:

  BNL : B. Andrews, B. Dowd, , K. Jones , A. Peskin, D. P. Siddons
  Mobil Corporation: W. Bell, M. Coles, R. Hazlett
  GTE Corporation

Types of Samples Studied with XCMT at NSLS

Samples ranged in size from less than 1 mm to 20 mm , with best resolution on the order of 3 microns

- **Reservoir sandstone, seal rock and catalysts : Mobil Corp.**
- **Synthetic rock : RPI**
- **Meteorites : University of Chicago**
- **Basalts : University of New Hampshire, National Taiwan University**
- **Insects , Wood : USDA, Dpt. of Forestry and Forest Products**
- **Porous Metals : Northrop - Grumman**
- **Plasma Sprayed Coatings : SUNY, Stony Brook**

Technical Achievements

- **3 microns resolution with porous samples**

- **Flexibility in Data Collection**
  - **Zoom capability--variable field of view; image samples over 1 inch**
  - **Subvolume correction for cylindrical porous samples written into software**
  - **Can redefine readout subarray of CCD for fast collection of time-dependent phenomena in a small area of interest (real-time flow, e.g.)**
  - **Can bin pixels; increases S/N, decreases readout-time for sample area**
  - **Variable energy of exposure offered by synchrotron X-Ray: reduces beam hardening effects as well as enhances contrast**

- **User-friendly automated data collection & reconstruction (PRT starting up)**

- **Improved data collection & reconstruction time: total of 20 minutes for 4x4 binned set, i.e., 329 slices each with over 50,000 resolution cells (over 10 million voxels)**

nsls IR UV X

Phantom: 100 μ D glass spheres in capillary tube

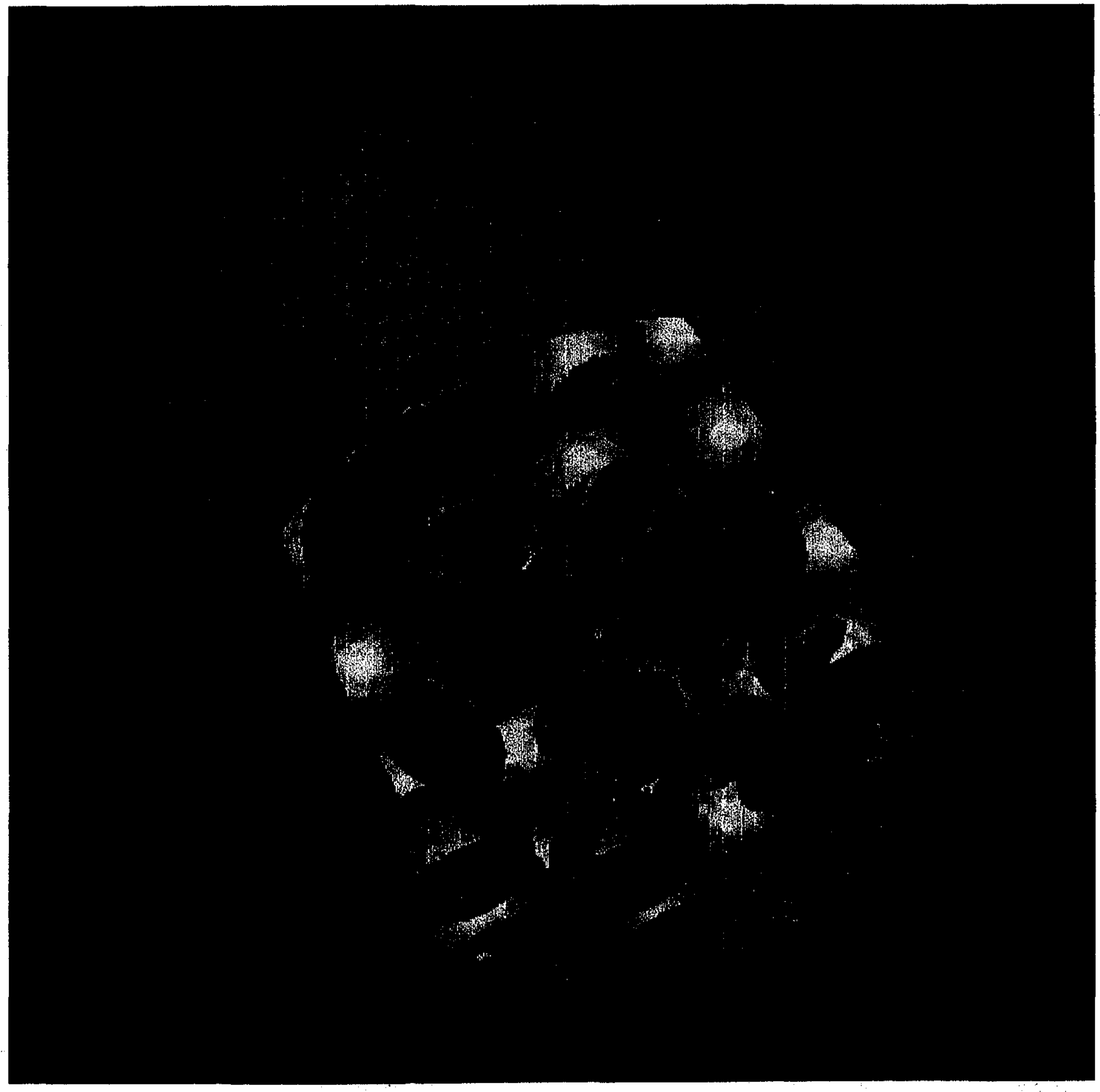

Tomography

Simple Reconstruction Theory

Single Projection

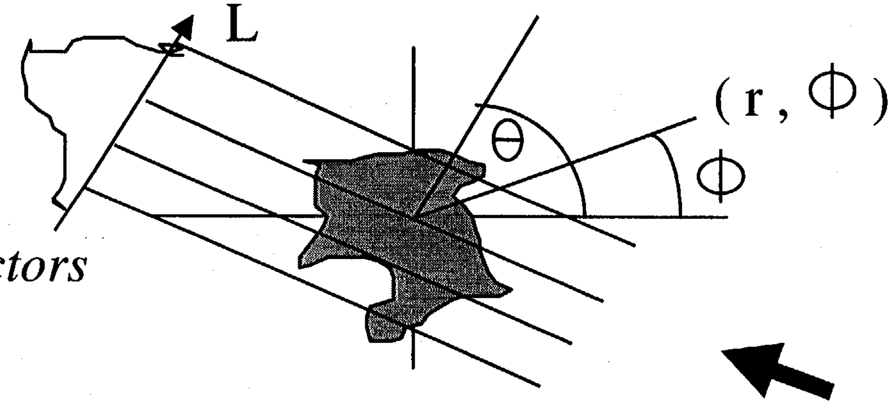

Ray Sum

$$r_\Theta(L) = \int_{lin} \mu(x,y)\, d(lin) = \ln\left[Io(L) / I(L) \right]$$

$$= \int\int \mu(x,y)\, \delta(x\cos\Theta + y\sin\Theta - L)\, dx\, dy$$

Reconstruction

Radon Transform R : relates $\mu(x, y)$ to projection data

$$r_\Theta(L) = [\, \mathbf{R}\, \mu\,](r, \Phi)$$

Data Collection and Reconstruction Requirements

Large data sets are needed to reconstruct volume

Number of Projection Views Required:

$\Pi * N / 2$ **N = Number of pixels in slice(row)**

If resolution requirements allow, Bin pixels for smaller data sets:

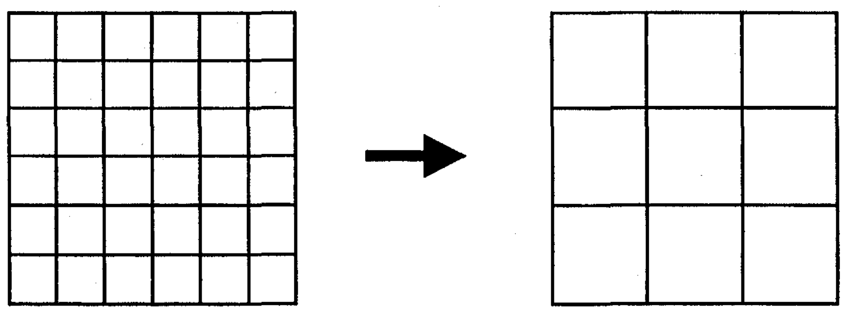

4 x 4 binning

Choose magnification with lens change -- automated

BNL XCMT Apparatus

Brookhaven X-Ray CMT Apparatus

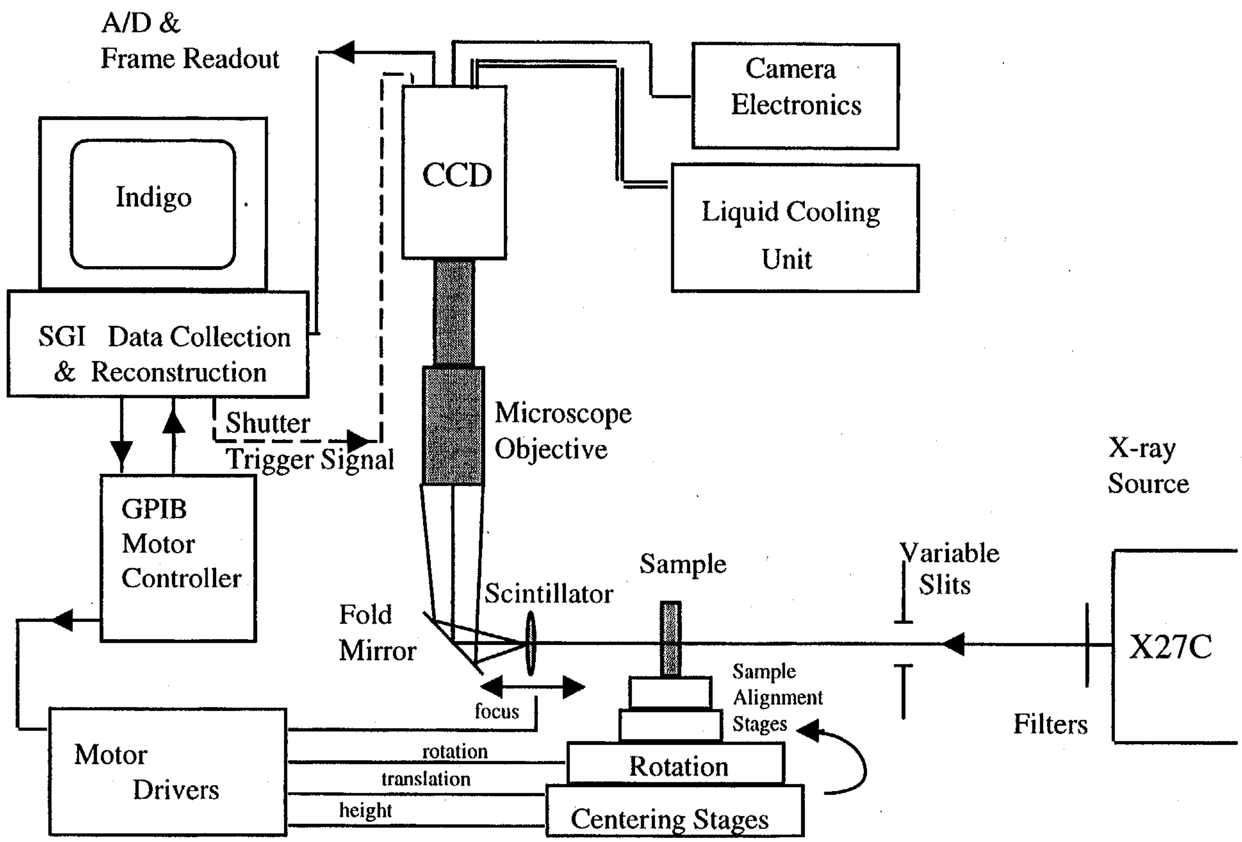

nsls

Data Collection Apparatus : Description

X-Ray Source

- Beamline X27
- Collimated, Monochromator

Image Collection

- YAG scintillator converts X-Ray absorption map to visible
- Commercial optics magnify and reimage phosphor onto CCD detector array
- .75 to 3x zoom lens; 1x, 5x, 10x mag. lens for variable FOV, resolution
- Inexpensive fold mirror allows positioning of CCD & optics at 90 degrees to X-Ray beam & minimizes scatter onto CCD array
- Photometrics cooled CCD camera with Kodak KAF-1400 or KAF-6300 chip

KAF-1400	KAF-6300
1317 x 1035 pixels, 6.8 μm pixel	3072 x 2048 pixels, 9.0 μm pixel
(8.98 mm x 7.04 mm)	(27.65 mm x 18.48 mm)

12 bit dynamic range

2×10^6 pixels/second readout time

Features binning & subarray readout

Data Collection Apparatus (cont.)

Image Collection : Software

- **Graphical Network -- Isee for Image Processing , Data Collection, Data Flow**
- **Ace linked in for motor control, alignment**
- **SGI Indy R5000**

Image Storage & Slice Reconstruction

- **Pre-process raw data, reconstruction using filtered backprojection**
- **Pentiums : Symmetric Multiprocessors (SMP) for processing multiple slices**
- **Fiber Optic Link to SGI Indigo or Reality Engine for volume rendering and viewing**

Volume Rendering & 3-D Viewing

- **Volume rendering software : IRIS , IBM Data Explorer**
- **Crystal Eyes , 3-D visualization facility**

User Facility

User Interface

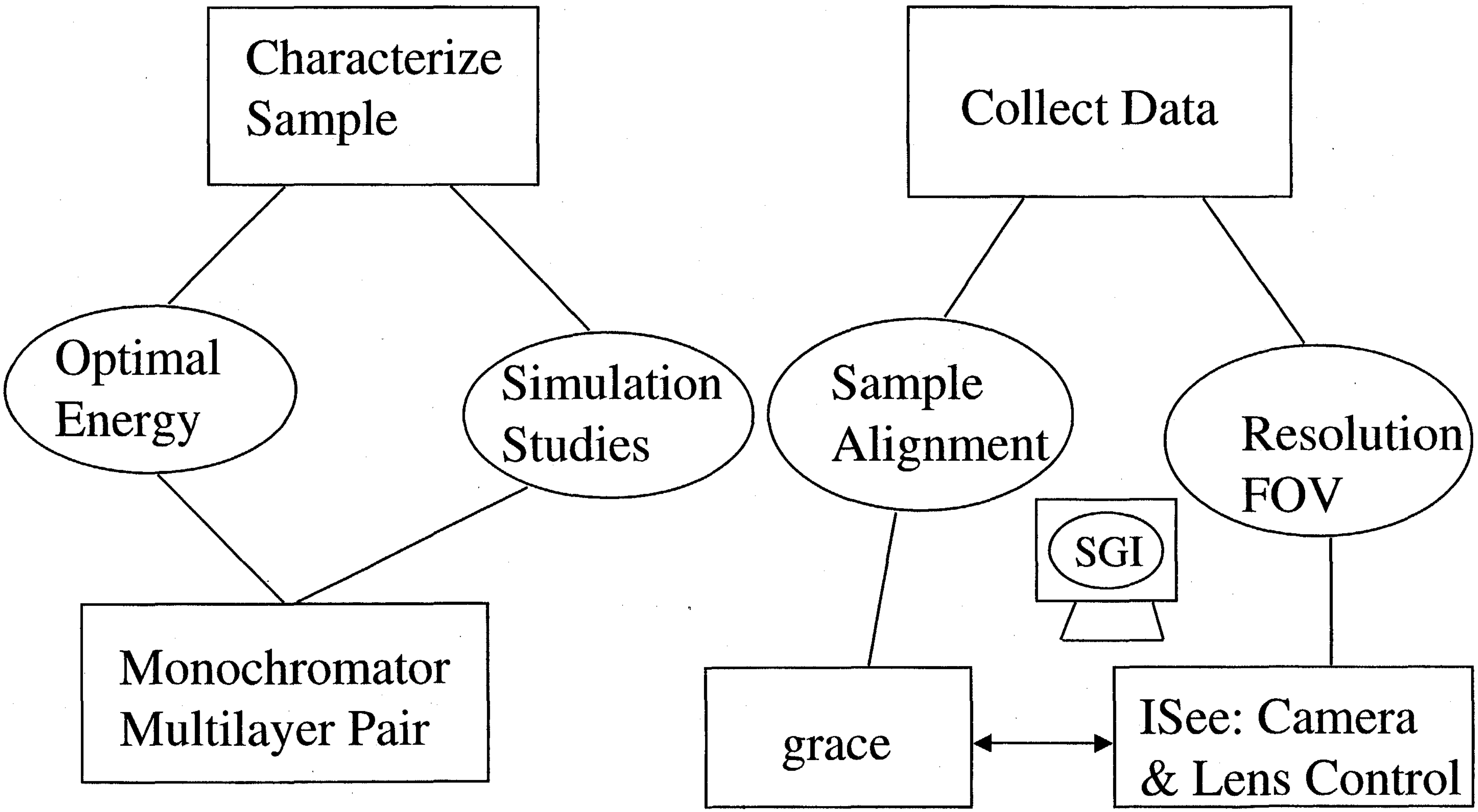

User Interface

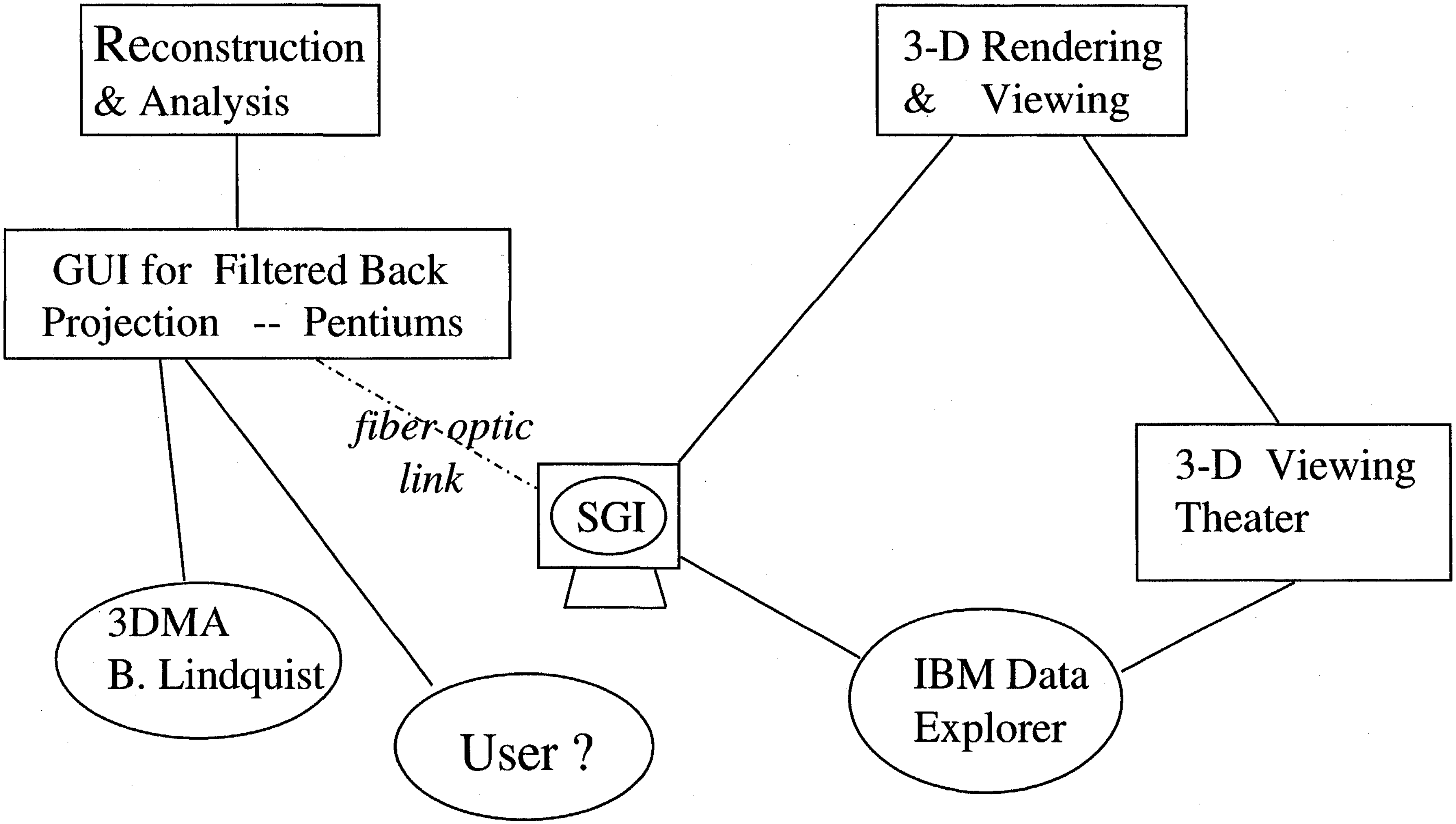

CMT Applications

Reservoir Sandstones

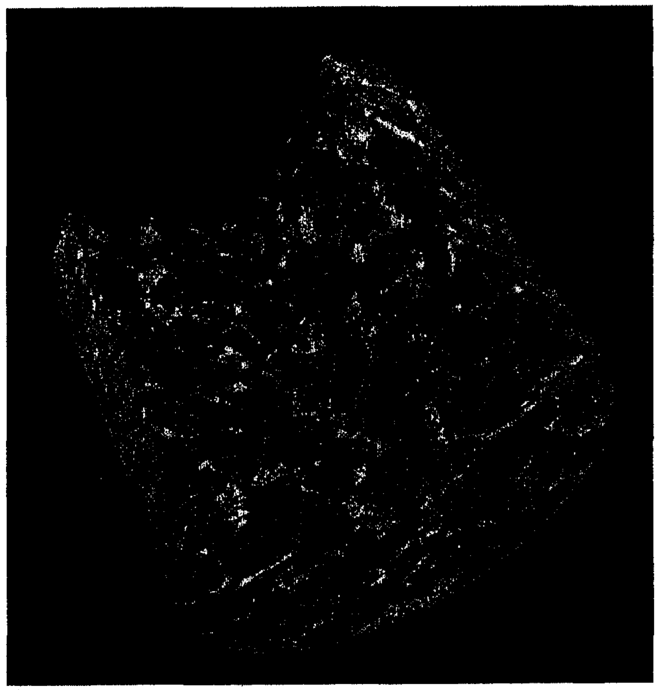

Volume Rendering of a reservoir sandstone from X-Ray CMT , D= 2mm
Pores (blue) are on the order of 15 to 20 microns

Literature References

Developments in Synchrotron X-Ray Microtomography with Applications to Flow in Porous Media

M.E. Coles, SPE, R.D. Hazlett, and E.L. Muegge, Mobil E & P Technical Center.
K.W. Jones, B,Andrews, B.Dowd,P. Siddons, & A. Peskin, NSLS.
P. Spanne, ESRF
W.E. Soll, Los Alamos National Laboratory

SPE 36531 : Presented at the 1996 SPE Annual Technical Conference and Exhibition, Denver, Colorado, 6-9 October 1996.

Work funded in part by ACTI grant from USDOE DE-AC0276CH00016

Reservoir Sandstone : Mobil Corporation

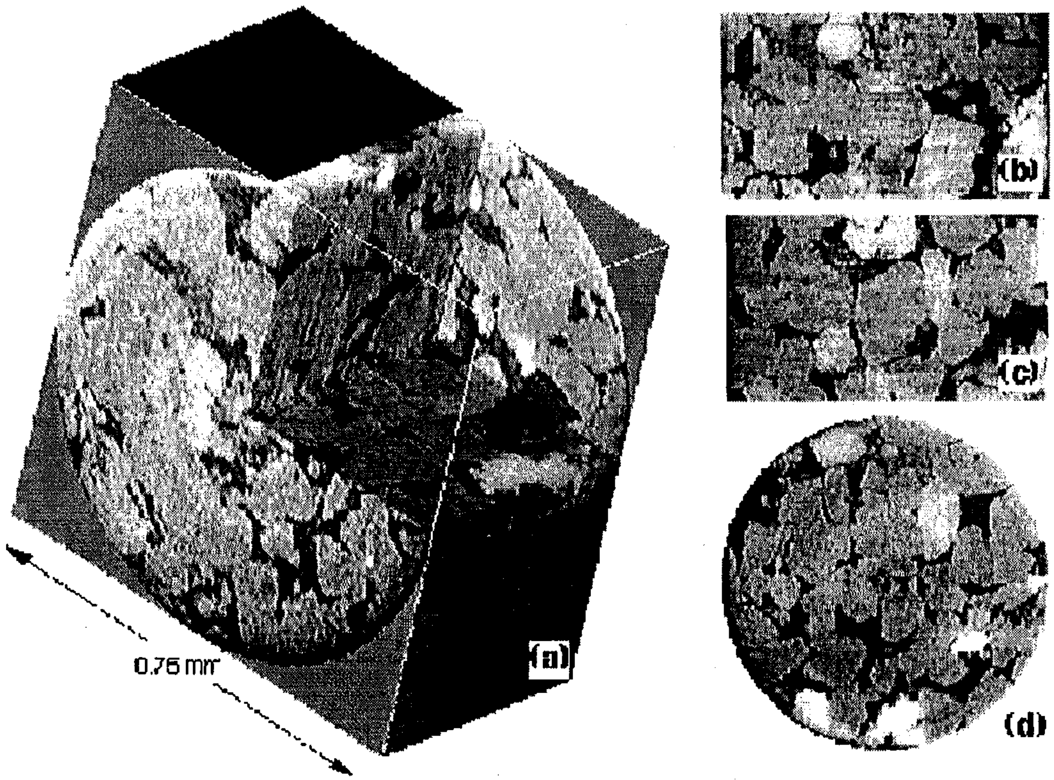

Reservoir Sandstone : Mobil Corporation

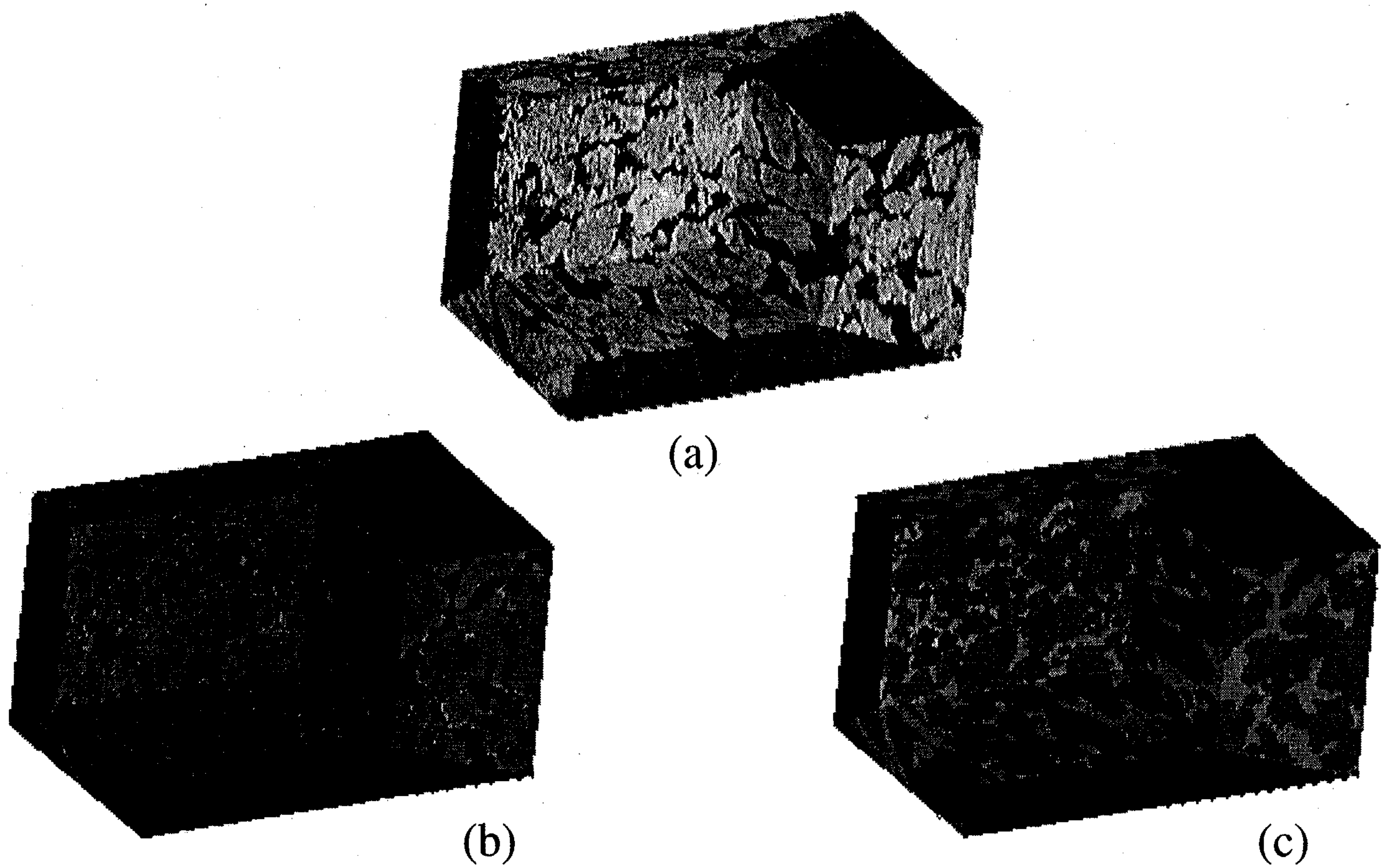

Figure 7. 3-D Cutaway images of a 5.8 darcy producing reservoir sandstone and network model predicted fluid distributions: a). CMT volume image, b). S_{iw} image, c). S_{or} image. Gray = rock; black = oil; white = water.

Reservoir Seal Rock : Mobil Corporation

Figure A-1 a
Mercury Porosimeter Data
Seal Rock GOM 10,000 ft

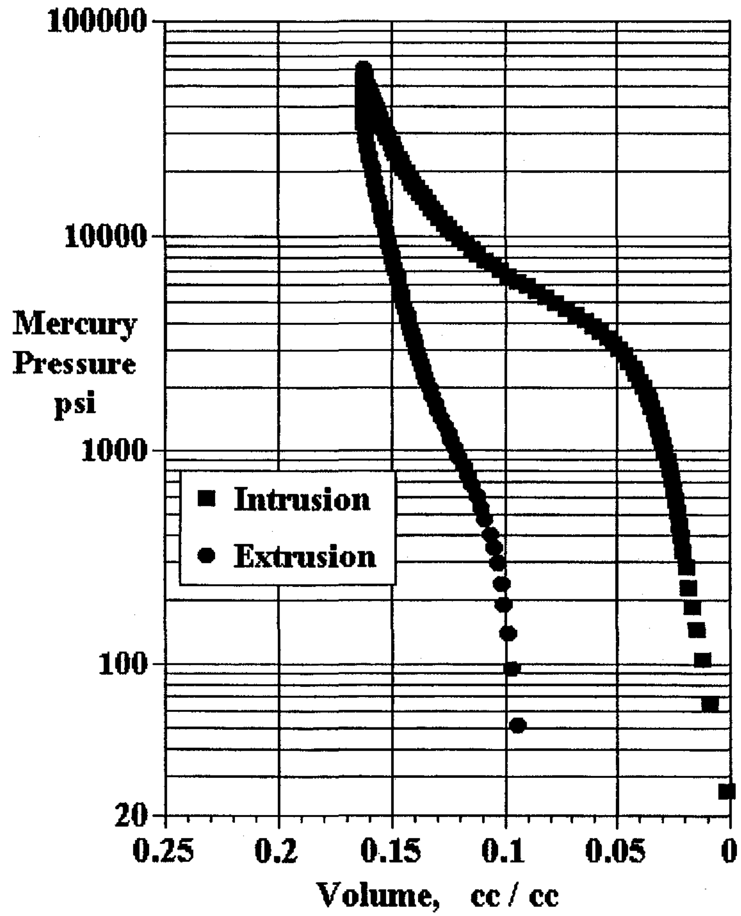

X-Ray Microtomography Applications to the Characterization of Oil Reservoir Seal and Source Lithologies

Weldon Bell, R.D.Hazlett (Mobil Corp.)
B.Andrews, B.A.Dowd, K.W.Jones, A. Peskin, D.P. Siddons (BNL)

BNL 52517 : Abstract in NSLS Activity Report 1996

Reservoir Seal Rock : Mobil Corporation

Hydrocarbons (oil & gas) migrate through porous rocks in the reservoir, primarily upward. The barriers to further upward migration are called seals. The physical properties of the seal help determine holdup, flow and leak rate, accumulation of oil and its quality.

Studies of seal rock properties is ongoing. The material examined seals a deep producing reservoir in the Gulf of Mexico. Mercury porosimetry data shows significant pore sizes (necks and bodies) distributed around 400 & 2000 A diameters.

Figure A-1 c.: Hg Extrusion Poresize Distribution

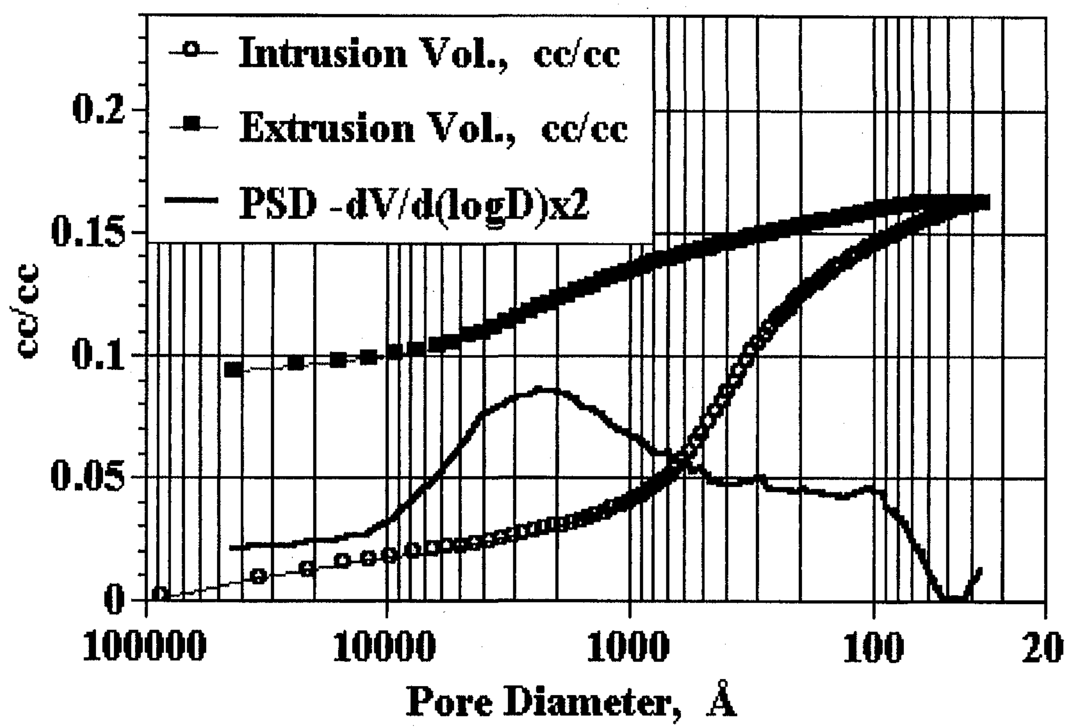

nsls

Reservoir Seal Rock

Figure A-1 b.: Hg Intrusion Poresize Distribution

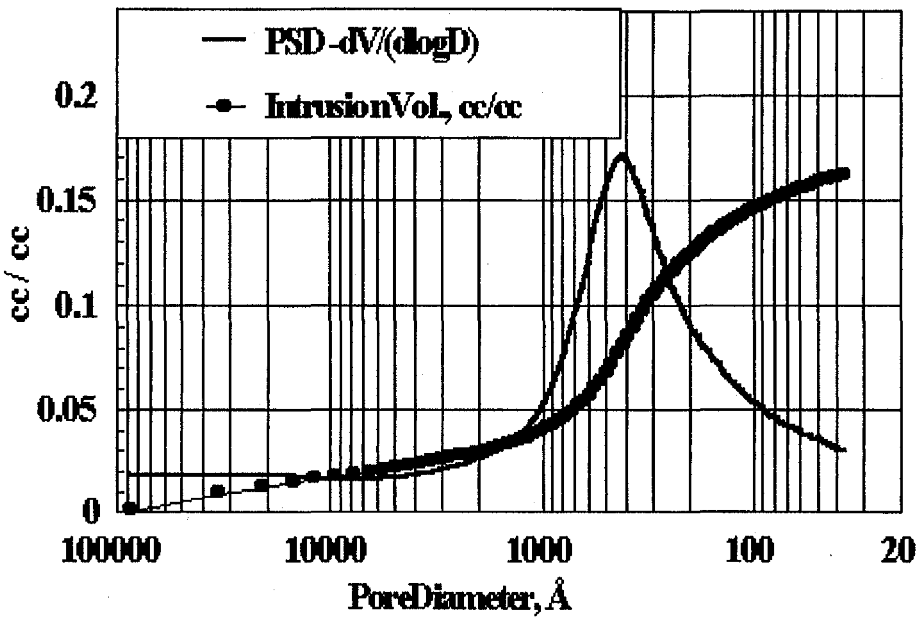

Status: Pore structure below resolution of CMT, however we have demonstrated ability to image fractures and unexpected voids; spatial distribution of minerals is also an area of interest.

nsls IR UV X

Subvolume Reconstruction

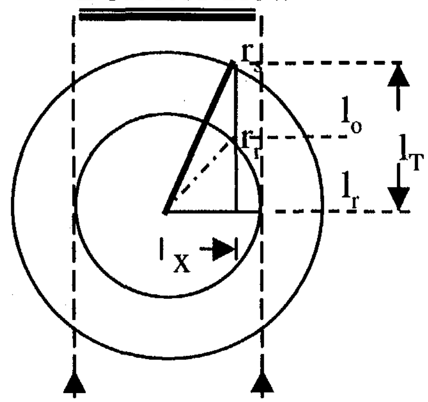

— r_r = radius of reconstructed area

-·· r_s = radius of sample

$2l_o$ = length of beam path outside reconstructed area

$2l_r$ = length of beam path through reconstructed area

Path lengths are a function of x, distance from the center of circle, which coincides with the center of the pixel row. From the geometry:

$$2l_o(x) = 2\left(\sqrt{r_s^2 - x^2} - \sqrt{r_r^2 - x^2}\right)$$

An average value of mu per pixel for the entire sample is calculated from the data. Each detector signal is then scaled by the factor $\exp[\mu\, l_o(x)]$ to effectively subtract out the effect of beam attenuation through the unreconstructed area.

This scaled data is then used to reconstruct the subvolume of interest.

Subvolumes

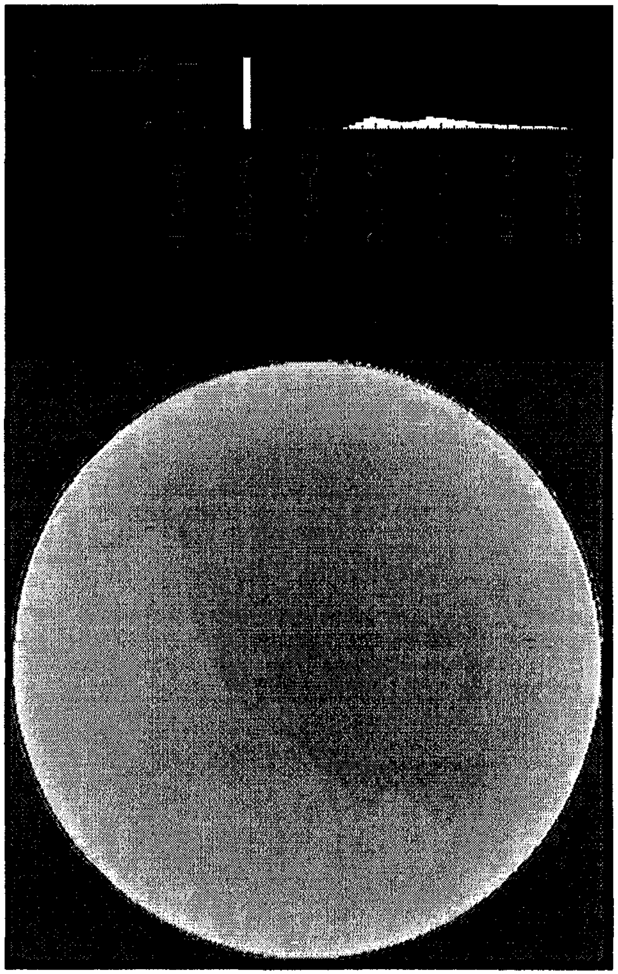

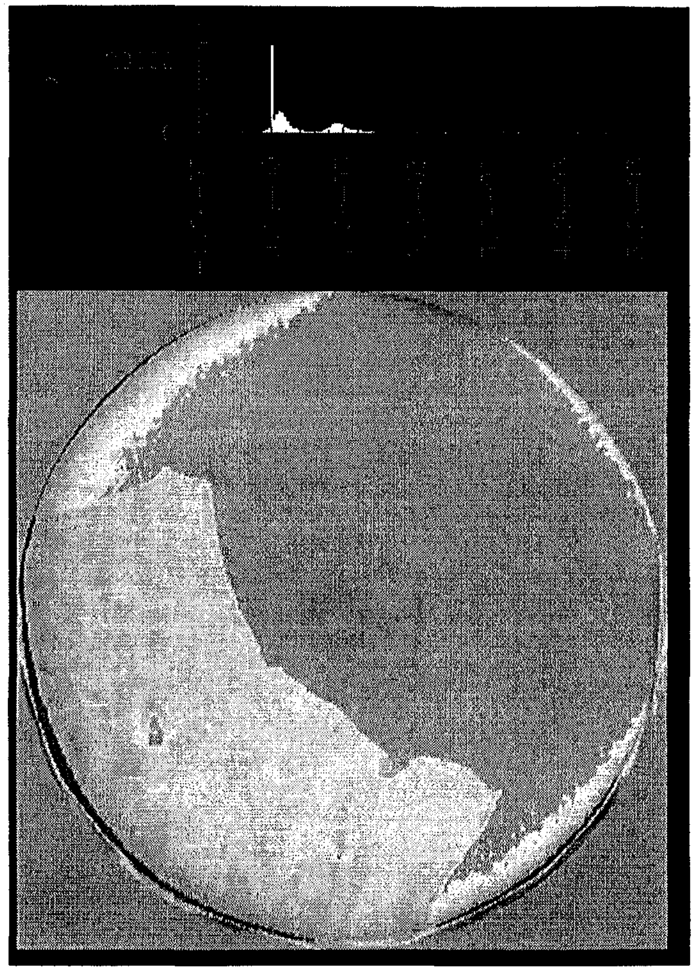

Basalts : Univ. of NH, National Taiwan Univ.

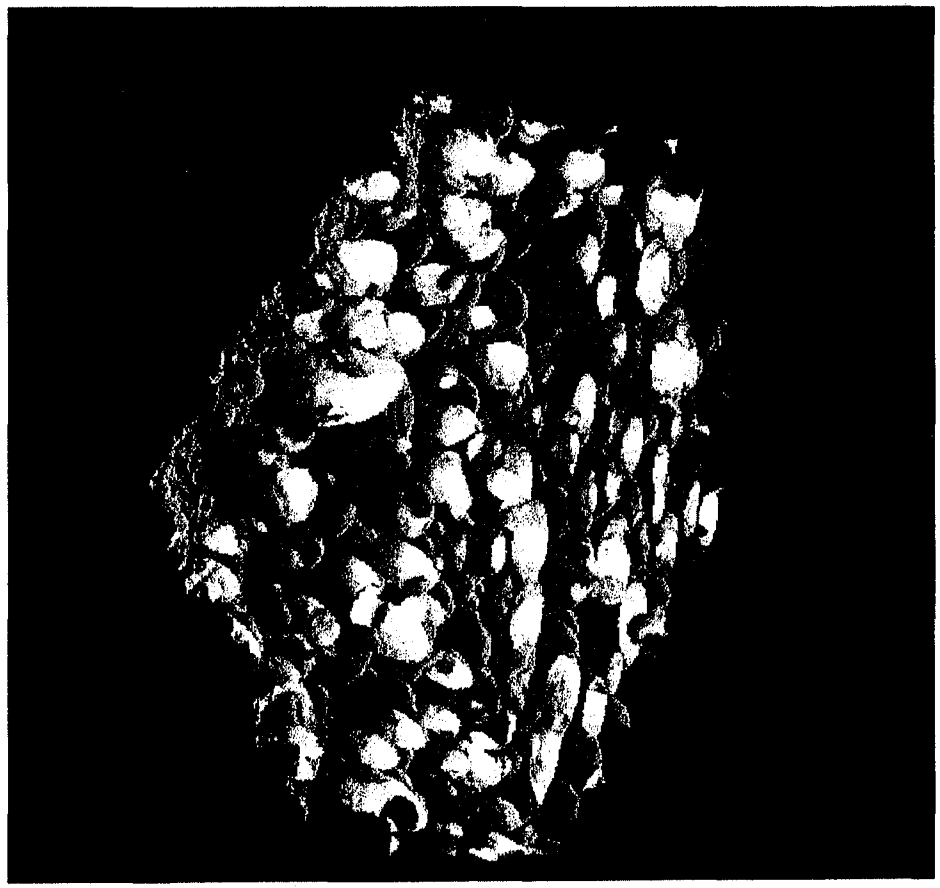

CMT is being used to
study the shape and size
distribution of
bubbles in basaltic lava flow.

Reference:

X-Ray Microrography of Basalts

D. Sahagian (UNH), B.A.Dowd, K.W. Jones, D.P. Siddons (NSLS), S-R Song (Nat. Univ. of Taiwan)

BNL 52517: Abstract in NSLS 1996 Activity Report

Porous Metals : Grumman - Northrop

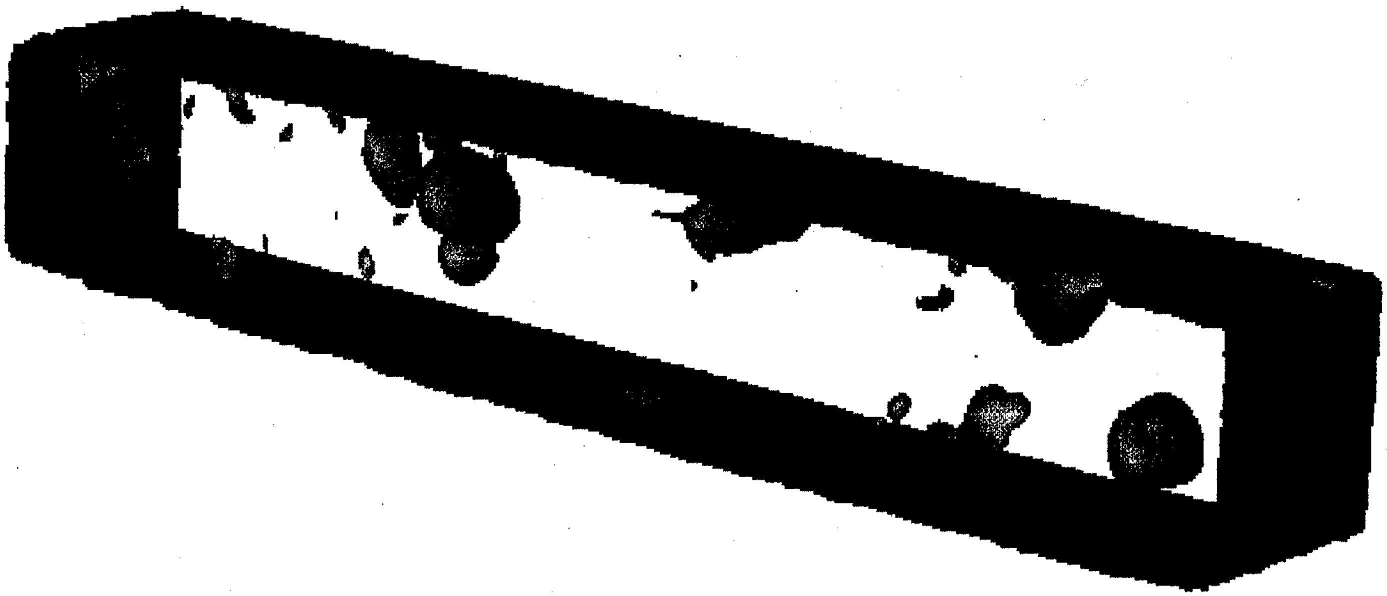

nsls

Fungal Deterioration in Wood

Reference:

Synchrotron Applications in Forestry and Forest Products

B.Illman, USDA/FS Forest Products Lab., Univ. of Wisc.

B.A.Dowd, NSLS

Synchrotron Radiation News, Vol 10:2,March/April 1997

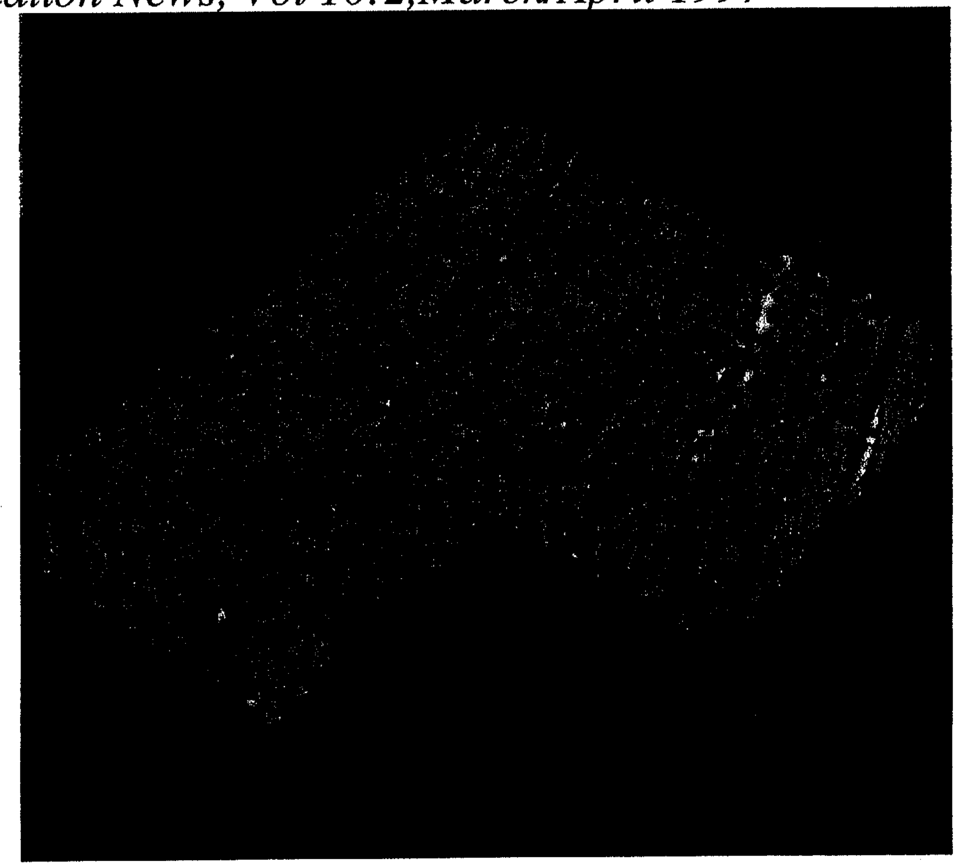

nsls IR UV X

Future Plans

- **Addition of Monochromator for Source Energy Optimization for Contrast Enhancement & Reduction of beam hardening artifacts**
  (*completed -- September 1997*)

- **Combine 3rd generation scheme with scanning (1st generation) technique to cover large samples without loss of resolution from zooming out**

- **Two dedicated X-Ray Microtomography Stations**
  - **PRT, User-dedicated facility**
  - **R&D facility for various tomographic techniques, such as phase contrast, fluorescence, edge-enhancement techniques, k-edge subtraction**

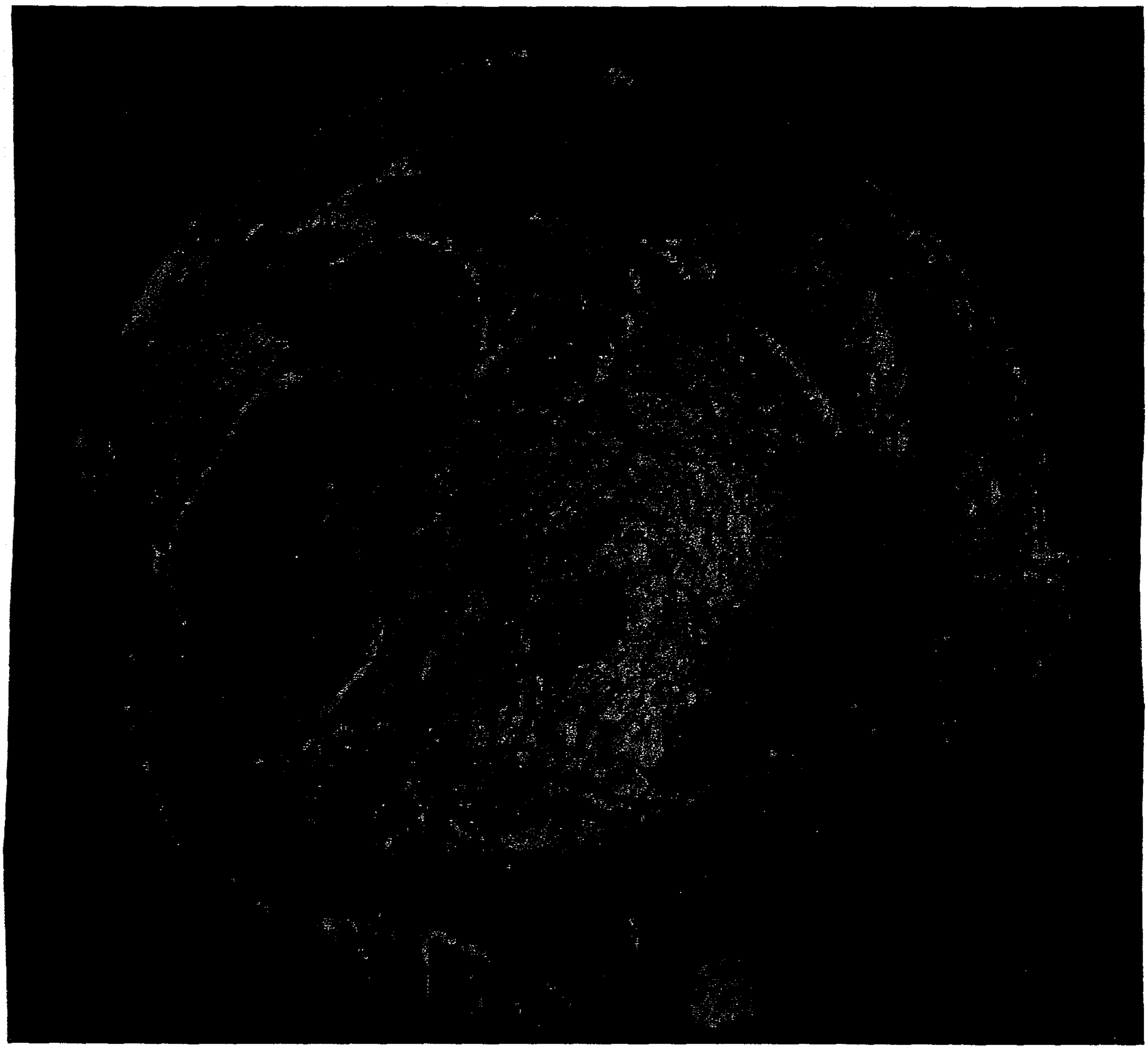

Figure 1. 3-dimensional image of beetle head reconstructed

Part VI

Barbara Illman
USDA/FS Forest Products Laboratory, University of Wisconsin

"XCMT Applications in Forestry and Forest Products"

MICROTOMOGRAPHY APPLICATIONS IN FORESTRY AND FOREST PRODUCTS

INTRODUCTION

Synchrotron x-ray techniques are being applied to problems in forestry and forest products. The research in conducted at the National Synchrotron Light Source (NSLS) at Brookhaven National Laboratory with current work on x-ray computed and microtomography at beamline X27. The problems that we are studying have fundamental similarities: the dynamic interaction of organisms and the chemical mechanisms responsible for the interactions

FOREST ECOLOGY

Several beamlines at the NSLS are being used to answer important questions about one of the most damaging insects affecting North American forests. Spruce ecosystems of Alaska are currently affected by outbreaks of the spruce bark beetle, *Dendroctonus rufipennis* (Kirby) and its symbiont fungi. Forests of white and Lutz spruce are subject to mortality from the bark beetle, where infestations have expanded throughout south-central Alaska since 1974 and have killed trees on over a million acres of forest. These large-scale outbreaks can affect forest community structure and successional pathways. The beetles' ability to exploit the forest resource is augmented by their pheromonally mediated cooperative behavior and their associations with microbial symbionts. Spruce-bark beetle-fungal systems offer an opportunity to evaluate the effects of ecological interactions across multiple spatial and temporal scales, across multiple trophic levels, and among diverse taxa. Understanding these relationships could greatly improve our ability to evaluate and devise appropriate forest management practices, and anticipate the impacts of multiple abiotic, biotic, and anthropocentric stresses.

We are using computed microtomography (CMT) to better understand beetle structure and function, to assist in identification of fungal species, and to locate fungi on/in beetles in order to determine the insect system(s) used to vector the symbiont into trees. CMT has been used to provide information about beetle structure. In the following figure, a microphotograph of a beetle head is given with three microtomography reconstructions of slices from the head and one microtomography reconstruction of head volume as seen from the bottom. The CMT images provide needed information about the juxtaposition of circulatory and respiratory systems, about cytoskeleton relation to eye and mouth parts, and about density-determined differences between internal structures and an unknown high density region found in the beetle.

BIODETERIORATION OF WOOD

Initial CMT images of fungal decay of wood is given in the following figure. Intact wood structures are resolved at about 3 microns in microtomographic reconstructions of wood volumes without fungal degradation (Figure 3a). In the reconstructions in Figure 3b, destruction of wood structures can be seen in wood during degradation by the wood decay fungus, *Postia placentae*. Availability of microtomography will aid in answering several questions about the mechanisms of fungal degradation of lignocellulose.

FUTURE RESEARCH

Many problems in forestry and forest products can be addressed using synchrotron technologies. CMT will be used with synchrotron x-ray fluorescence spectroscopy (SXRT) and x-ray absorption spectroscopy (XAS). CMT will be used to image the micro-environment of tree - insect - fungal interaction, pine root - fungal - soil relationships, and time-dependent wood - fungal relationships.

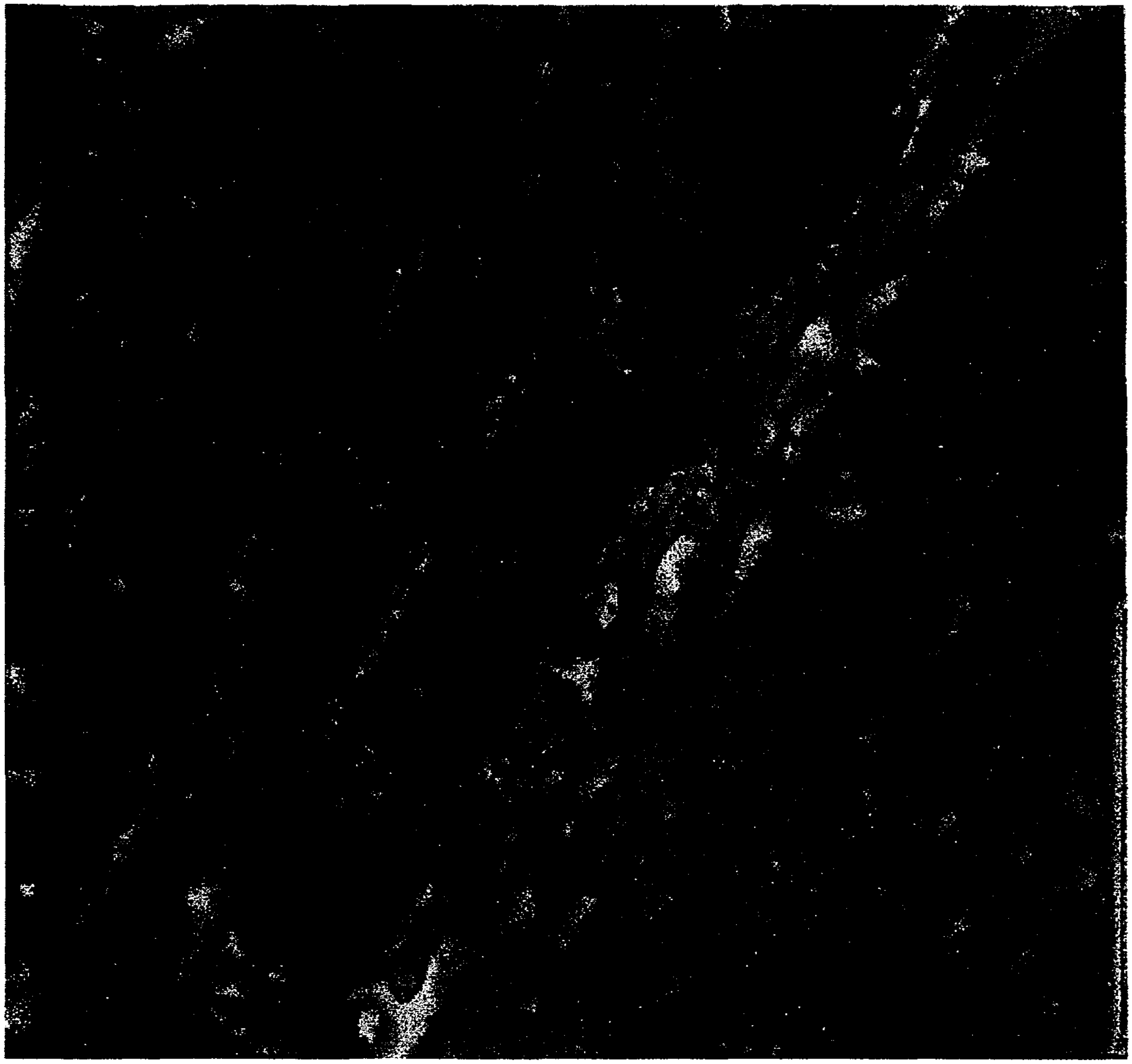

Figure 2. Microphotography and four microtomographic reconstructions of the spruce bark beetle. Dendroctonus rufipennis.

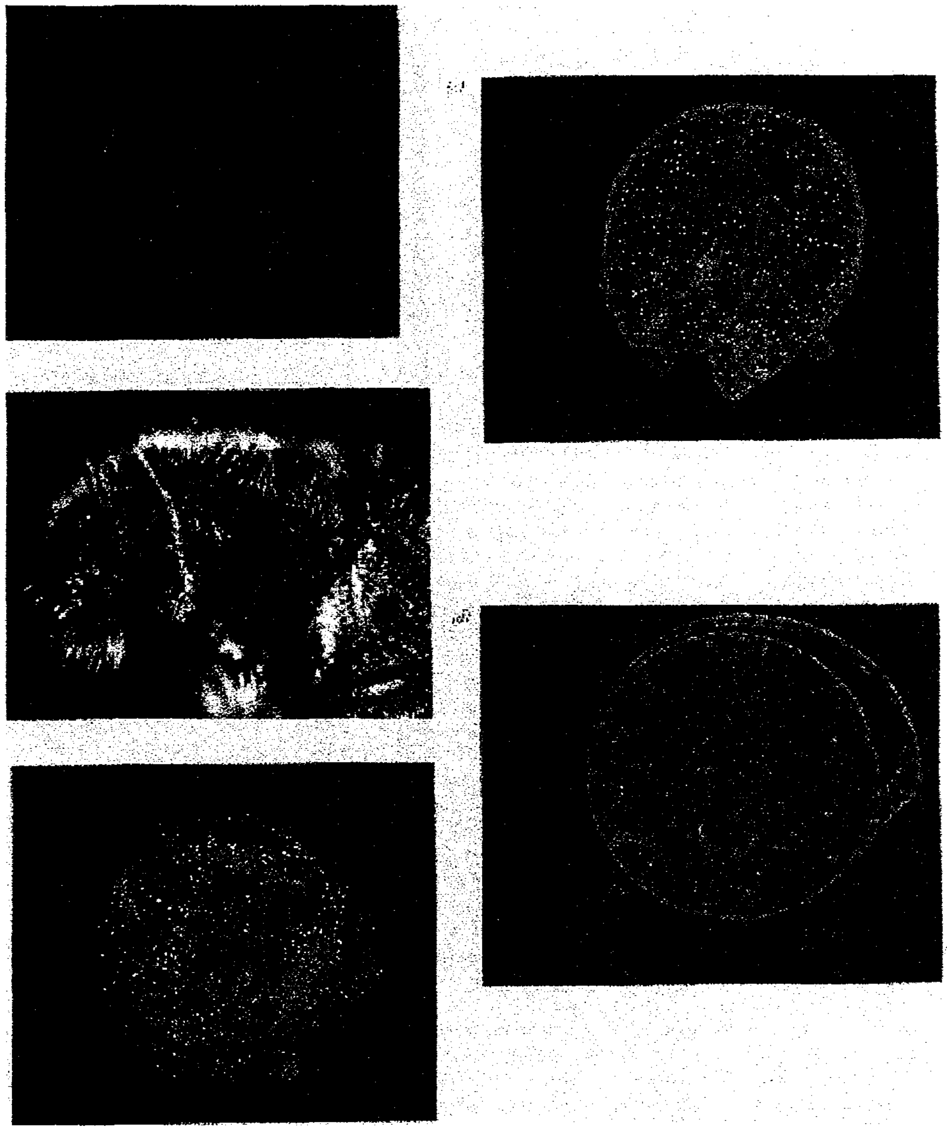

Figure 3. Microtomography of wood structures taken from the interior of a solid piece of wood.

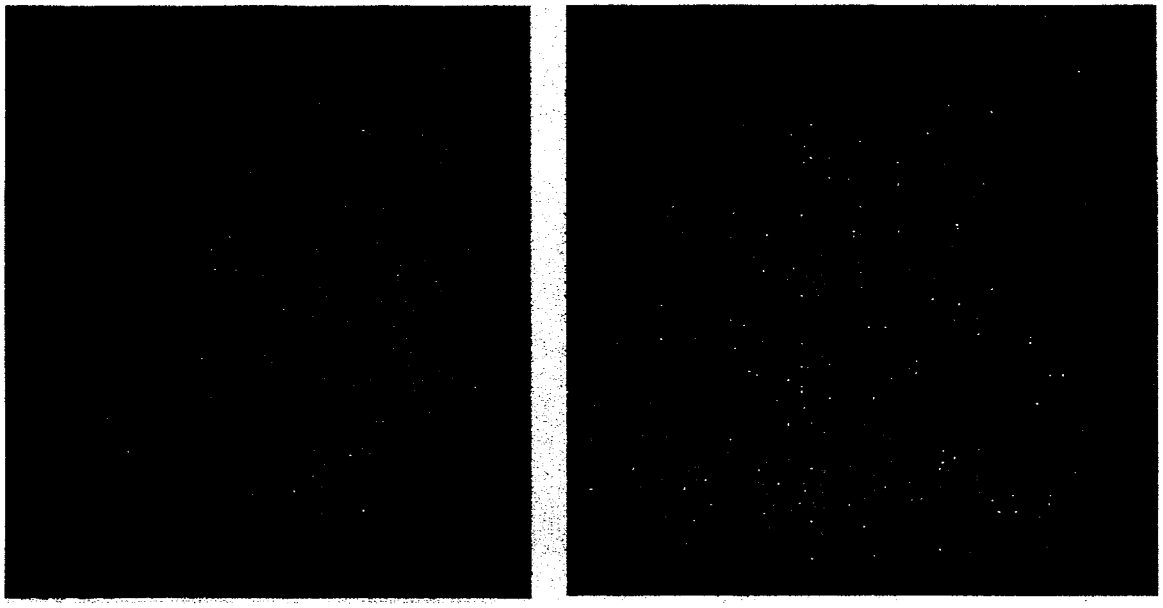

Figure 4. Microtomographic reconstruction of pine wood. (a) Reconstructed volume of solid wood without degradation by fungi. (b) Reconstructed volume of wood degraded by the brown-rot fungus, Postia placenta.

Part VII

Brent Lindquist
SUNY, Stony Brook

"3DMA: Investigating Three Dimensional Pore Geometry from High Resolution Images"

3DMA:

Investigating Pore Geometry using Tomography, Computational Geometry, Graph Theory and Statistics

Brent Lindquist

SUNY - Stony Brook and UT - Austin

Joanne Fredrich

Sandia National Laboratories

Arun Venkatarangan
Hyunmi Yang, Wonho Oh

SUNY - Stony Brook

David Coker

SUNYIT - Utica

Images courtesy

- Joanne Fredrich (Sandia)
- Keith Jones, Sheng Rong Song (BNL)
- John Dunsmuir (Exxon)
- Mark Perkins (KCC)
- Loveena Kapur (UT)

Research Support

- U.S. DOE Geosciences Program
- Sandia National Laboratories
- Kimberly–Clark Corporation
- Exxon Research and Engineering Company

Goal: development of computational tools to provide routine geometric analysis of volumes

$$512^3 \rightarrow 1024^3$$

data set + (small) input file | 3DMA > **output**

data set: tomographic data file

output:

distributions
visuals
predictions

- freeware
  ftp://www.ticam/pub/lindquis
  med_ax_mar97.tar.gz
- manual on www
  http://tomo.sunyit.edu/coker

Rock properties are stochastic

→ measure distributions

- quantify form of distribution
- predictive value of first moment (average)
  eg. Carman-Kozeny

$$K = \frac{\phi^3}{2\tau(1-\phi)^2\alpha_s^2}$$

Rock structure is 3D

→ Volumes instead of thin sections

- 2D observations can only capture isotropic 3D scalars

3D tomographic image

- synchrotron X-ray
- laser scanning confocal

Segmentation

- diffusion-based
- kriging

Erosion

- medial surface
- medial axis

Pore geometry

- porosity
- specific surface area
- pore size distribution
- 2-point covariance/variogram
- throats/nodal pores
- coordination numbers
- path length/tortuosity

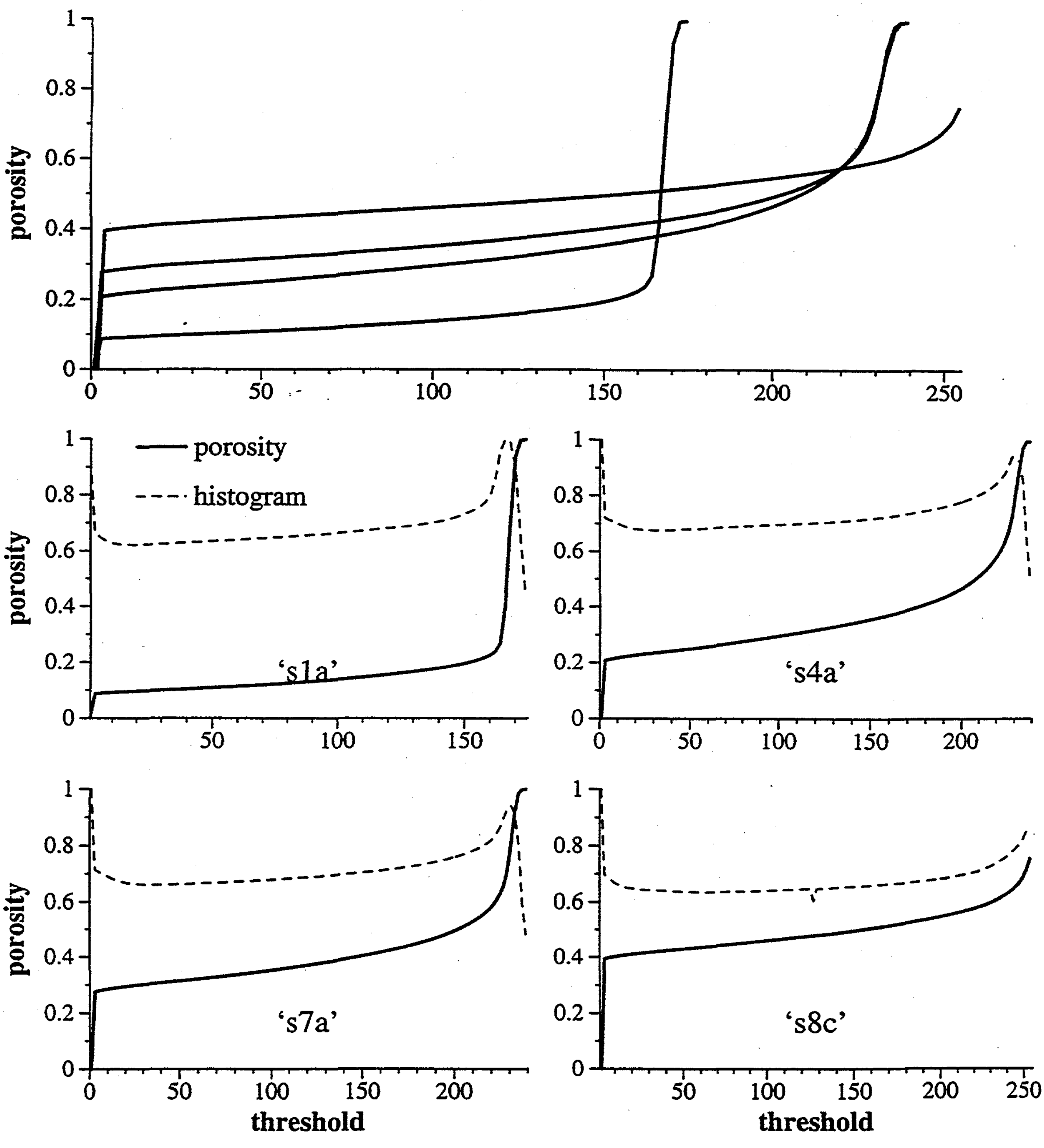

porosity
threshold
porosity
histogram
's1a'
's4a'
's7a'
's8c'

diffusion-based image enchancement

$$I_n(x) = \nabla \cdot [c_{n-1}(x) \nabla I_{n-1}(x)] \ . \qquad (1)$$

$$c_n(x) = g(\|\nabla I_n(x)\|) \ . \qquad (2)$$

$$g(\|\nabla I\|) = \exp\left(- \left(\frac{\|\nabla I\|}{K} \right)^2 \right) \ . \qquad (3)$$

Inside an object, ∇I small, $g(\cdot) \approx 1$.

Across edges, ∇I large, $g(\cdot) \approx 0$.

Privileges high-contrast edges over low-contrast edges.

Segmentation by Kriging
w. oh

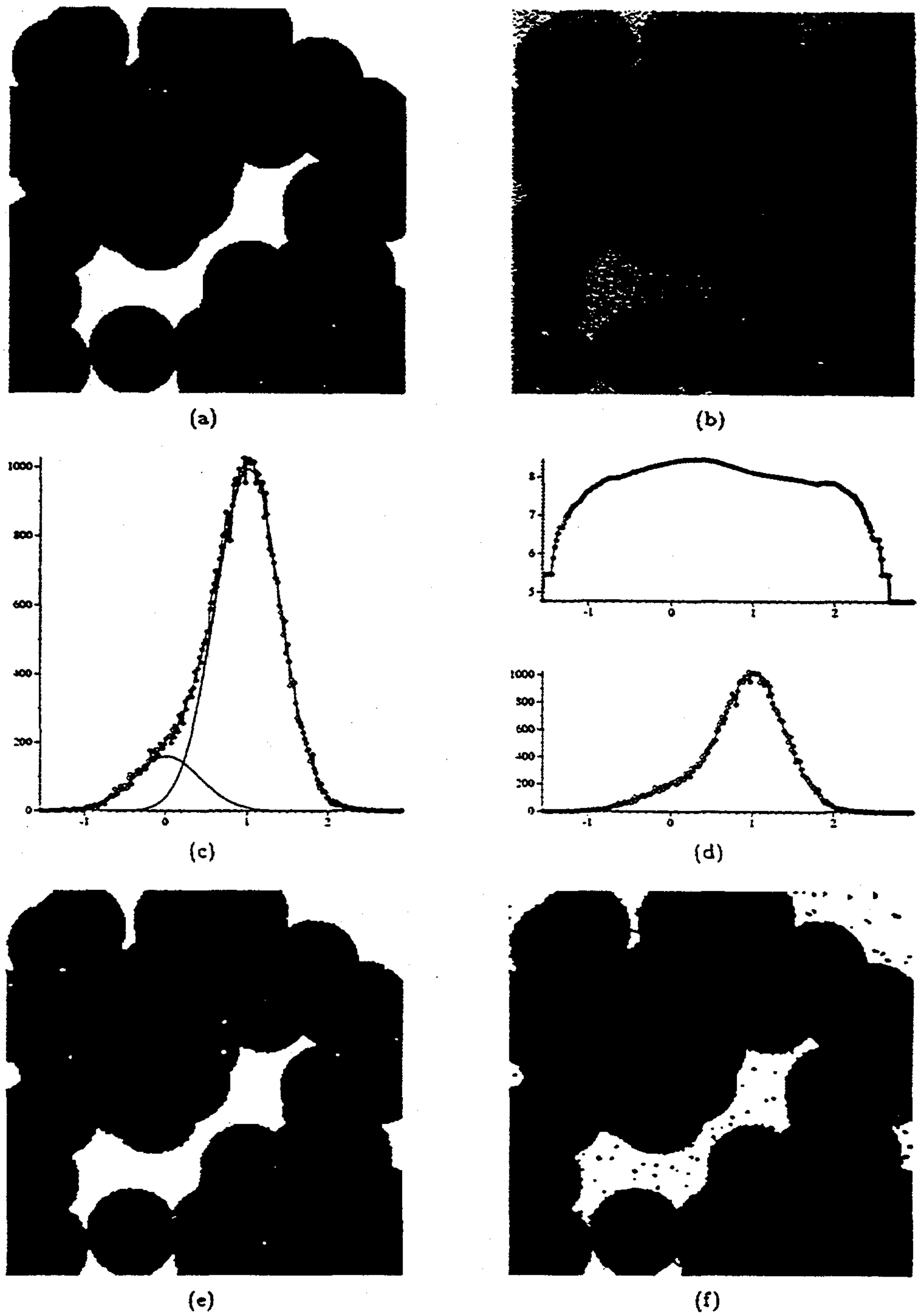

Figure 3: Result for $\sigma_w = 0.4, \sigma_b = 0.4$

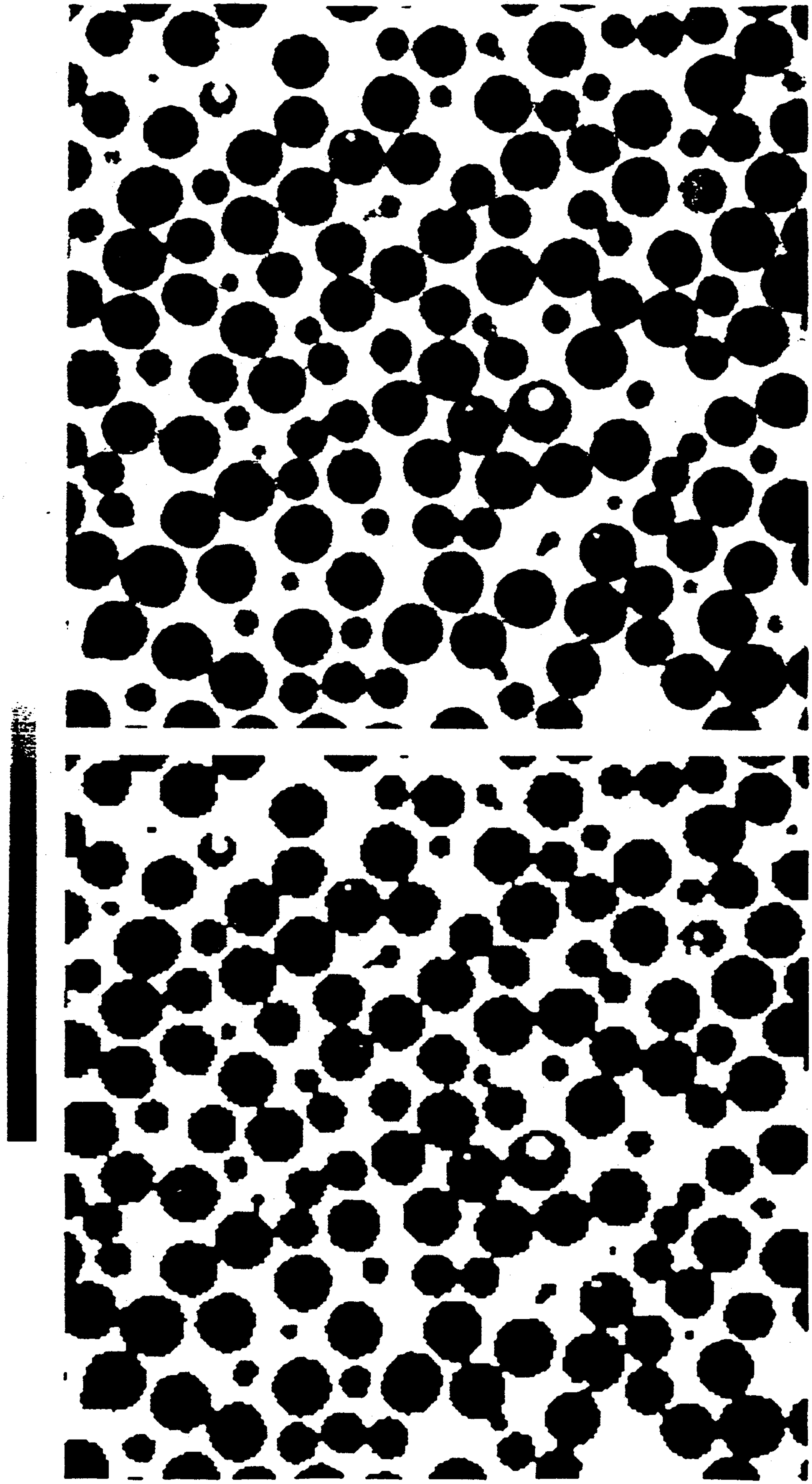

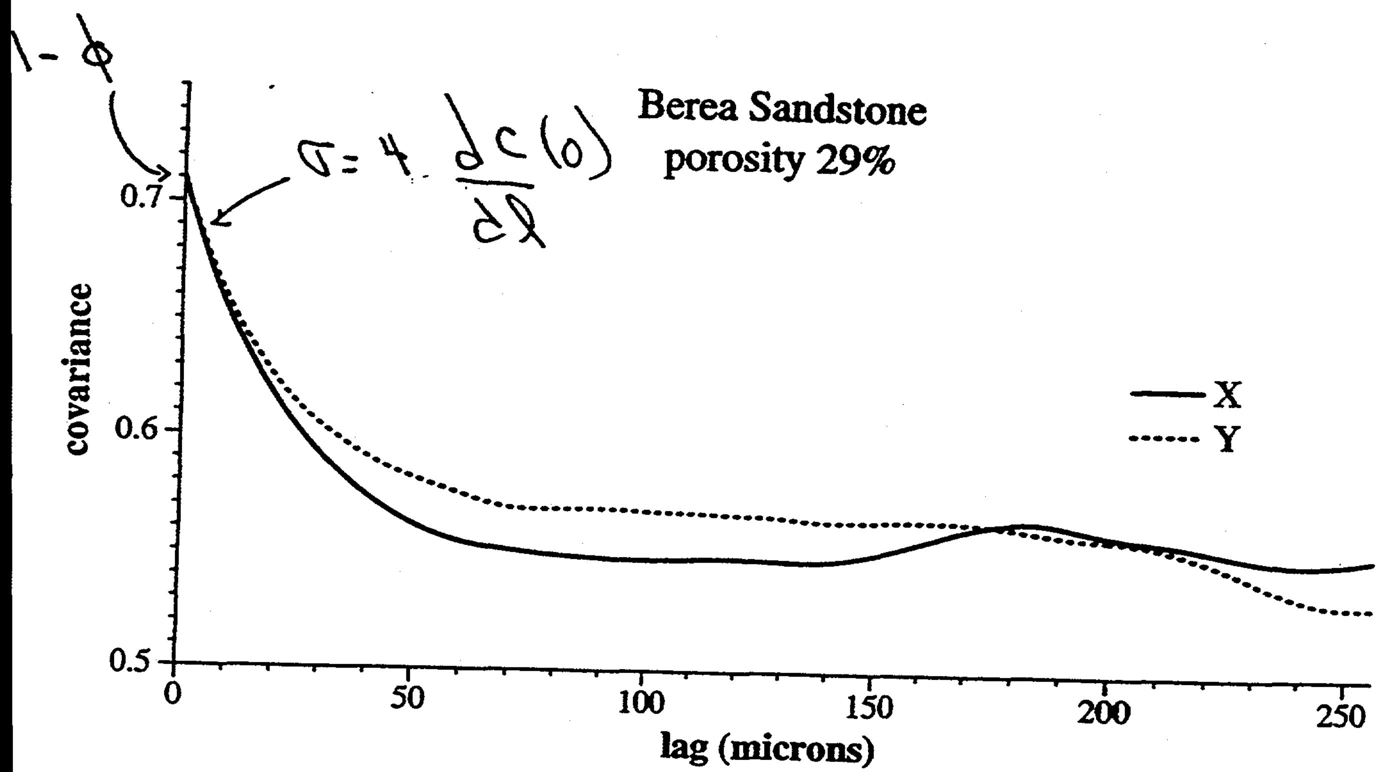

1 - φ
σ = 4 dC(0)/dl
Berea Sandstone
porosity 29%
covariance
0.7
0.6
0.5
X
Y
0
50
100
150
200
250
lag (microns)

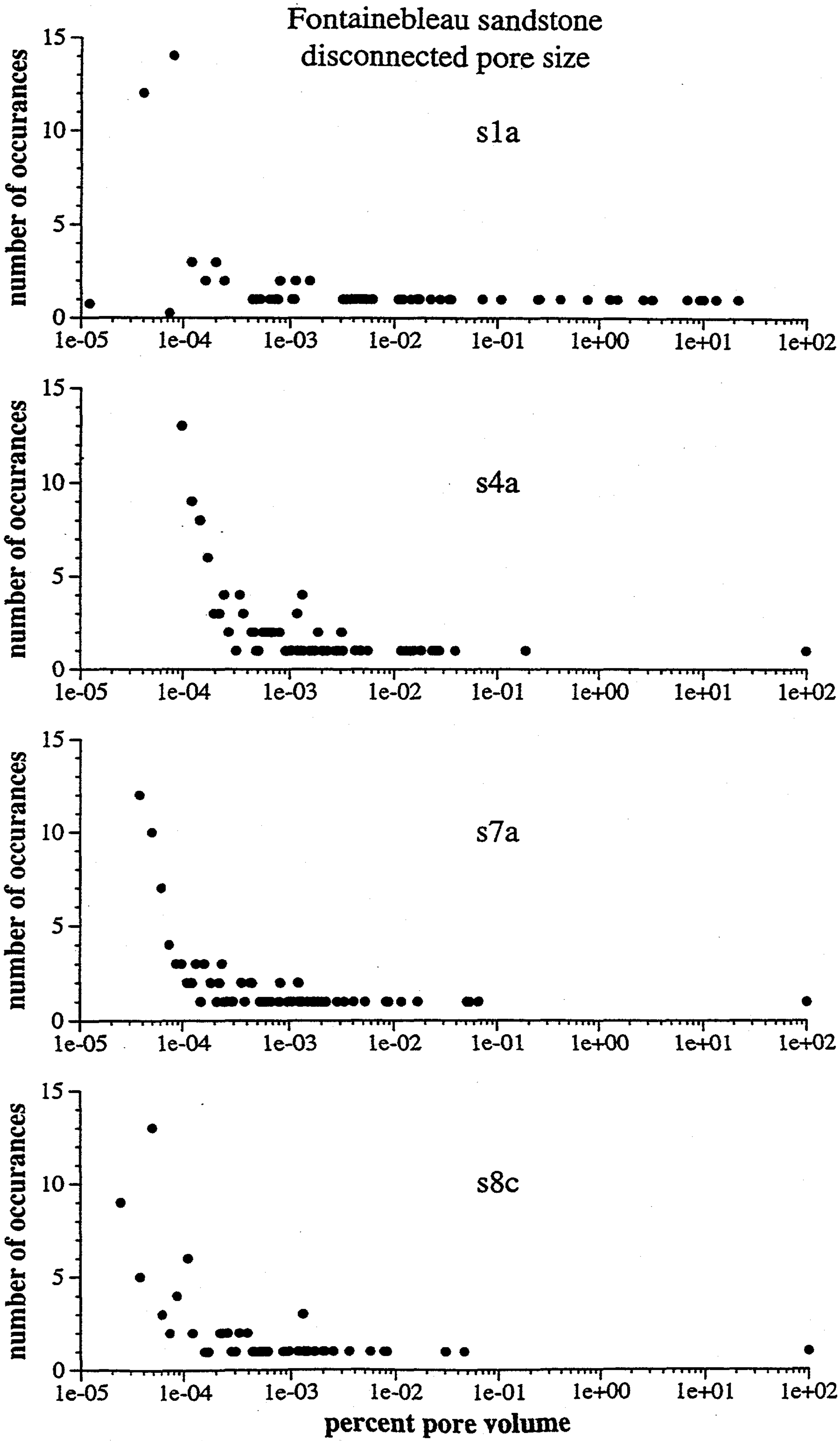
Fontainebleau sandstone
disconnected pore size
s1a
s4a
s7a
s8c
number of occurances
0
5
10
15
1e-05
1e-04
1e-03
1e-02
1e-01
1e+00
1e+01
1e+02
percent pore volume

Sandstones
Erosion distributions

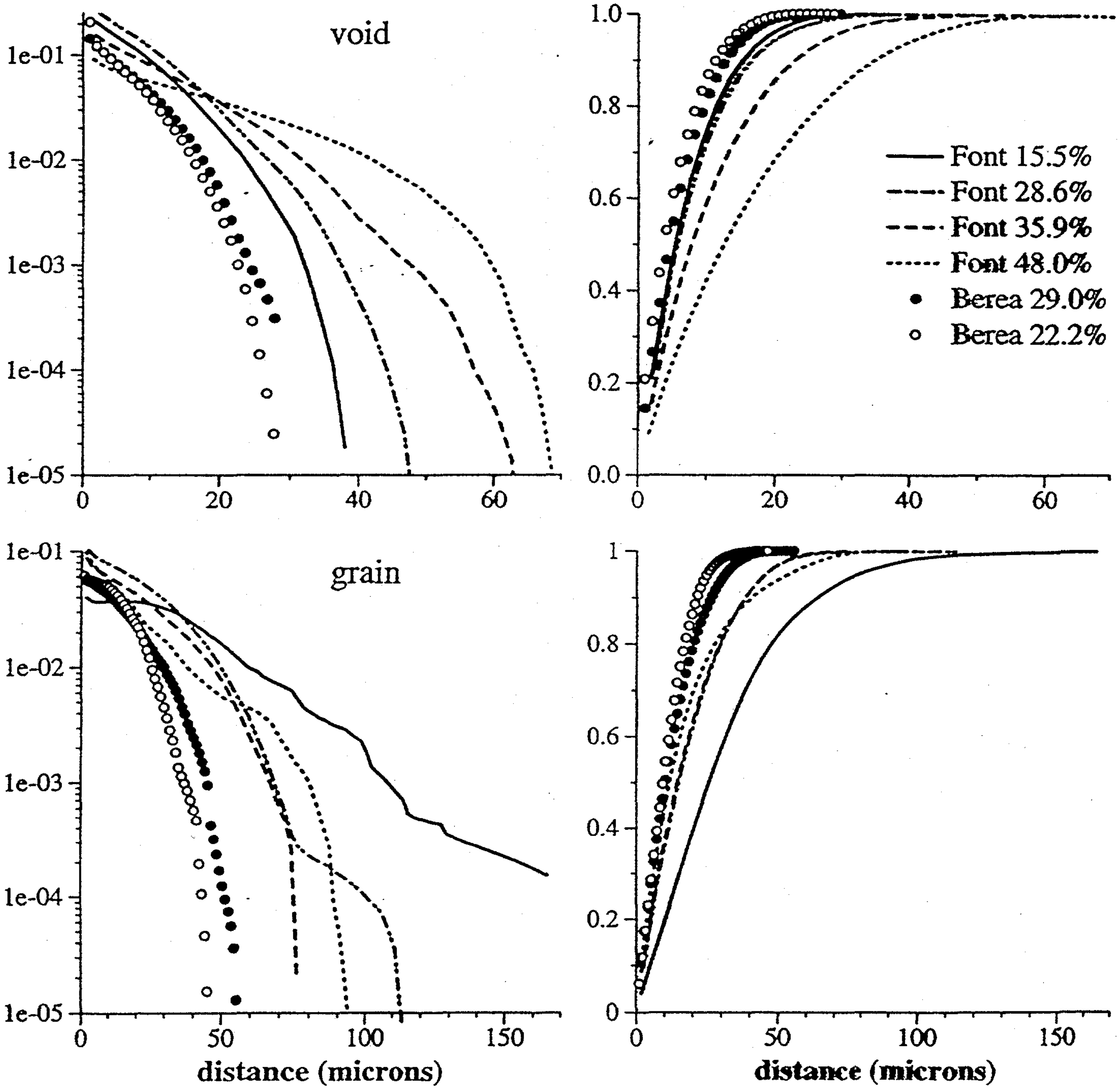

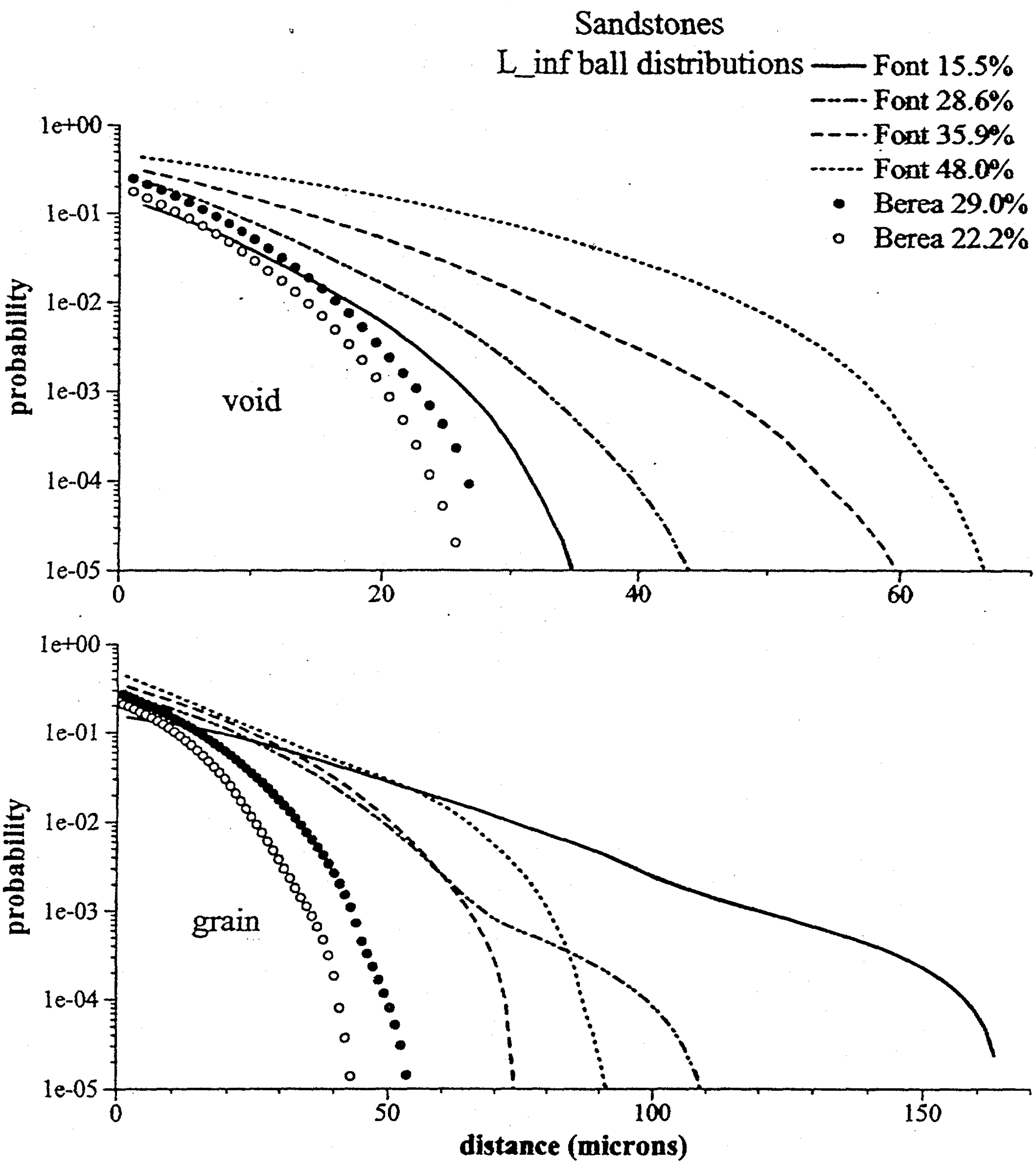

Sandstones
L_inf ball distributions
Font 15.5%
Font 28.6%
Font 35.9%
Font 48.0%
Berea 29.0%
Berea 22.2%
probability
void
1e+00
1e-01
1e-02
1e-03
1e-04
1e-05
0
20
40
60
grain
0
50
100
150
distance (microns)

Medial Axis Transform

Thinning (erosion) procedure

Reduces 3D object to its medial surface (MS)

Retains objects topological properties
number of

- connected components
- embedded cavities
- holes

Properties of each MS point

1) Equidistant from $\geq$ 2 surface points of the object.
2) 2 of these surface points lie on the opposite sides of the MS.
3) No surface points lie closer.

Medial Surface → Medial Axis (MA)

If the object contains no embedded cavities, the MS can be further reduced to a medial axis, a union of one dimensional curves.

(If the object contains embedded cavities, a medial surface segment surrounding the cavity is retained.)

The MA lies in the medial position of the MS. It retains all important 1D characteristics of the geometry of the original 3D dimensional object.

We characterize the discrete medial axis as the union of

- 1D 'paths'
- branching 'clusters'
- surface segments

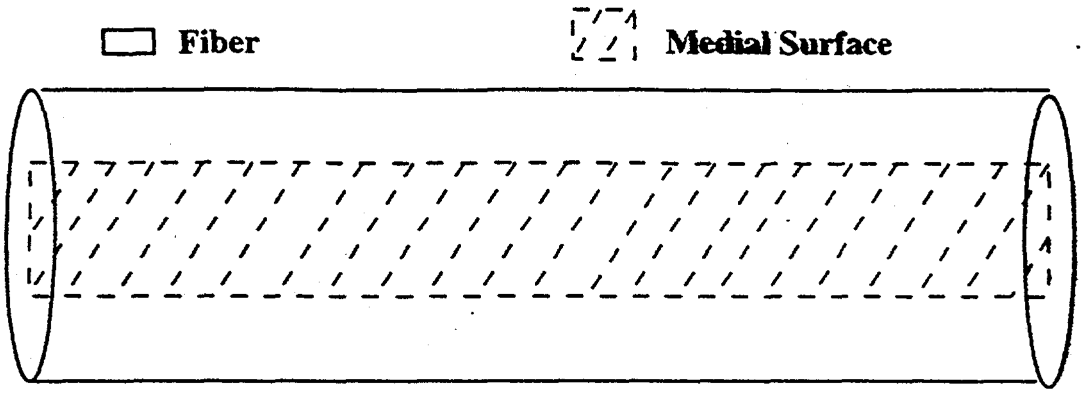
Fiber
Medial Surface

1a

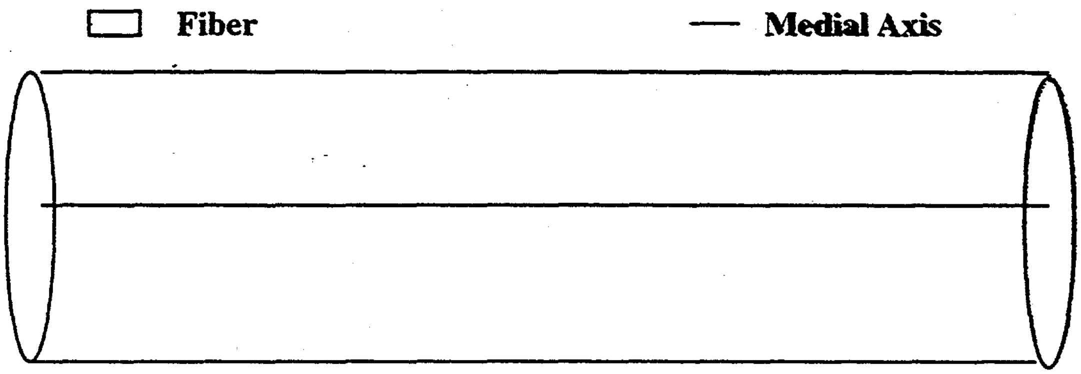
Fiber
Medial Axis

1b

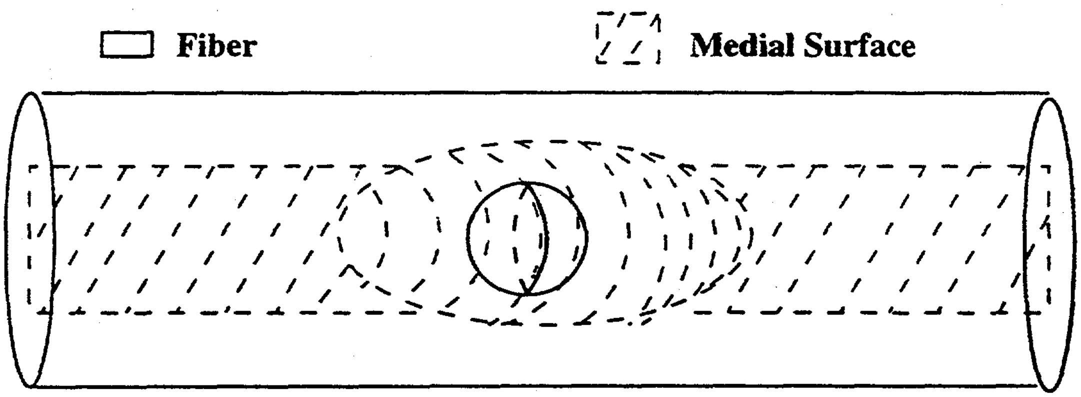
Fiber
Medial Surface

1c

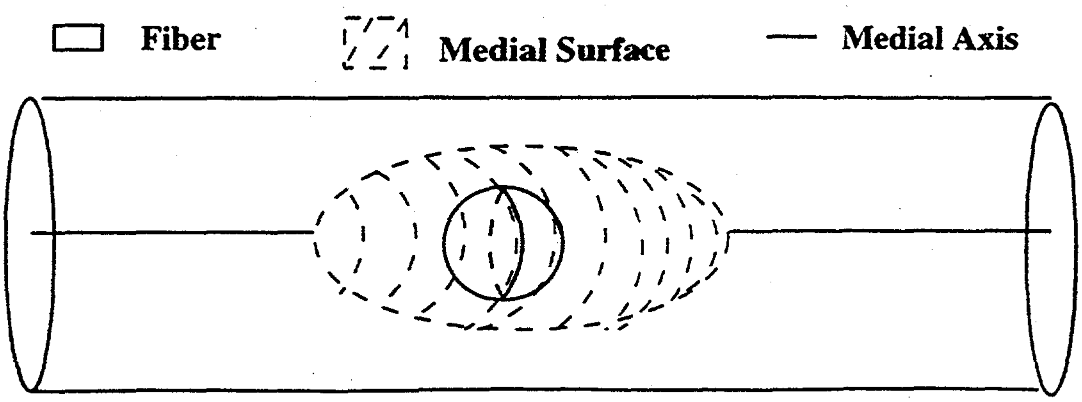
Fiber
Medial Surface
Medial Axis

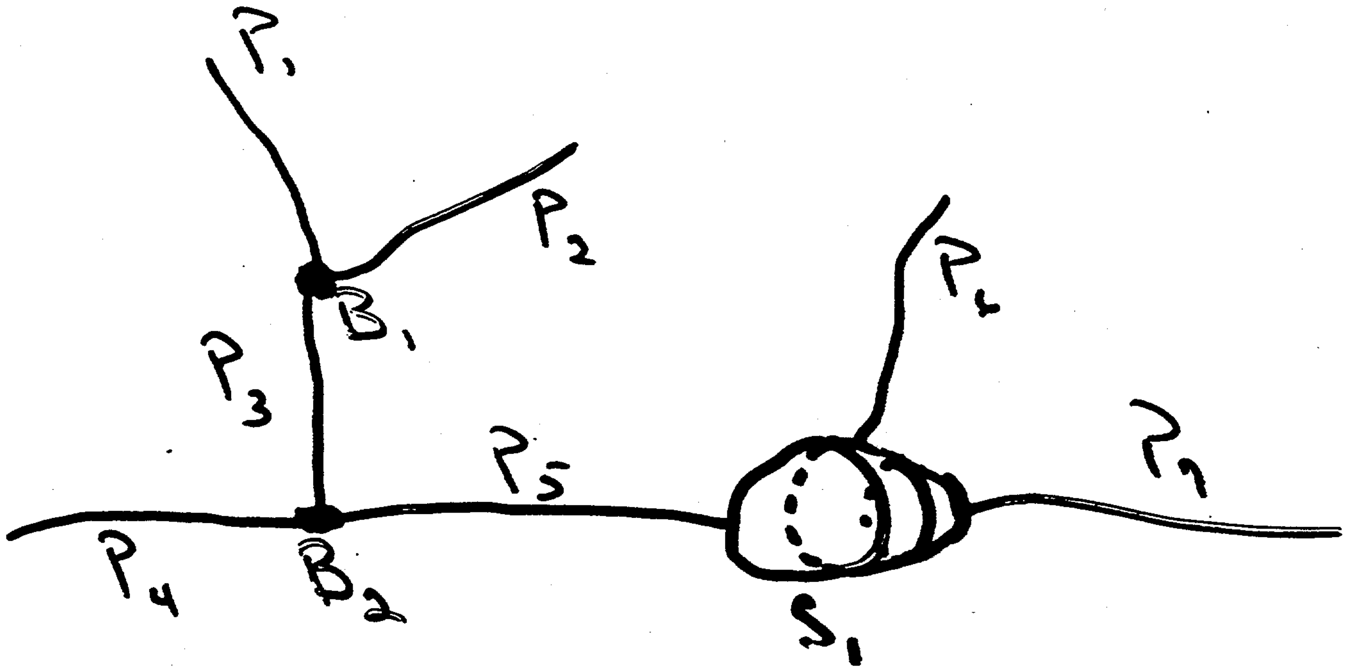

• Branch cluster

~ path

Fontainebleau sandstone
disconnected medial axis segments

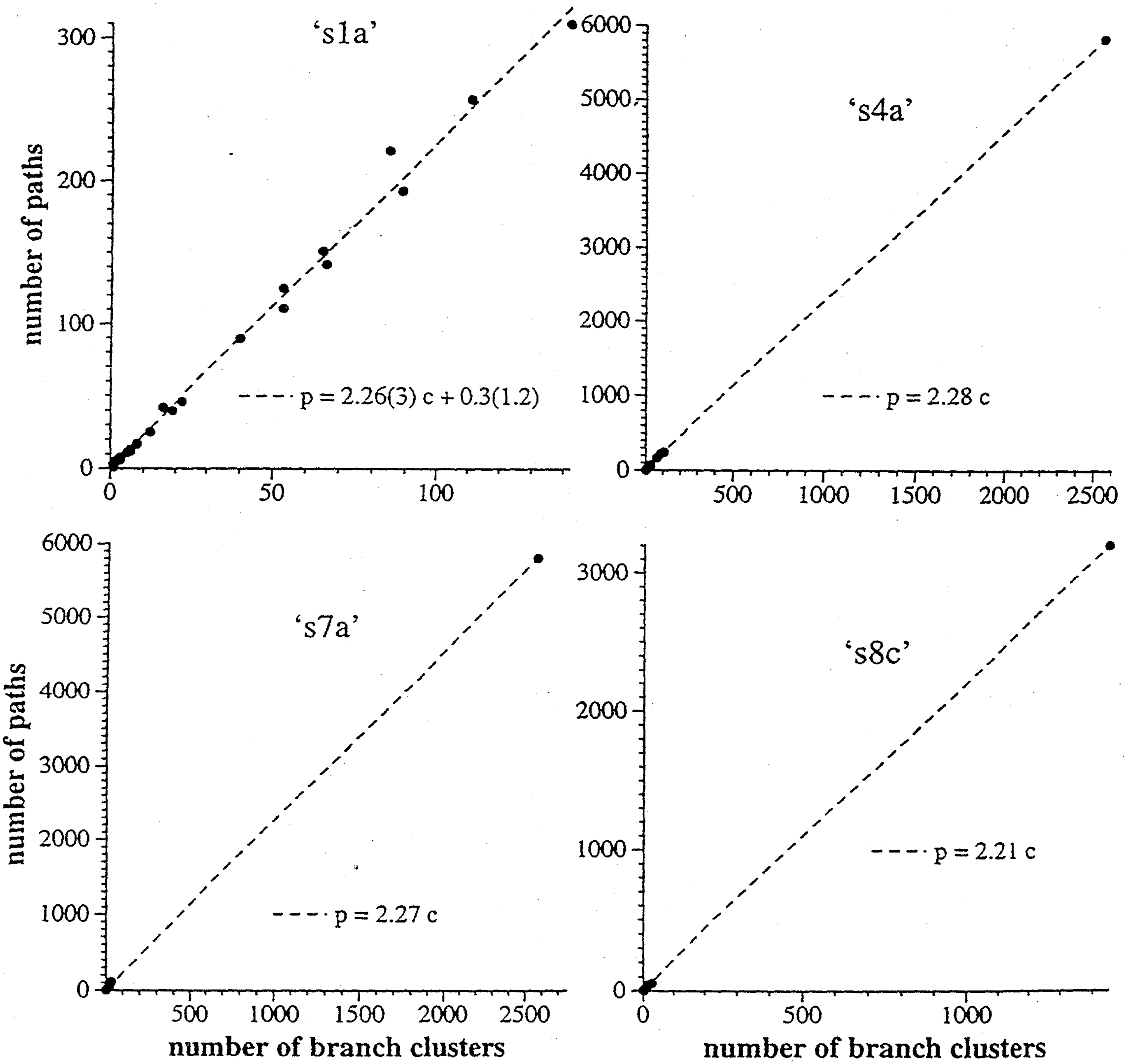

Fontainebleau sandstone
Coordination numbers

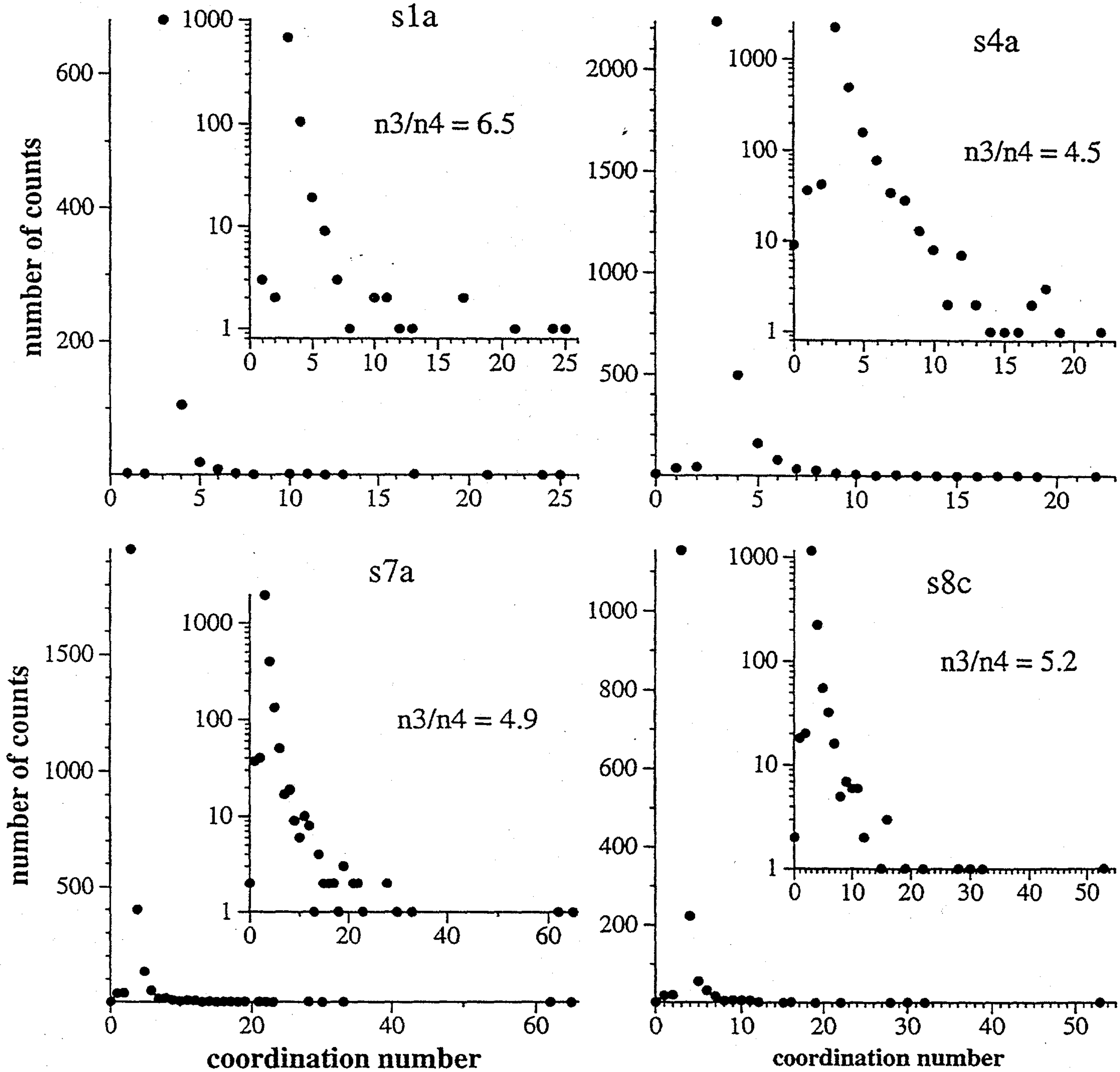

Fontainblean sandstone

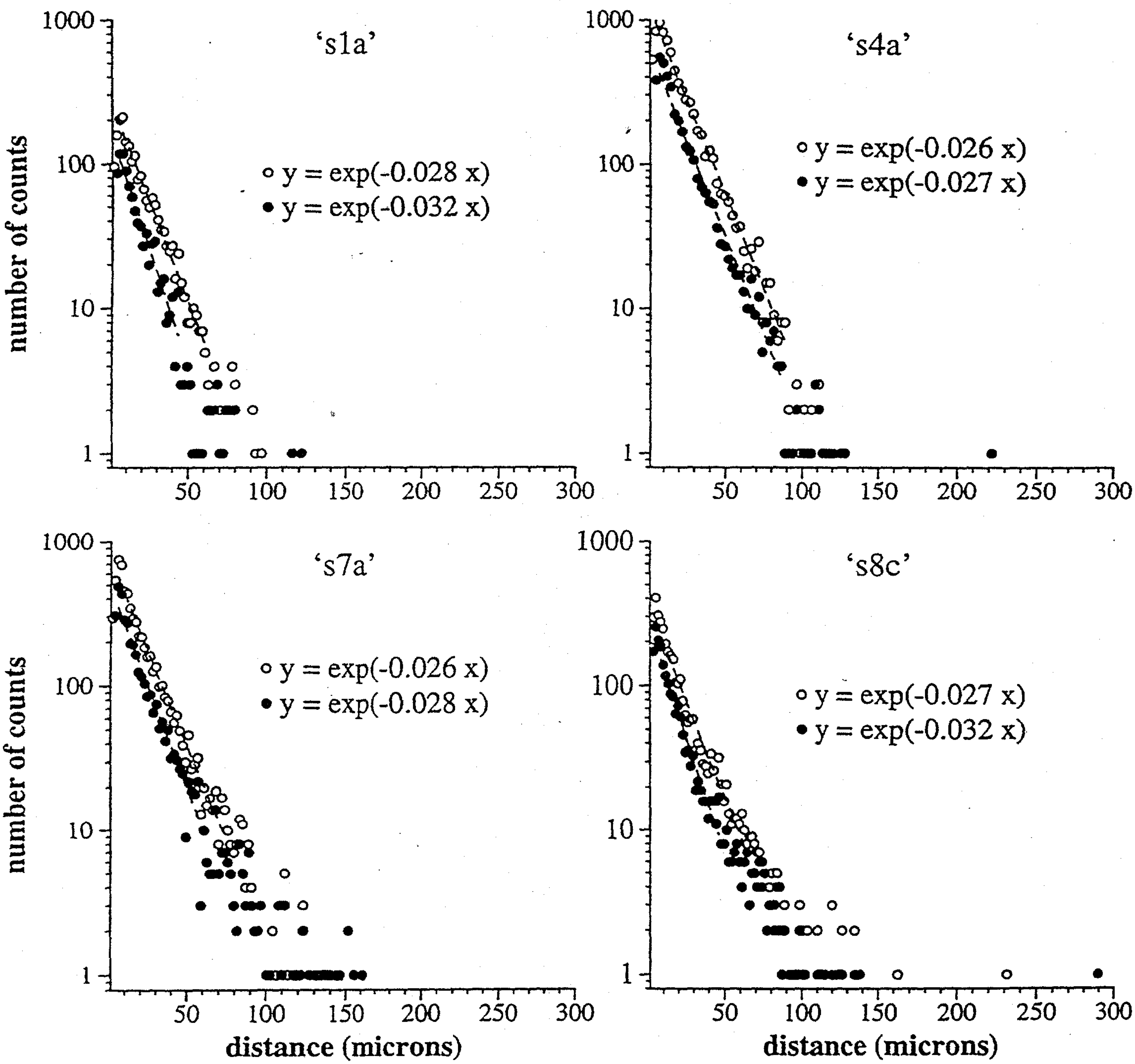

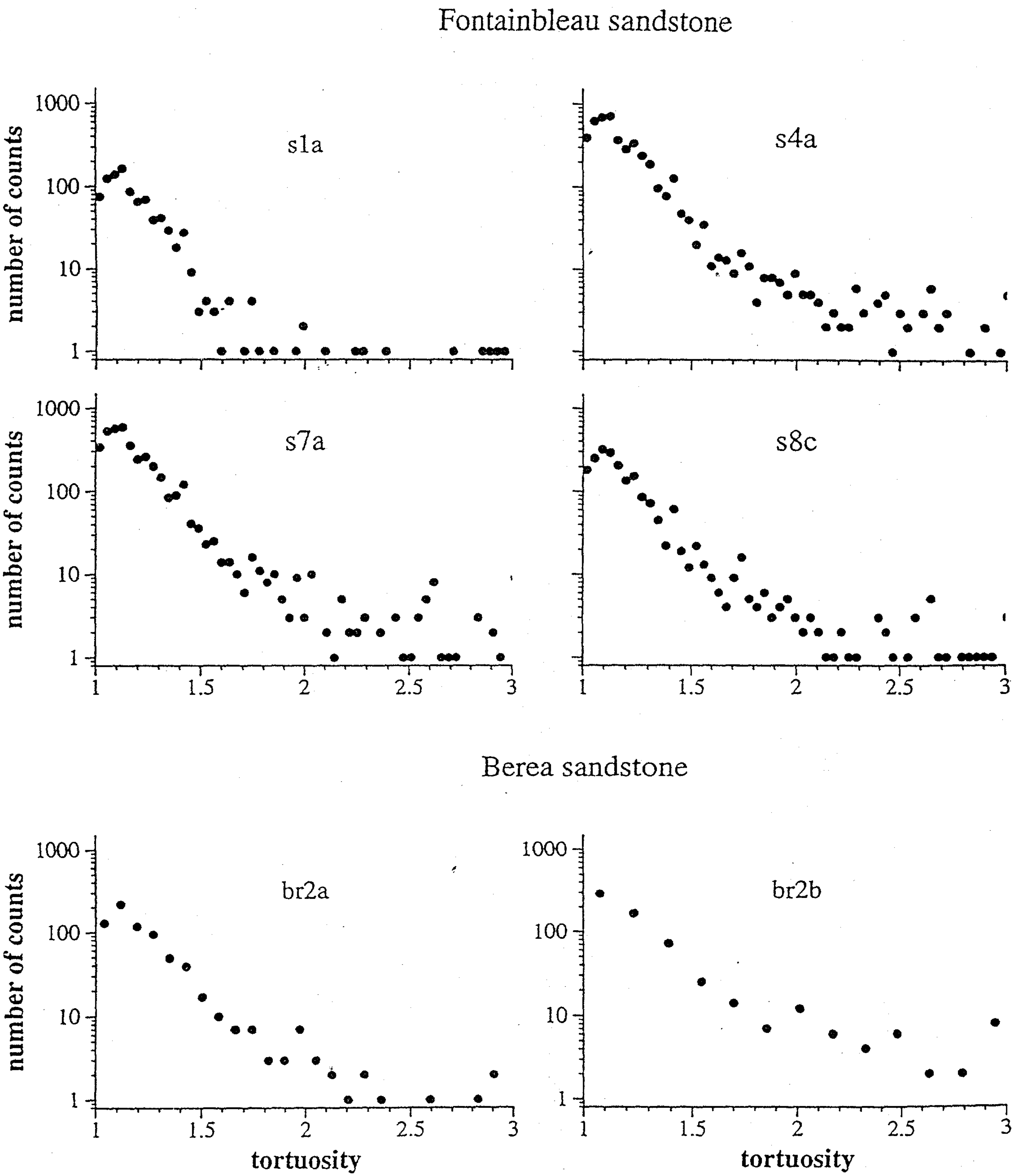
Fontainbleau sandstone
s1a
s4a
s7a
s8c
Berea sandstone
br2a
br2b
number of counts
tortuosity
1000
100
10
1
1.5
2
2.5
3

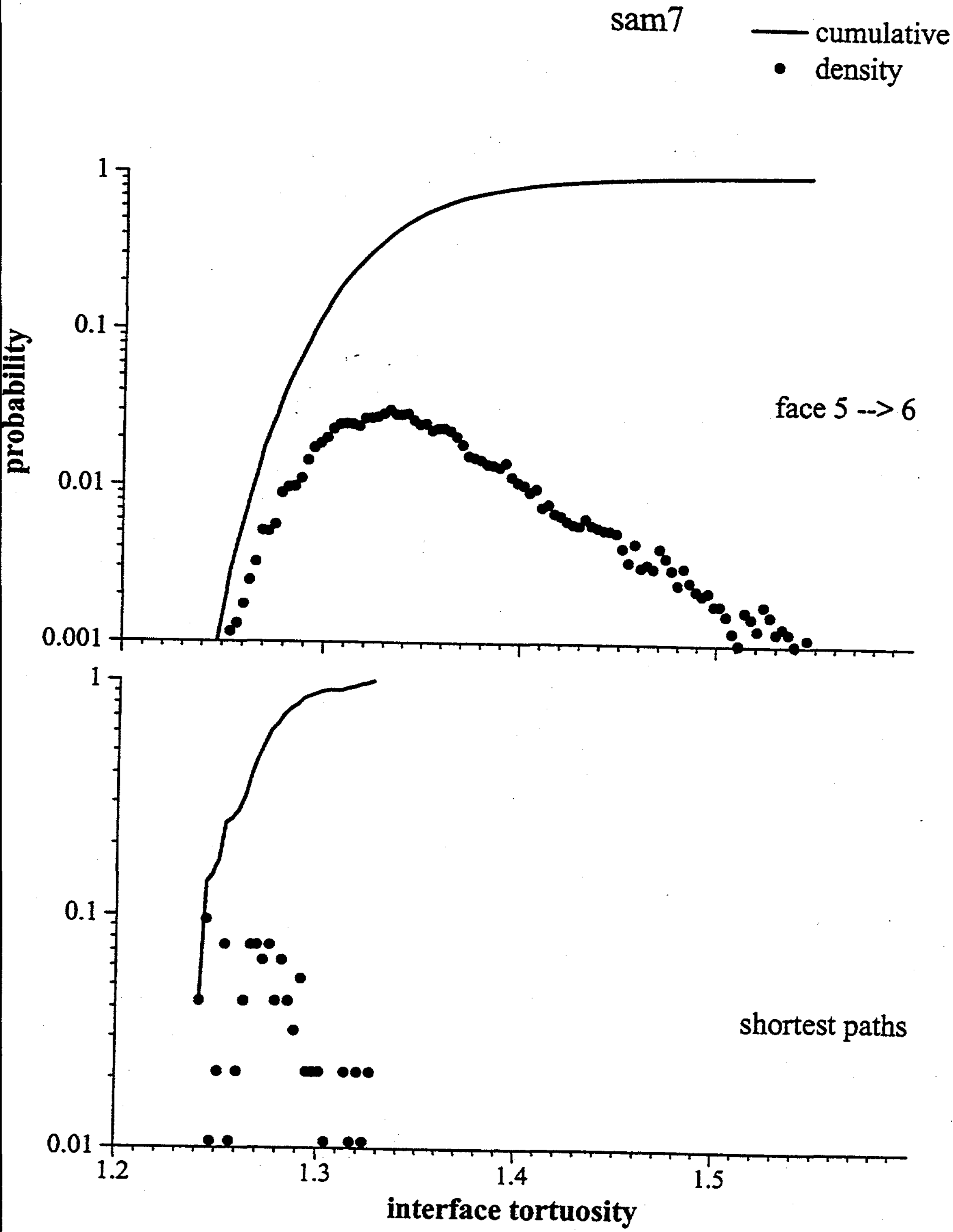
sam7
cumulative
density
probability
1
0.1
0.01
0.001
face 5 --> 6
1
0.1
0.01
shortest paths
1.2
1.3
1.4
1.5
interface tortuosity

Part VIII

Sheng-Rong Song
Dept of Geology, National Taiwan University

"X-ray Computed Microtomography Studies on Volcanic Rock"

Synchrotron X-Ray Computed Microtomography (CMT) Study on Volcanic Rocks

- **Sheng-Rong Song :** Dept. Geology, National Taiwan University
- **Keith W Jones :** Dept. Applied Science, BNL
- **W Brent Lindquist :** SUNY at Stony Brook
- **Betsy A Dowd :** Natl. Syn. Light Source, BNL
- **Dork L Sahagian :** EOS, Univ. New Hamshire, Durham
- **Peter P Siddons:** Natl. Syn. Light Source BNL

Aims:

- Study the degassing of magma and mechanisms of eruption
- Study the paleoelevation or paleoatomsphere pressure
- Study water flowing model in hazardous waste disporsal site

$V_t/V_b=P+\rho gh/P$

- V_t and V_b are the volumes of the model bubble sizes at the top and bottom of the flow
- P : atmospheric pressure at emplacement
- ρ : lava density
- g :gravity
- H: flow thickness

Current methods:

- 2D→3D: Petrographic, Stereoscopic and Scanning Electron Microscopes
- Filled with polymers, HF dissolve the rocks and counts the ploymers
- Laboratory Experiments: Mercury porositmetry, Vacuum impregnation and BET absorption

Samples:

- vesiculated basaltic lavas
- calcite-filling vesiculated basaltic lava
- basaltic reticulite
- trachytic and rhyolitic pumice

Results:

- Morphology
- Segmentation
- Physical properties:
  1. Vesicularity
  2. Connectivity
  3. Specific Surface Area

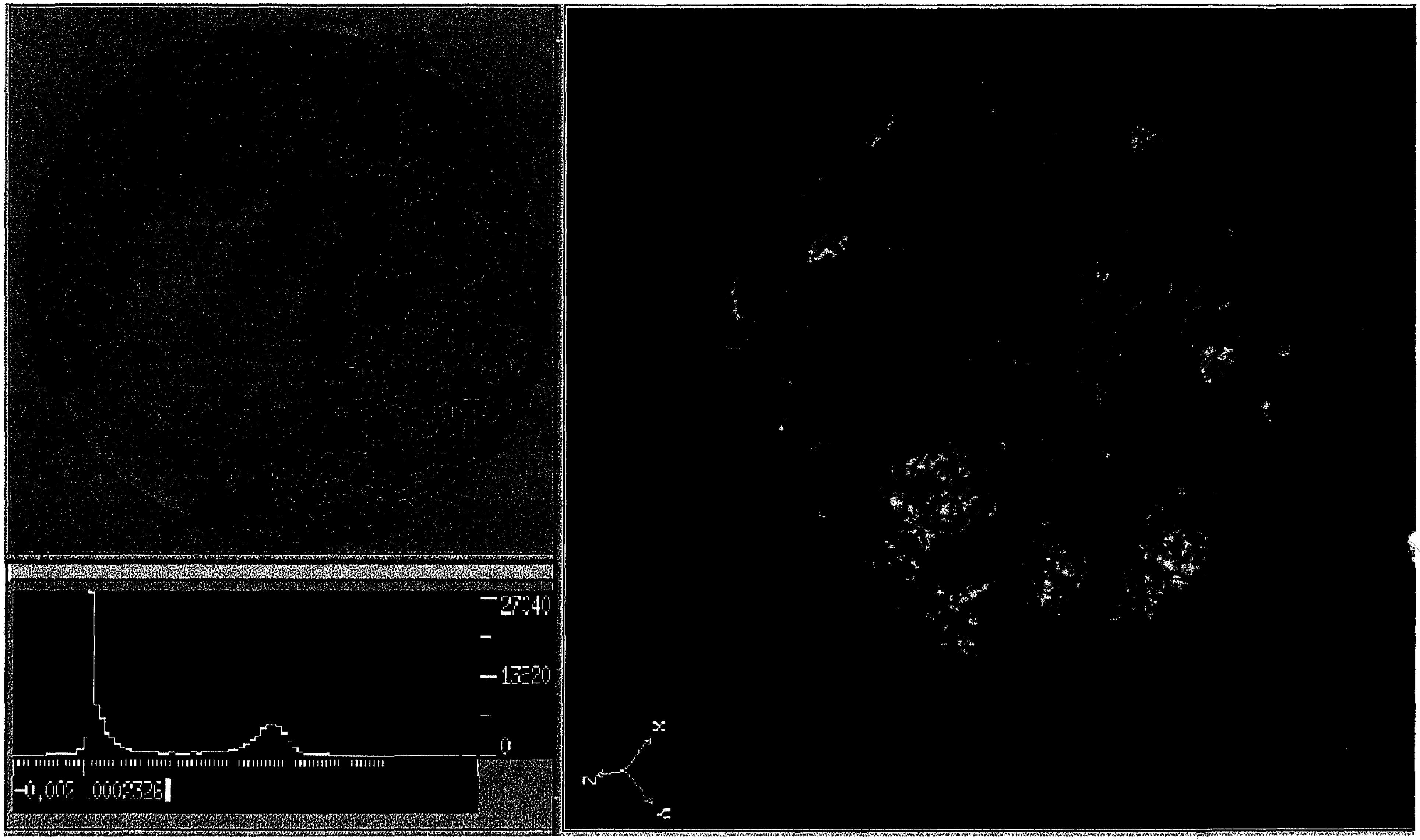
27240
13620
0
-0,002
0002326
x
y
z

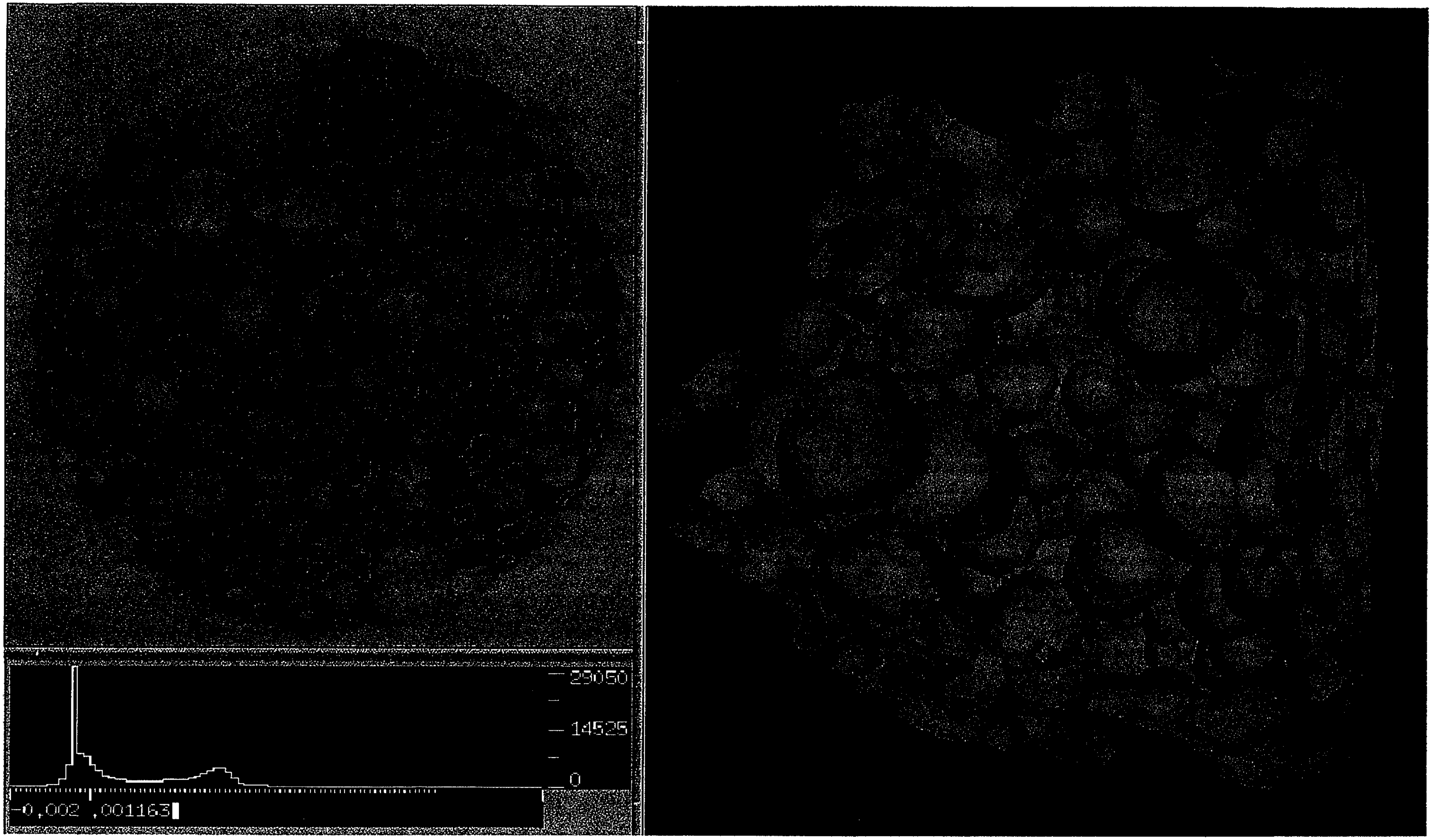

29050
14525
0
-0,002 ,001163

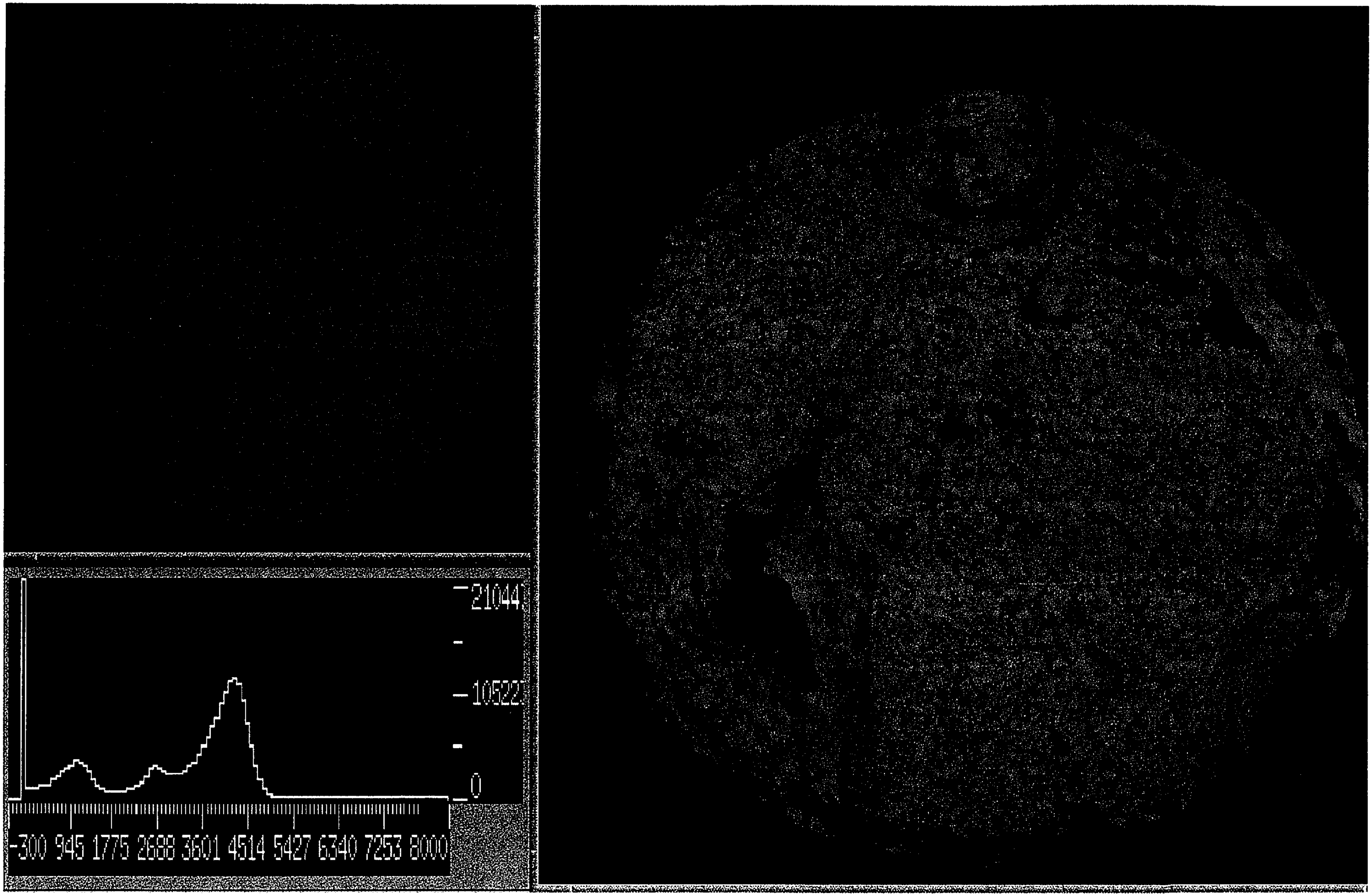
21044
10522
0
-300 945 1775 2688 3601 4514 5427 6340 7253 8000

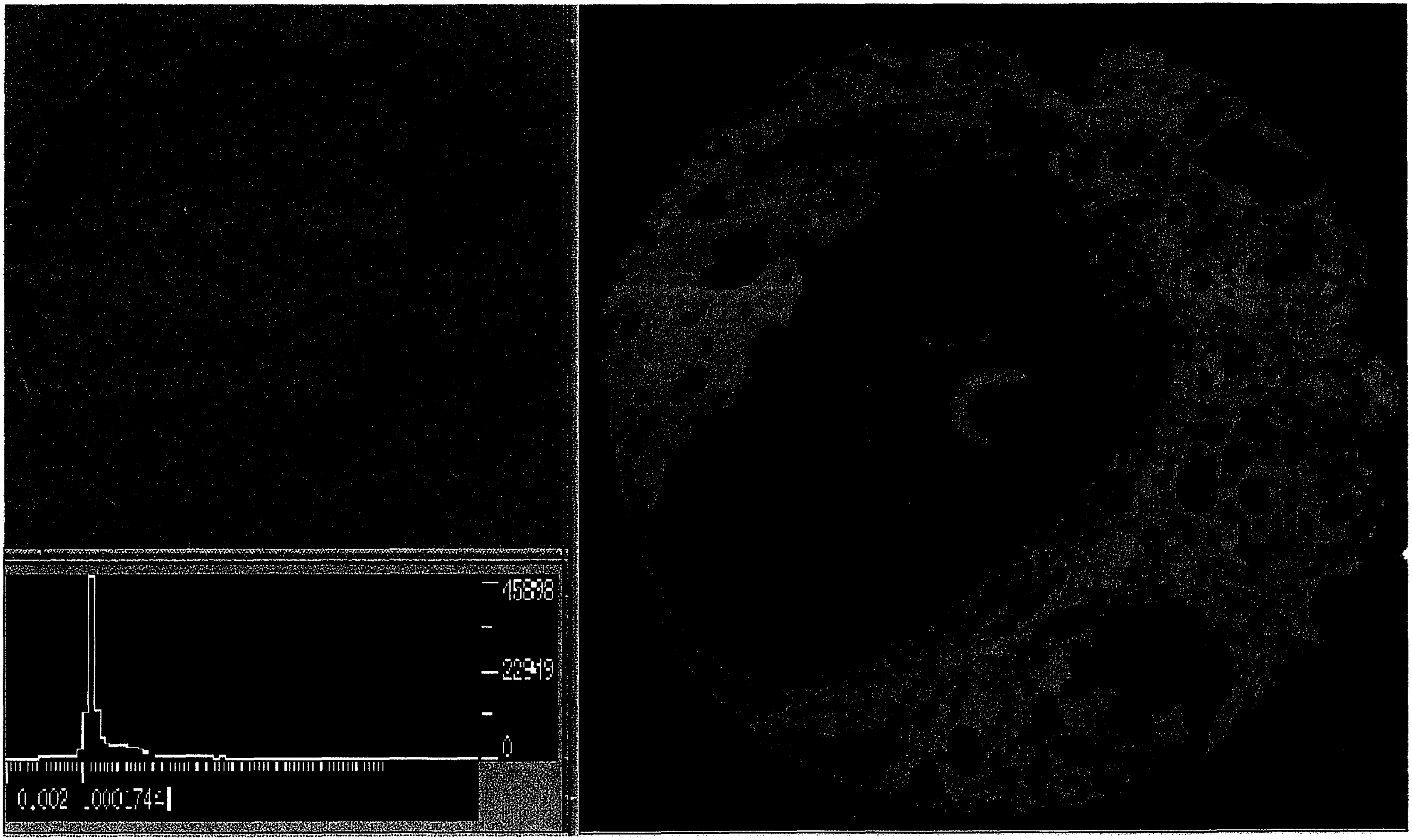
45838
22919
0
0.002

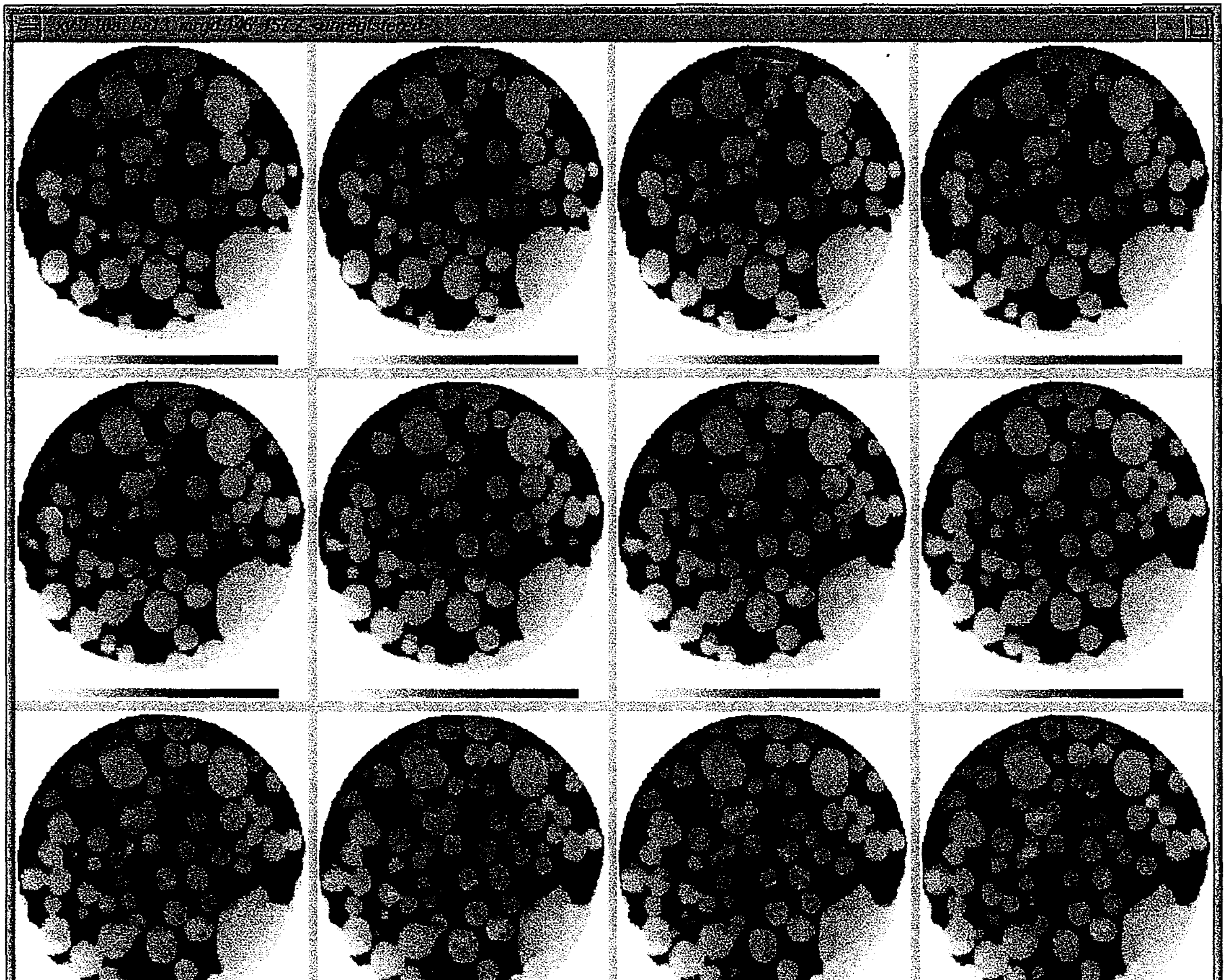

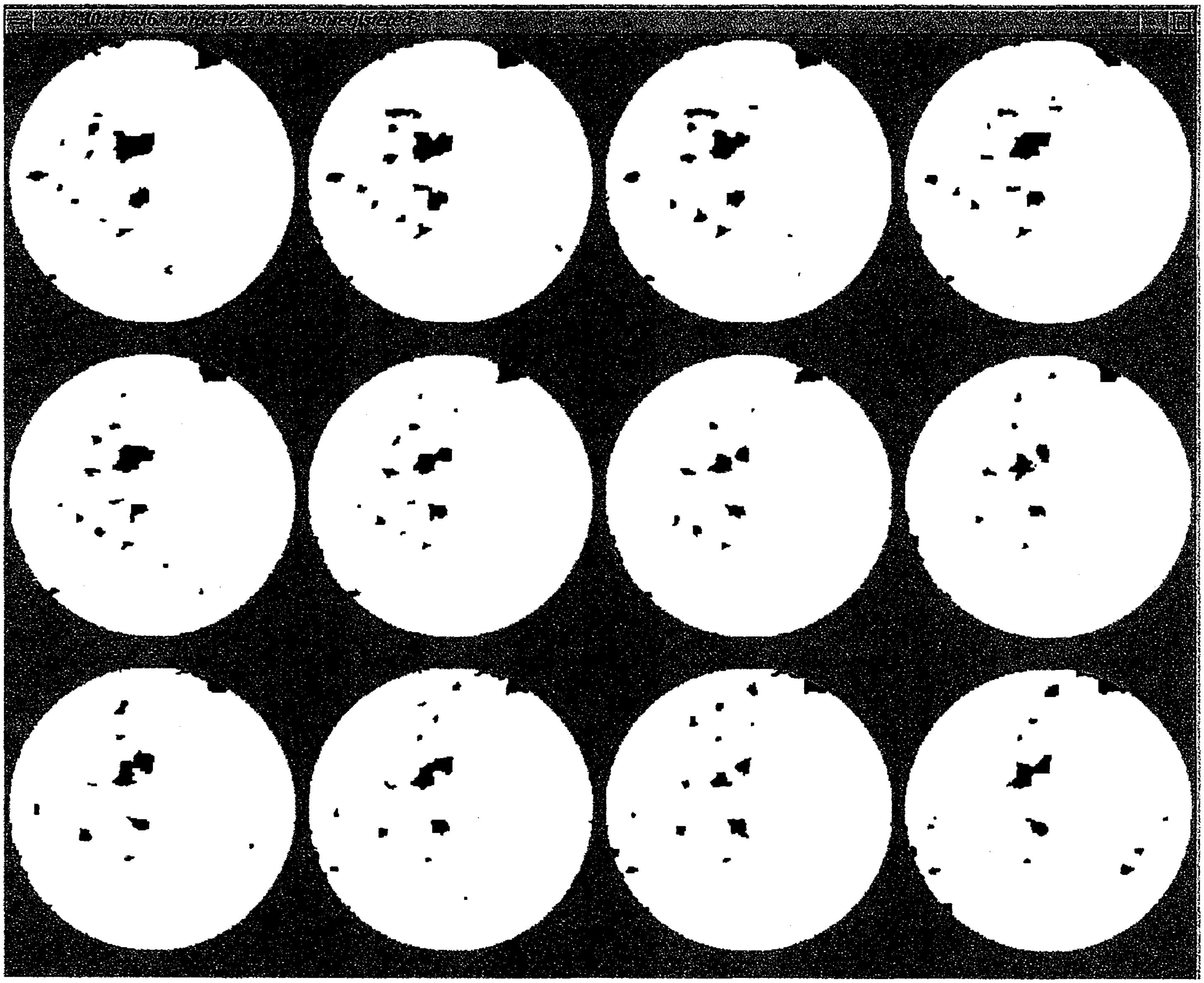

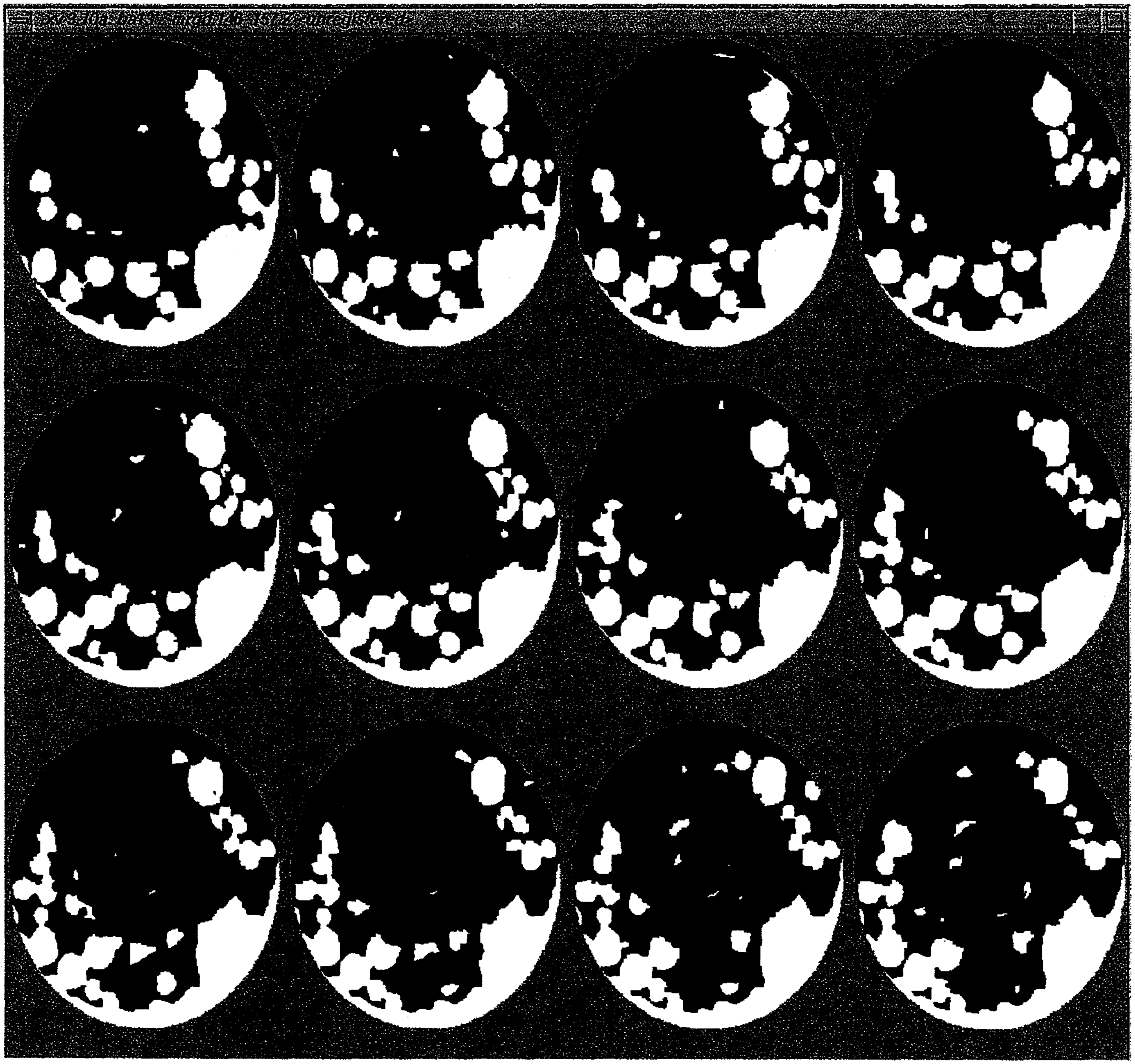

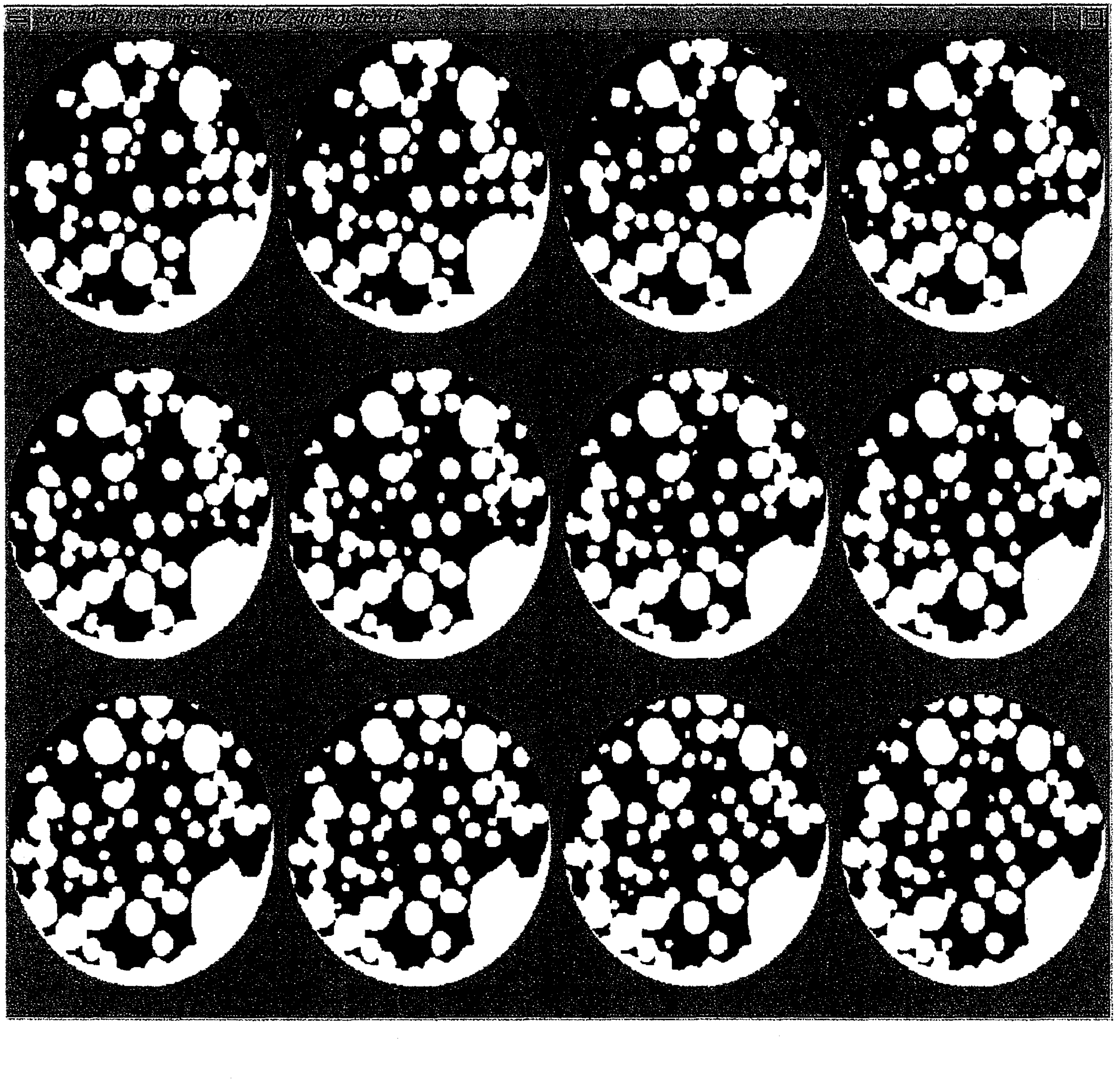

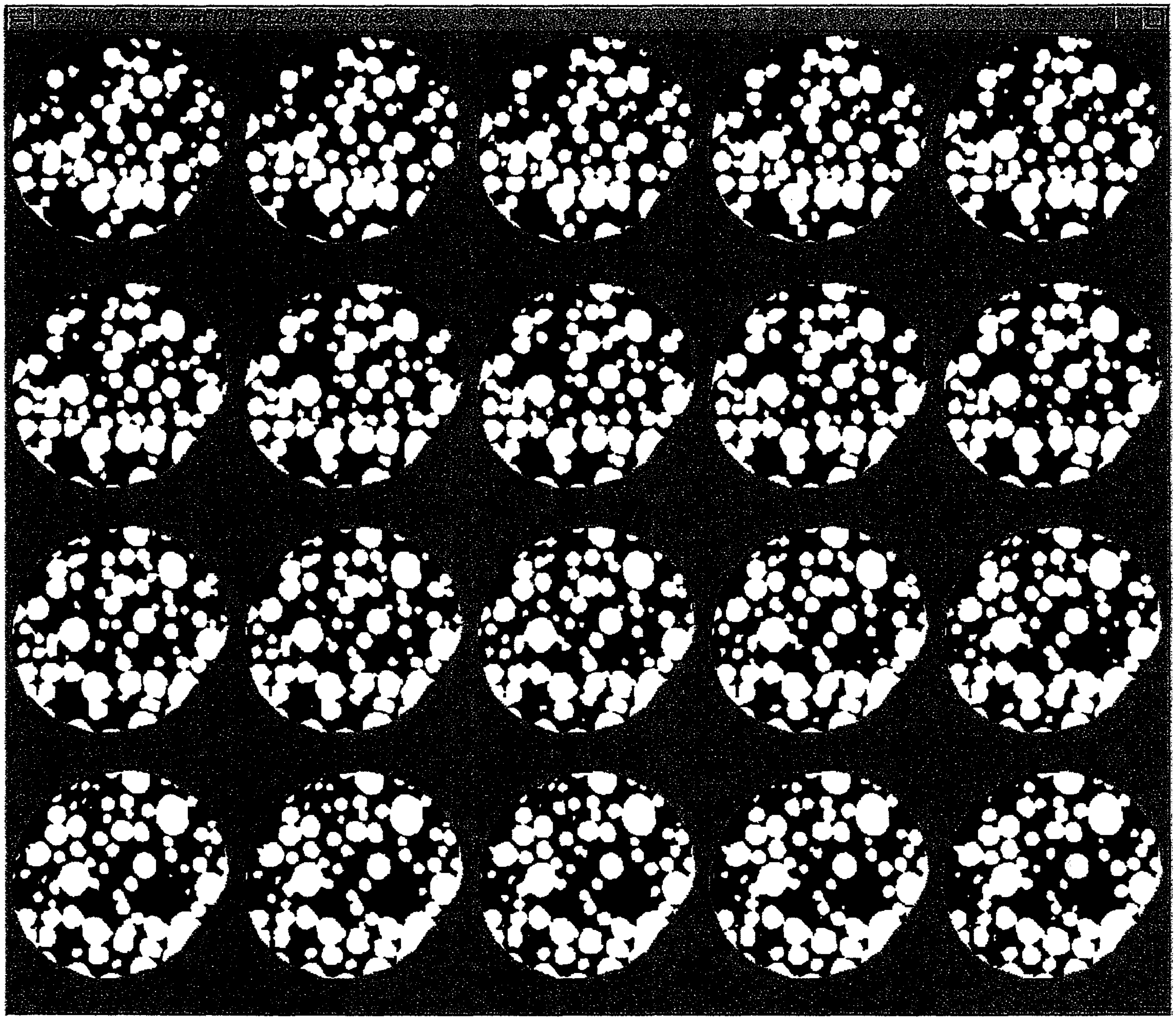

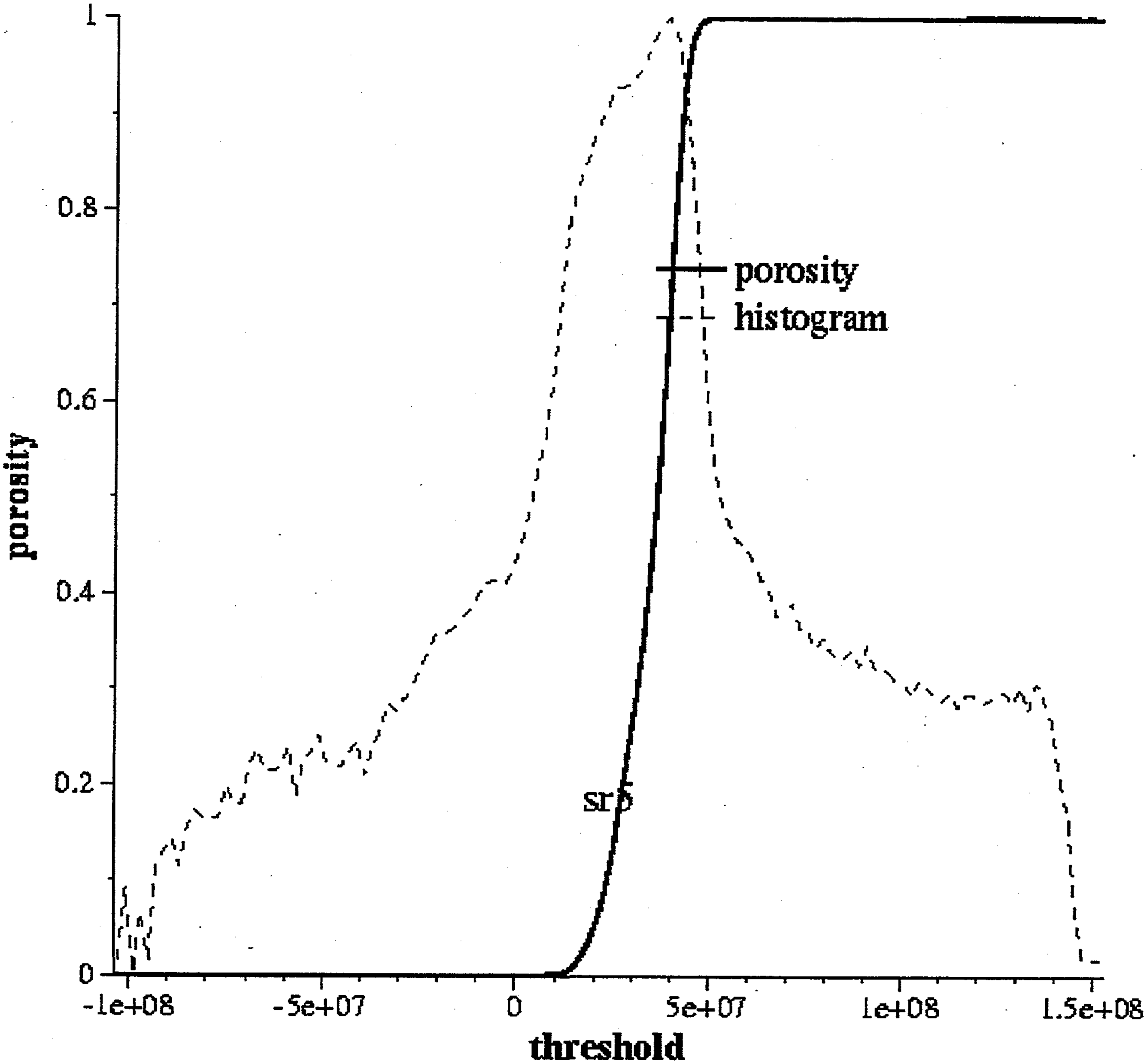

porosity
histogram
sr5
porosity
threshold
0
0.2
0.4
0.6
0.8
1
-1e+08
-5e+07
0
5e+07
1e+08
1.5e+08

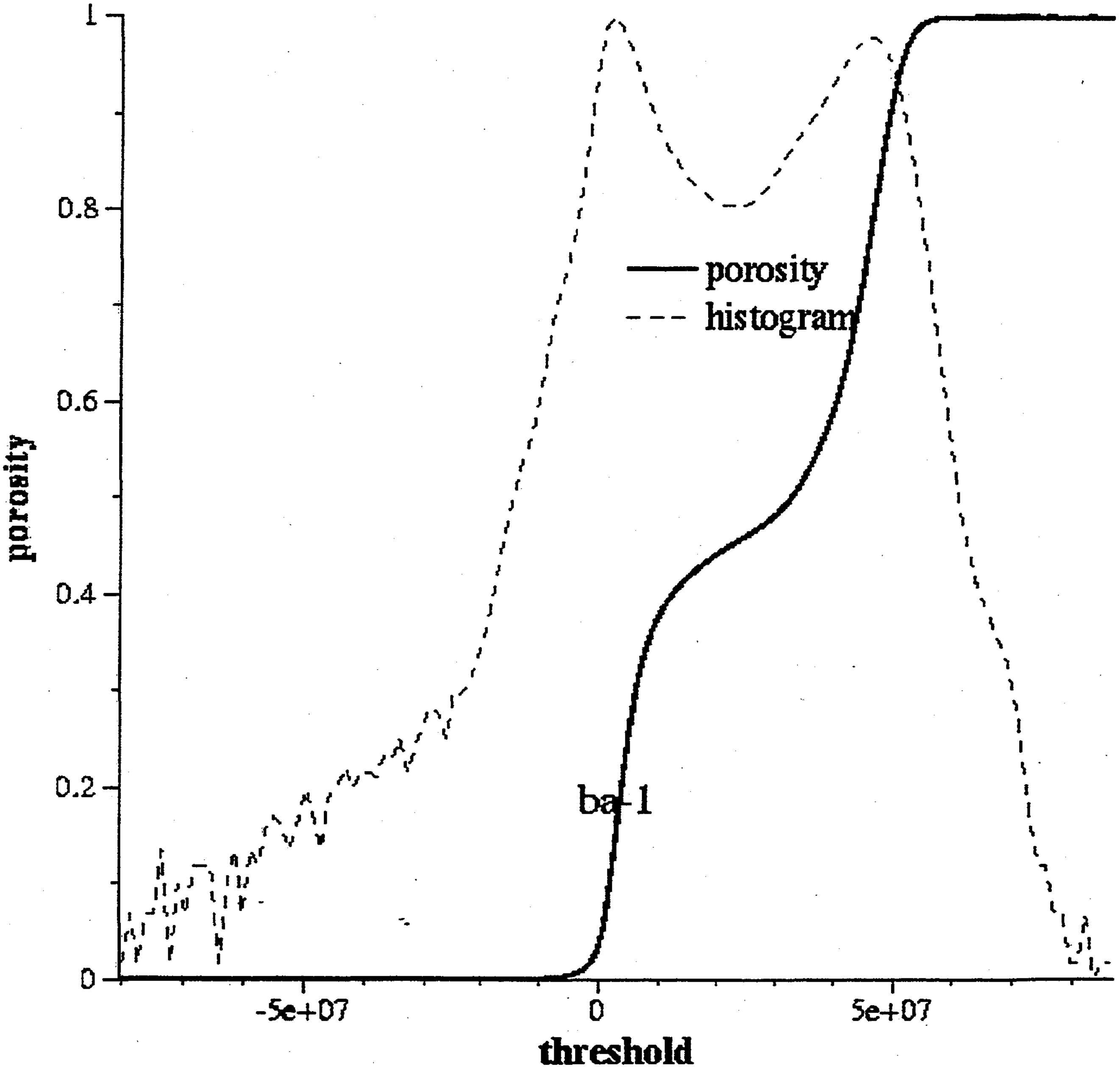

1
0.8
0.6
0.4
0.2
0
porosity
-5e+07
0
5e+07
threshold
porosity
histogram
ba-1

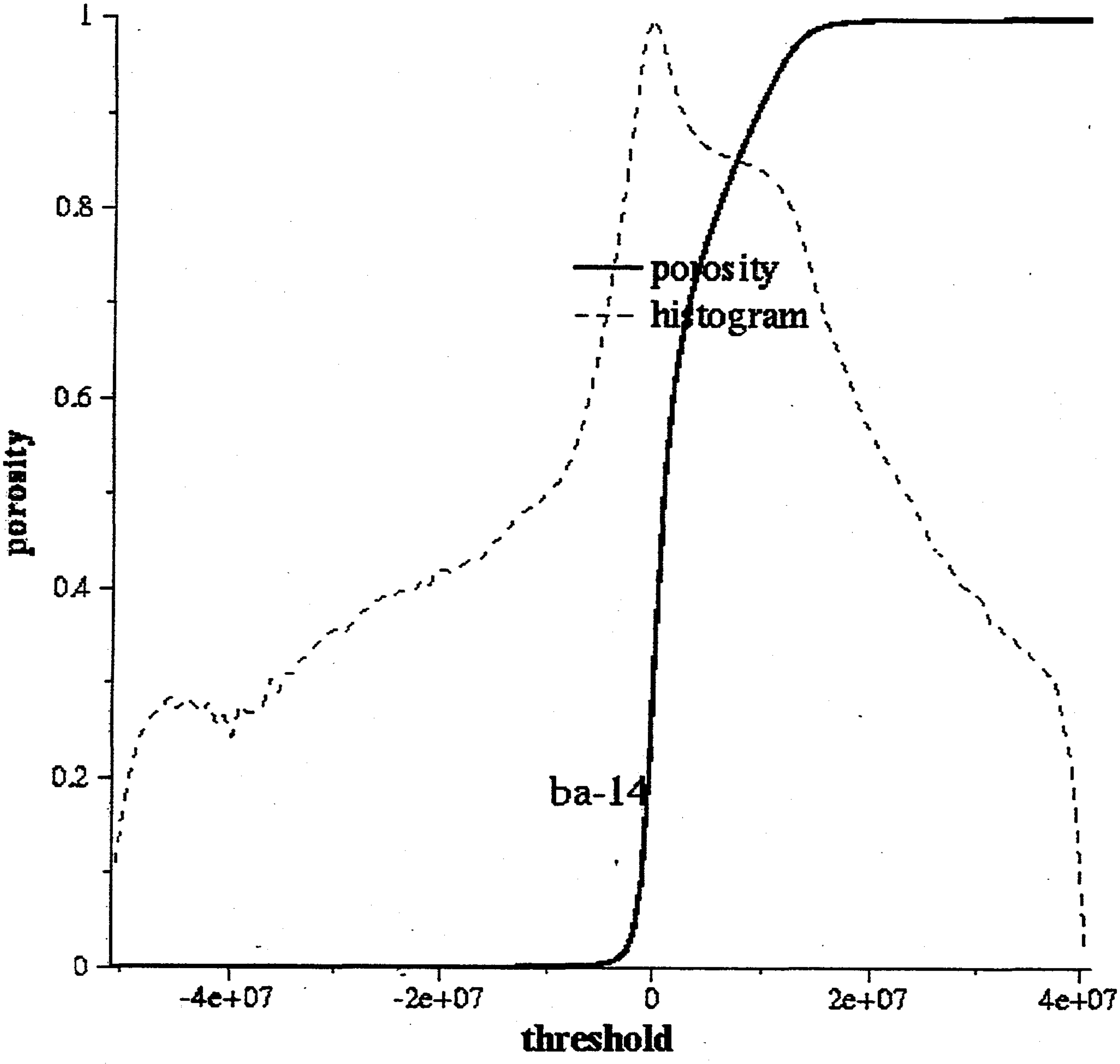

1
0.8
0.6
0.4
0.2
0
porosity
porosity
histogram
ba-14
-4e+07
-2e+07
0
2e+07
4e+07
threshold

The results of physical properties of volcanic rocks.				
Sample No.	Vesicularity (%)	Connectivity (%)	Specific surface area (3dma	Specific surface area (2-point
Ba1	44.47	92.72	0.049276	(0.034418, 0.030950)
Ba3	46.00	98.67	0.132231	(0.085820, 0.085649)
Ba14	83.49	99.97	0.131151	(0.086417, 0.080497)
Ba15	73.28	99.94	0.201494	(0.120772, 0.116625)
sr5	18.02	95.31	0.055746	(0.021299, 0.017450)
Cbs4	59.80	98.67	0.220397	(0.126655, 0.112434)
Cbs8	82.43	100.00	0.274949	(0.176243, 0.140572)

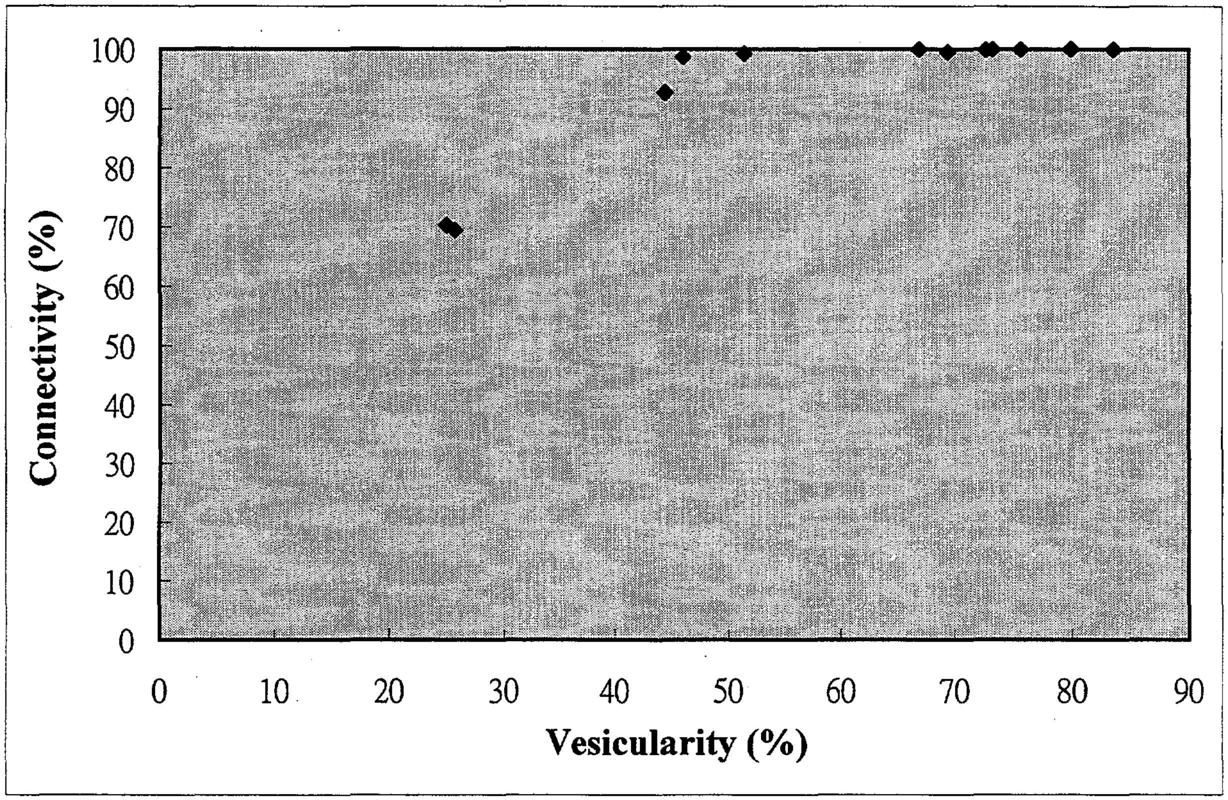
100
90
80
70
60
50
40
30
20
10
0
Connectivity (%)
0
10
20
30
40
50
60
70
80
90
Vesicularity (%)

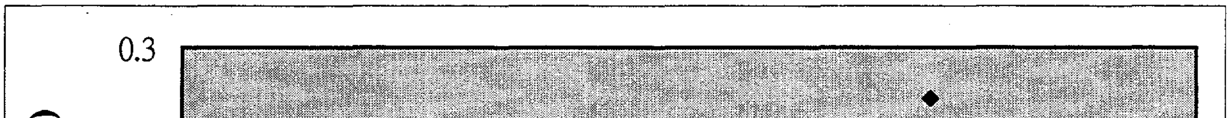
0.3
0.25
0.2
0.15
0.1
0.05
0
Specific surface area (3DMA)
0
10
20
30
40
50
60
70
80
90
Vesicularity (%)

Conclusions:

- Synchrotron X-ray computed microtomography (CMT) with medial axis analysis is a good non-destructive technique to quickly get results of the morphology and physical properties of bubble in volcanic rocks.

- For vesicle-filling rocks the CMT is also a good method to study the properties of original bubble.

Part IX

Ballard Andrews
Brookhaven National Laboratory (BNL)

"3-D Visualization of Tomographic Volumes"

Interactive Visualization for Tomography

A. Ballard Andrews (CCD/BNL)

Overview:

- X-Ray Micro-Tomography Graphics Pipeline
- Visualization Techniques for 3D Tomography
- DX Application for Tomography
- 3D Stereo Viewing of User's Data

next

X-Ray Micro-Tomography Graphics Pipeline:

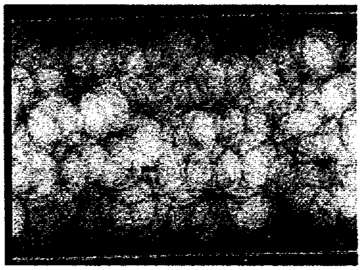

- RawData

- Sinogram

- Reconstruction (FBP, 2D FFT, Local, Wavelet)

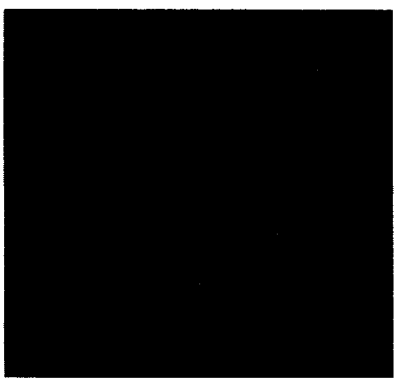

- Rendering (Volume or Surface)

prev next

Visualization Techniques for 3D Tomography

Volume rendering

- Voxel based; Map data elements directly onto image (screen) space without using geometric primitives as intermediate representation.

- No data thrown away; Interior information may be viewed. Avoids problem of accurate representation of surface

- Ray tracing requires long rendering times compared to surfaces Entire data set must be traversed.

Methods:

- Ray Tracing(back to front)

Ti(x, y) = transparency of pixel (x,y)'s ray segment in ith cell

Ci(x, y) = color added on pixel (x,y)'s ray segment in ith cell

Fi(x, y) = frame buffer value at pixel (x,y)

For all pixels (x,y)
For all ray segments i in back to front order
F(x, y) = Ti(x, y) x F(x, y) + Ci(x, y)

- Ray Tracing(front to back):

For all pixels (x,y)
For all ray segments i in front to back order
F(x, y) = F(x, y) + T x Ti(x, y) x Ci(x, y)
If Ti(x, y) = 0 (i.e., pixel is opaque) break

Surface rendering

- indirect geometry based technique for converting 3D scalar fields into surface representations (polygons)

- fast rendering for < 100,000 polygons. Data set traversed once for given threshold value to obtain surface. Hardware rendering used to produce images.

- for every volume element, must decide whether or not a surface passes through it. This can produce false negatives (holes) or positives (spurious surfaces)

Methods:

- Marching Cubes:

- Create a cube
eight data values (slice k and k+1)

- Classify each vertex
vertex outside (< value) or inside surface (> value)

- Build an index
binary labeling of each vertex (between 0-255)

- Get edge list
foreach index, access a list of cube edges that contain a triangle vertex (from symmetry of cube, all 256 cases can be generated from 15 cases)

- Interpolate triangle vertices
foreach triangle edge, find the vertex using linear interpolation of the data values
$x = i + (value - d(i))/(d(i + 1) - d(i))$

- Calculate and interpolate normals
foreach triangle edge, find the vertex normals from the gradient of the data
$nx = d(i+1, j, k) - d(i-1, j, k)$
$ny = d(i, j+1, k) - d(i, j-1, k)$
$nz = d(i, j, k+1) - d(i, j, k-1)$

- NB. Ambiguous cases (6) can create holes
Occur on any cube face that has adjacent vertices with different states, but diagonal vertices in the same state

- Marching Cubes:

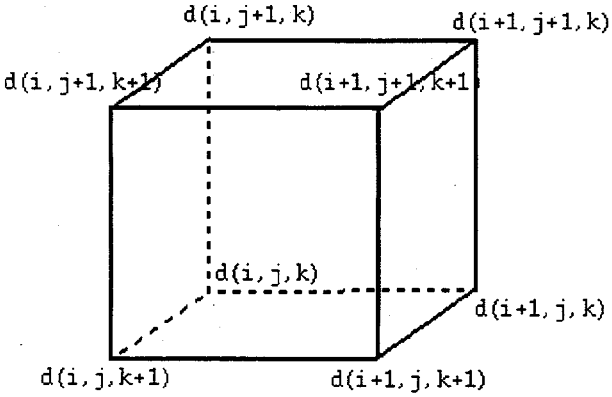

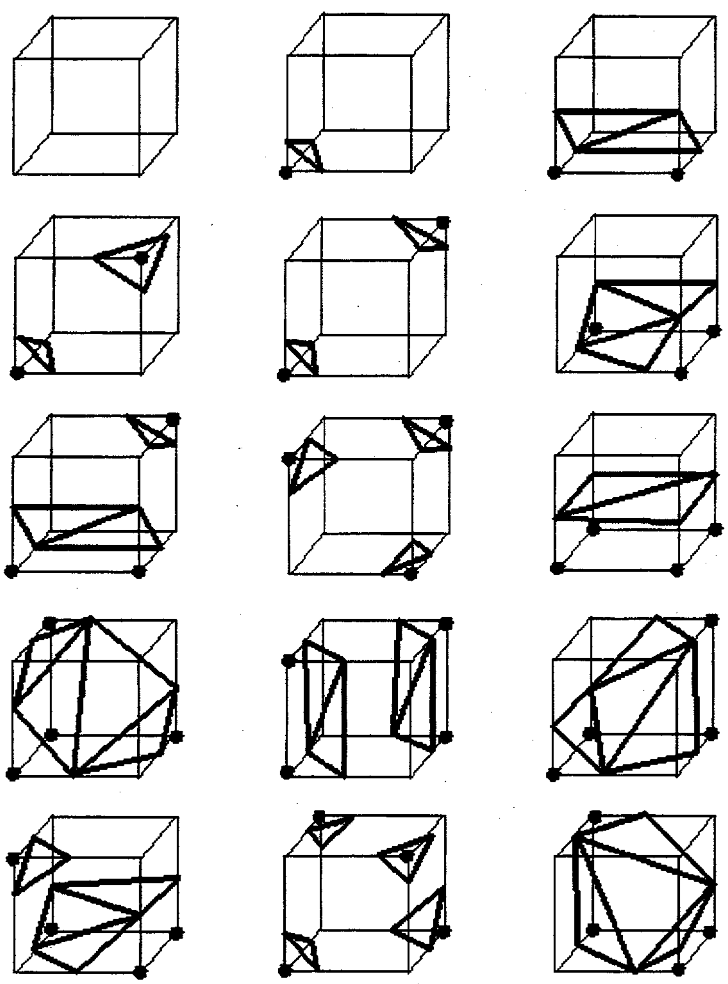

- Example (Volume rendering):

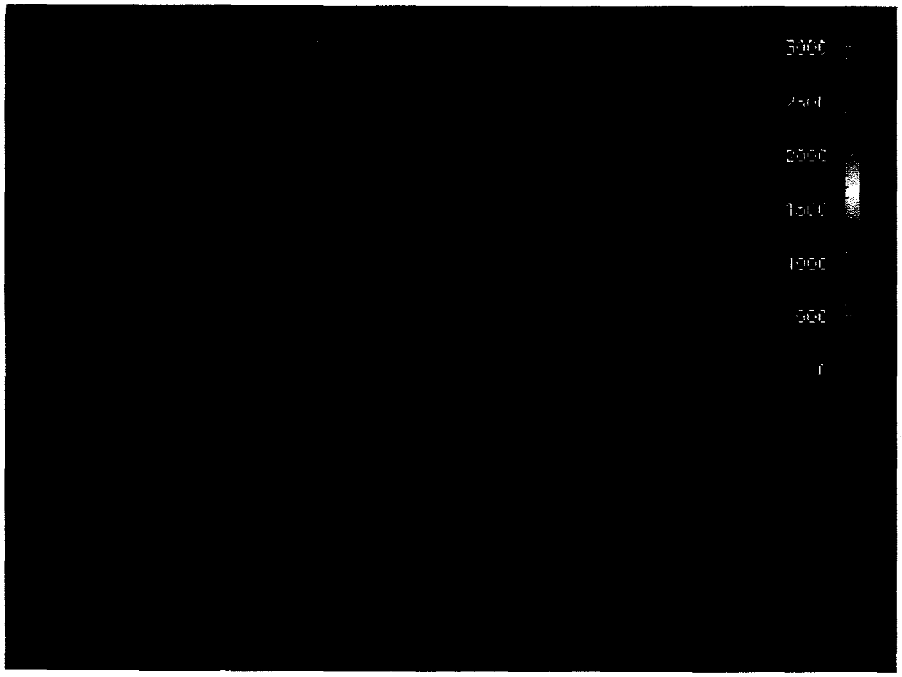

- Example (Surface rendering):

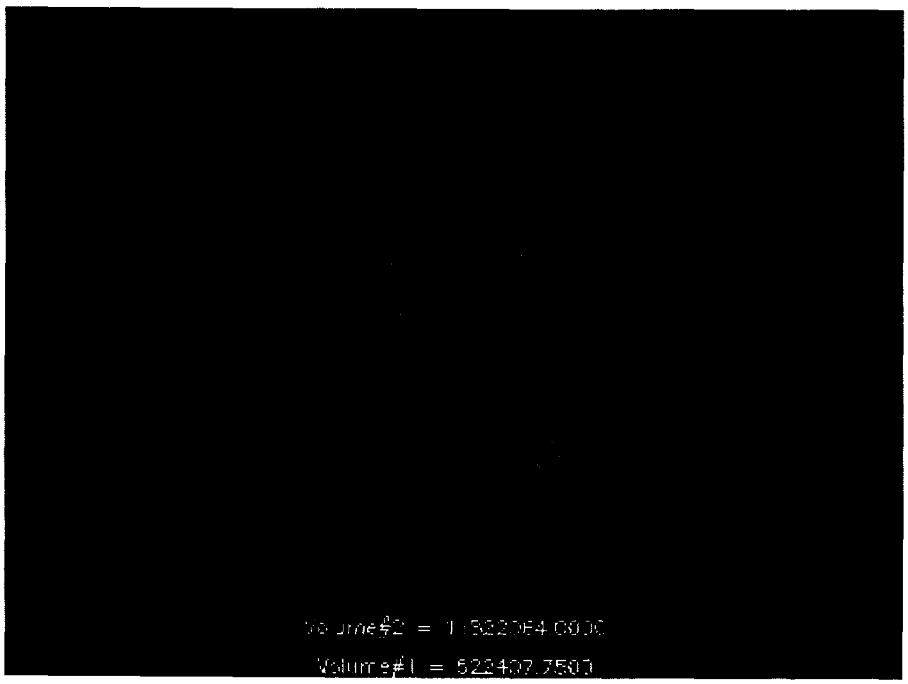

[prev][next]

Examples (Surface simplification):

Original Surface:

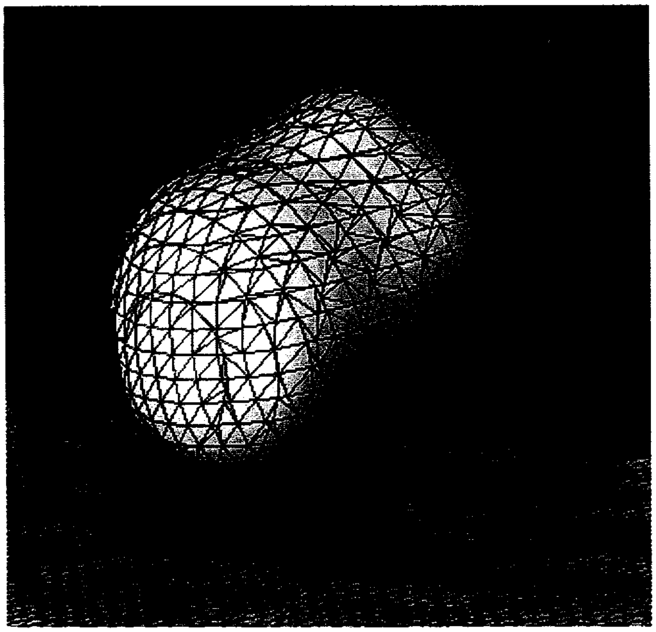

After Decimation (77% reduction in polygon count):

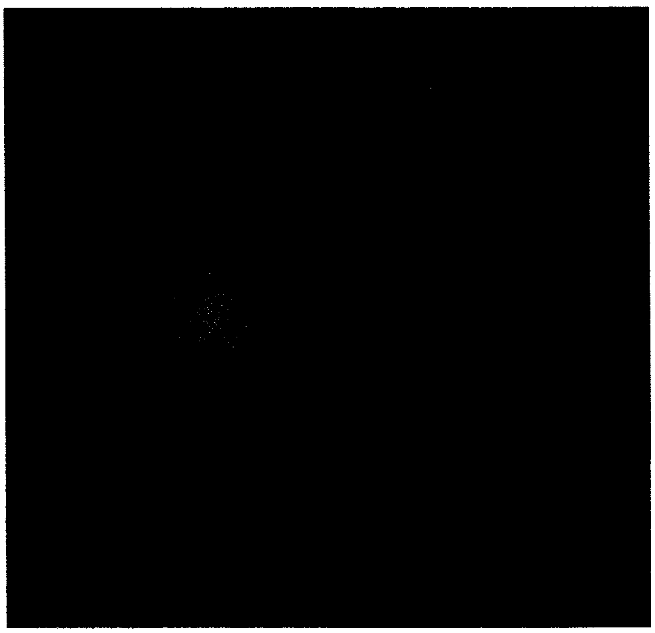

prev next

DX Application for Tomography

Motivation:

- Real time rendering of 3d volumes permits interactive data visualization, query, mapping, transformation, etcetera.

Features:

- Easy to use interface with customized control panels.

- Data manipulation:
  object selection
  navigation
  subsetting, reduction, refinement

- Data interrogation:
  interactive measurement (length, area, volume).

- Data transformation:
  image processing (filtering, edge detection, morphological)
  binarization/segmentation
  histogram, statistics
  color and opacity mapping
  annotation

-Saving and retrieval of processed data sets:

prev next

API:

- IBM Visualization Data Explorer (DX):

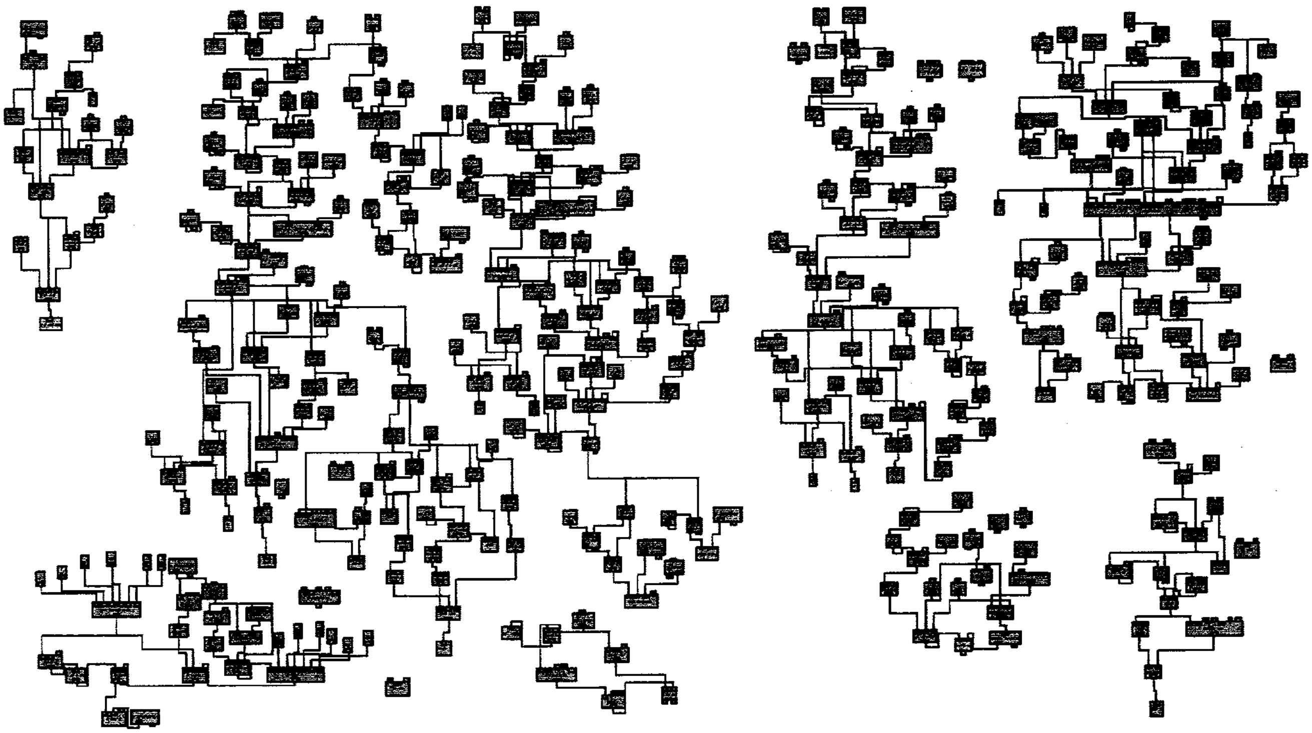

[prev][next]

Stereo Projection

Stereo Display System

The display system in the 3D Theatre is driven by a Silicon Graphics Reality Station with one CPU, a single Reality Engine and two Raster Manager Boards. Dual viewports can be created using a Multi-Channel Option box (MCO). The stereo effect is achieved in a conference room setting by rear-screen projection using high resolution, high brightness, digital projectors with low-persistence phosphors fitted with polarizing filters to generate the left eye/right eye images. A specially designed 10 foot (diagonal) screen, treated to preserve light polarization, is then viewed through polarized glasses. We refer to this time-parallel implementation as '**polar-eyes**' to distinguish it from the more widely used time-slicing method '**crystal-eyes**', which is found on desktop stereo viewing systems and comes packaged with many commercial applications . In order to maintain compatibility with these applications and provide additional flexibility the system is configured with a switch box so that the stereo viewing is possible in both modes of operation. On a per cost basis, the initial investment for **polar-eyes** viewing is greater than that for **crystal-eyes** (because of the dual projectors and the MCO box), however the cost of the extra projector is compensated by the low cost of the lightweight polarizing glasses, which make it possible for 'standing-room only' audiences of up to 25 people (limited primarily by the present room size) to simultaneously view the data. Secondly, the 'polar-eyes' system offers twice the screen resolution of time-multiplexed systems because two full screen left and right eye images are drawn with 1024 lines each. For displaying 3D models we use Iris Performer, which provides a real-time rendering library that is optimized to take advantage of the graphics hardware on the SGI. The viewing algorithm produces an image which appears to float in the middle of the room. Data files are prepared in a 3D object file format such as Inventor. The 3D scene graph is controlled by a mouse and function keys. Models with up to a million polygons can be displayed.